# Computation of Stability Boundaries in Parallel Flows

**Thomas Cantrell**
**May 2021**

**Student ID: 10170539**
Project Supervisor: Prof Richard Hewitt
Course unit: MATH40000

# Contents


**1 Abstract** **5**

**2 Introduction** **5**
2.1 History and background . . . . . 5
2.2 Methodology . . . . . 7
2.2.1 Numerical methods . . . . . 8

**3 Derivation of the Orr-Sommerfeld equation** **11**

**4 A test problem - linear one-dimensional eigenvalue problem** **15**
4.1 Numerical results . . . . . 16
4.1.1 Error analysis of the eigenvalues . . . . . 18
4.1.2 Convergence of the numerical scheme . . . . . 19

**5 The Orr-Sommerfeld eigenvalue problem** **21**
5.1 Formulating the discretized equations . . . . . 21
5.2 Numerical results . . . . . 23

**6 One-dimensional boundary value problem and an iterative method** **30**
6.1 Establishing the iterative scheme . . . . . 31
6.2 Numerical results . . . . . 32

**7 Orr-Sommerfeld boundary value problem** **34**
7.1 Establishing the iterative scheme . . . . . 34
7.2 Numerical Results . . . . . 37

**8 Computation of the neutral stability curve** **40**
8.1 Discussion of some experimental results . . . . . 44

**9 Chebyshev polynomials and the spectral-tau method** **47**
9.1 Formulation of the Orr-Sommerfeld problem with the spectral-tau method 52

**10 Numerical results of the spectral-tau method** **57**
10.1 Analysis of spurious eigenvalues . . . . . 58
10.2 Analysis of eigenvalue spectrum and most unstable eigenmodes . . . . . 60
10.3 Curves of neutral stability . . . . . 67

**11 Comparison with finite-difference methods** **69**
11.1 Comparison of the local iterative method and the spectral-tau method . . 69
11.2 Computation of the critical Reynolds number . . . . . 71

**12 Conclusions and discussion** **74**
12.1 Extension to Poiseuille-Couette flow . . . . . 75
12.2 Conclusions . . . . . 77

**Appendices** **79**
A Spectral-tau method for Poiseuille-Couette flow . . . . . 79
B Examples of MATLAB code used . . . . . 81
B.1 Finite-difference implementation . . . . . 81
B.2 Spectral-tau method implementation . . . . . 82

# 1 Abstract

The linear stability of plane Poiseuille flow is studied by examining the solution to the Orr-Sommerfeld eigenvalue problem by the implementation of two numerical methods. The numerical schemes utilised are that of finite-difference methods and spectral methods, where it is shown that the spectral-tau method obtains very accurate results more economically in comparison to a second-order central-difference scheme employed. A local iterative method derived from the second-order finite-difference scheme is utilised to obtain approximations to the least stable eigenvalue with the use of an estimated guess and a corrector. These numerical schemes are compared in terms of their accuracy, order of convergence and computational expense by comparison of the numerical results produced. The spectral approach is also applied to a hybrid plane Poiseuille-Couette flow, where the boundaries are allowed to move tangentially relative to each other, the results of which are commented on in this work.

---

# 2 Introduction

## 2.1 History and background

The theory of hydrodynamic stability is a branch of applied mathematics that was first notably developed by Helmholtz, Kelvin, Rayleigh and Reynolds in the latter half of the nineteenth century. The principal interest of study in hydrodynamic stability theory is the transition from laminar to turbulent flow, and more specifically the description of the breakdown in laminar flow in space and time. The transition between these two states has been of high interest and extensively studied since the mid-nineteenth century, with aims to analyse and examine under which conditions this breakdown of laminar flow takes place and turbulent flow develops. In 1883, Reynolds clearly explained the observance of an instability, in a series of classic experiments on the instability of flow through a pipe (Reynolds, 1883). In these experiments water was drawn through glass tubes submerged in a tank of water, with the experiment constructed such that a band of coloured water enters the tube with the clear water. It was found that drawing water at a sufficiently low velocity through a tube created a streak of colour in a straight line, thus demonstrating stable laminar flow. He further demonstrated that above a critical velocity at which the flow is driven through the tube the smooth laminar flow observed previously, breaks down. Reynolds observed that the streak of colour mixed with the surrounding clear water, filling the remaining part of the tube with coloured water. The results observed by Reynolds (1883) are shown in figure 1.

The description of the breakdown of laminar flow in the series of experiments conducted by Reynolds, illustrated by the drawings in figure 1, shows the remarkably chaotic motion of turbulent flow observed initially at the onset of instability. Another phenomenon observed by Reynolds was that of turbulent spots in the flow. These were initially described by Reynolds as flashes of disturbance that would come on at a particular length of the tube and then switch off seemingly returning to laminar flow, only for another turbulent spot to occur after a certain length along the tube. Therefore the experiments carried out by Reynolds clearly illustrated the need for the development of a theory which is able to describe, characterise and predict the transition from laminar flow

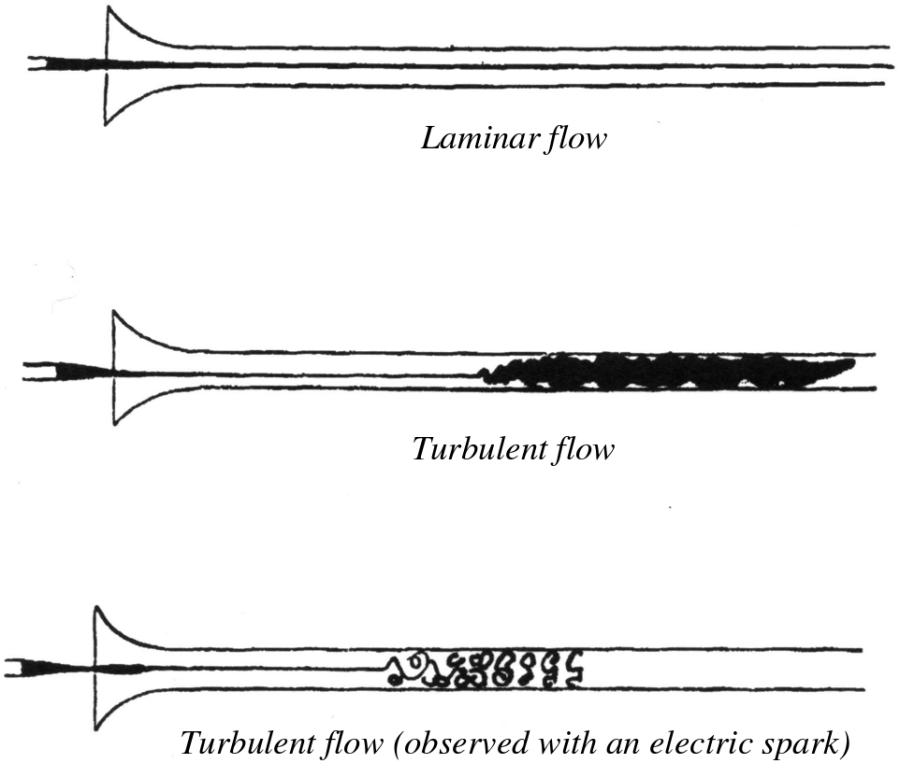


FIGURE. 1 Illustration of the observations made by Reynolds in 1883 in his classic series of experiments. The streak of colour carried by the flow in the pipe is shown for laminar flow as well as two examples of turbulent flow (Reynolds, 1883).

to turbulent flow in various scenarios. This is where the foundations of hydrodynamic stability, both in a theoretical and experimental sense, are found.

There have been many different approaches in developing the theory of hydrodynamic stability by well-known applied mathematicians such as Rayleigh, Taylor, Helmholtz and Kelvin. This is due to different assumptions being made for different scenarios, most notably is the assumption of viscosity. In the characterisation of the Kelvin-Helmholtz instability, the assumption that the fluids in the system are inviscid was made by Kelvin and Helmholtz to characterise the instability. The Kelvin-Helmholtz instability is observed when two fluids of different densities separated by an interface have a large difference in their velocities and the effects of gravity. The result is a turbulent interaction between the fluids, characterised by wave generation at the interface. Helmholtz (1868) first published work on the instability with Kelvin (1871) publishing his work on the instability later in the nineteenth century. This particular instability, which is described by wave generation at the interface, is often seen in nature in strikingly beautiful yet chaotic settings. For example Kelvin-Helmholtz instabilities have been observed in the cloud formations in the atmospheres of planets, such as Jupiter and Saturn, where the layers of the atmosphere pass over each other at different velocities creating an interface between them. A more commonly seen example of the Kelvin-Helmholtz instability is when wind blows over the surface of water. Hence, in some scenarios disregarding the effects of viscosity still allows us to describe physical phenomena. This is a key difference in comparison to the experiment conducted by Reynolds which is intrinsically viscous.

The problem of evaluating the stability of fluid flows where viscous effects are taken into account was established independently by Orr in 1907 and Sommerfeld in 1908. The type of channel flow studied by Orr (1907a,b) was plane Couette flow, where the parallel boundaries surrounding the viscous fluid are allowed to move tangentially relative to each other. Whereas Sommerfeld (1908) studied plane Poiseuille flow, where a pressure gradient acting in the streamwise direction drives the fluid through the channel. The combination of their work led to the derivation of the Orr-Sommerfeld equation, thus establishing a basis for future problems in the study of hydrodynamic stability with the inclusion of viscous effects. Initially the attempts to obtain a solution to the Orr-Sommerfeld equation did not yield many meaningful results as only a few very simple solutions could be found analytically. Therefore many applied mathematicians in the early twentieth century appealed to asymptotic analysis. However, as computational implementations of numerical methods became increasingly feasible, finite-difference methods were used to solve the Orr-Sommerfeld equation numerically. Although this was a significant advancement in successfully obtaining a solution, the development of spectral methods allowed for a very accurate solution and thus a meaningful interpretation of the numerical results corresponding to the stability of the flow.

In studying the linear stability of channel flows to infinitesimal disturbances, the fundamental parameters that correspond to the transition to turbulence are estimated. The linear stability analysis of plane Poiseuille flow yields the conclusion that pressure driven flow between two parallel rigid boundaries is unstable to infinitesimal disturbances (Orszag, 1971). Whereas, plane Couette flow is found to be stable to infinitesimal disturbances (Davey, 1973). In the experiments conducted by Reynolds (1883) the transition to turbulence of Poiseuille flow is observed above a critical Reynolds number. However, in contrast to these famous experiments, Poiseuille flow in a pipe is found to be linearly stable to infinitesimal disturbances (Davey and Drazin, 1969). Although the linear stability analysis of plane Poiseuille flow correctly predicts a transition to turbulence above a threshold for the flow parameters, the critical values of these parameters observed in experiments are often in disagreement with the linear theory (for example see Alavyoon *et al.* (1986)). This discrepancy between the theoretical prediction of transition versus the observed experimental results highlights the need to account for nonlinear effects and the importance of a nonlinear theory. The improved agreement among theoretical and experimental results allows us to better understand transition to turbulence.

In more recent history the study of hydrodynamic stability has had far-reaching applications. For example, the stability of fluid flows is important in the fields of aerodynamics, atmospheric sciences, astrophysics, oceanography, combustion, biology and engineering. In the case of aerodynamics, the prediction of the region of laminar to turbulent flow on an aircraft is significantly important, if this is predicted incorrectly, this could lead to an infeasible or flawed engineering design. Therefore in studying the stability of fluid flows, we can examine fundamental flows which have a wide range of applications in the mentioned fields of study. The simplest of fluid flows one can consider are that of parallel channel flows, where a fluid flows between two rigid parallel boundaries.

## 2.2 Methodology

To begin the analysis of the stability of plane Poiseuille flow, we must first define the fields of velocity and pressure. The flow defined by these fields is known as the base or basic flow. The traditional classical method for solving a system of linear equations

obtained from the governing equations is that of normal modes, where small disturbances of the fields are resolved into modes. The success of this method relies upon the ability to obtain a complete set of normal modes, as this allows us to develop a picture of an arbitrary initial disturbance. Each normal mode has an associated growth rate $\sigma$, which determines the stability of the normal mode. If $\sigma > 0$ a mode is said to be unstable, if $\sigma < 0$ then the mode is stable and if $\sigma = 0$ then the mode is neutrally stable. If we are to consider temporal stability then we concerned with disturbances that grow with time, alternatively if we consider spatial stability then we consider disturbances that grow in space. In this report where we consider the stability of pressure-driven flow, we will be concerned with temporal stability, that is the wavenumber of a normal mode is taken as real while the frequency is considered to be complex.

For the case of plane Poiseuille flow, the three-dimensional problem can be reduced to a two-dimensional problem in the search of the onset of instability by Squire's theorem, then introducing a streamfunction we reduce the governing equations to an eigenvalue relation in the form of the famous Orr-Sommerfeld equation (Squire, 1933). In order to obtain a solution to this eigenvalue problem we are required to use numerical methods. In this report finite-difference and spectral methods are the numerical methods used to obtain a solution to the Orr-Sommerfeld equation. A key development in obtaining an accurate solution to the Orr-Sommerfeld equation was achieved numerically in 1971 by using expansions in Chebyshev polynomials, where the Reynolds number and wavenumber corresponding to the onset of instability were found to be $Re_c = 5772.22$ and $\alpha_c = 1.02056$ respectively (Orszag, 1971). The critical values of the parameters $\alpha$ and $Re$ have been computed by numerous authors, however these are the widely accepted values.

In order to obtain the boundaries of stability for the Orr-Sommerfeld eiegenvalue problem, we are required to compute the neutral stability curve for plane Poiseuille flow. The plot of neutral stability is significantly important as it allows us to observe the relationship between the parameters, namely the Reynolds number and wavenumber, and the resulting stability of the flow. Hence, in computing the curve of neutral stability, a boundary is found in the plane of the parameters separating the region of instability from the region of stability. The minimum Reynolds number on the curve corresponds to onset of instability, below which all Reynolds numbers correspond to a flow that is stable.

### 2.2.1 Numerical methods

There have been many variations of numerical methods used to solve the Orr-Sommerfeld eigenvalue problem. Among the first methods used to solve the Orr-Sommerfeld equation, were finite-difference methods and methods of asymptotic analysis. In finite-difference methods the derivatives at a given point are approximated by the points surrounding it. The formulation of numerical schemes using finite-difference methods can be constructed with a prescribed order of convergence to the exact solution. As a result, potentially very complex numerical schemes with higher orders of convergence have the ability to provide a highly accurate solution with fewer nodal points. Conversely, much simpler numerical schemes will require more nodal points to obtain a solution with the same degree of accuracy.

Spectral methods are another set of numerical methods which were applied to the Orr-Sommerfeld eigenvalue problem, after finite-difference methods had already been used. As well as many other areas of applied mathematics, spectral methods have been found to be extremely useful in accurately solving many problems in hydrodynamic stability

theory, including the Orr-Sommerfeld eigenvalue problem. The solution to the differential equation is written as a sum of basis functions, where the coefficients are determined in such a way as to best approximate the true solution. Furthermore, the implementation of the spectral method is normally achieved by the collocation, Galerkin or tau approach. In the tau approach, which is considered the simplest to implement, a series expansion of an orthogonal set of basis functions are used to approximate the solution. The crucial difference between finite-difference methods and spectral methods is that finite-difference methods take a local approach, whereas spectral methods take a global approach in approximating the solution. For this reason, spectral methods have exponential convergence, hence the methods provide attractive and desirable error properties.

In the case of plane Poiseuille flow the values for the wavenumber and Reynolds number corresponding to the onset of instability are used to compare and assess the accuracy of various numerical methods implemented. For example, in the linear theory the widely accepted values corresponding to the onset of instability are $Re = 5772.22$, $\alpha = 1.02056$, which were found by Orszag (1971). Prior to the implementation of spectral methods to solve the Orr-Sommerfeld equation, agreement among these values was sought after for many years. Among the many methods, complex finite-difference schemes as well as orthogonal expansions have been used to obtain approximations to the solution of the Orr-Sommerfeld eigenvalue problem. For example, one particular study carried out by Thomas (1953), the critical Reynolds number was found to be $Re = 5780$ and $\alpha = 1.026$ using finite-difference methods . In this study it was claimed that the Reynolds number was well-determined, however it was stated that $\alpha$ was only determined as far as being in the interval $[1.02, 1.03]$ (Thomas, 1953). This has indeed been confirmed, as more accurate methods have been employed in more recent history. In the implementation of the technique of expansion in a set of orthogonal functions by Grosch and Salwen (1968), the critical values corresponding to the onset of instability were found to be $Re = 5750$, $\alpha = 1.025$. Moreover, the numerical results were found to be in agreement with Thomas (Grosch and Salwen, 1968).

In order to confirm further agreement and validity of numerical results obtained by different methods, the approximation to the least stable eigenvalue for $Re = 10,000$, $\alpha = 1.0$ is also often quoted in the literature. The least stable eigenvalue, again calculated by Orszag (1971), is given by $0.23752649 + 0.00373967i$ to eight decimal places. It is known that the least stable eigenmode is symmetric, which is a fact often used to confine the search for the least stable mode. This was used not only by Orszag but by other authors who wished to more accurately approximate the least stable mode, by disregarding eigenmodes that are known not to correspond to the least stable mode. For example, in a study conducted by Gary and Helgason (1970), using a sixth-order finite-difference scheme with 100 grid points, the approximation to the least stable eigenvalue was found to be $0.23752964 + 0.00374248i$.

In this report the linear stability of plane Poiseuille flow is studied by solving the Orr-Sommerfeld eigenvalue problem using both finite-difference and spectral methods. The accuracy, order of convergence and computational expense of these numerical methods are compared. A linear test problem is considered in order to consolidate the methodology for numerically solving the Orr-Sommerfeld equation, where this test problem demonstrates the utilisation of finite-difference methods for solving a differential equation. A local iterative method is derived from the finite-difference scheme employed in order to gain an approximation of higher accuracy to the features of the solution we are truly concerned with (namely the least stable mode). The spectral-tau method is also implemented where

the solution is then analysed and compared with numerical results in the literature. Both methods are used to calculate the neutral stability curves which illustrate the stable and unstable regions in the plane of the parameters. Finally, an empirical comparison is performed between the numerical results obtained from both methods and the extension to the hybrid flow plane Poiseuille-Couette flow is discussed.

# 3 Derivation of the Orr-Sommerfeld equation

The Orr-Sommerfeld equation is an eigenvalue problem which arises from the Navier-Stokes and continuity equations, that describes linear two-dimensional modal disturbances to parallel flow. In this derivation, the case of pressure driven flow of a viscous fluid between two parallel boundaries (plane Poiseuille flow) is considered. The pressure gradient acting on the fluid between the walls is applied so the pressure decreases in the streamwise direction. The Orr-Sommerfeld equation is derived from the linearised Navier-Stokes equations, which may be non-dimensionalised before. The solution to the governing equations for parallel laminar flow may become linearly unstable to infinitesimal disturbances if certain conditions are satisfied, the Orr-Sommerfeld is the eigenvalue relation that must be solved in order to determine these conditions. We find that a pressure gradient acting on the fluid in the streamwise direction corresponds to the parabolic velocity profile displayed in figure 2. This simple velocity profile is then perturbed to infinitesimal disturbances in the form of normal modes, which are wave-like solutions. The growth or decay of this wave-like perturbation velocity is determined from solving the Orr-Sommerfeld eigenvalue problem, where a wave-like solution that decays in amplitude in the streamwise direction is said to be stable. For particular combinations of the flow parameters, a wave-like solution that increases in amplitude in the streamwise direction is unstable, and one that neither increases nor decreases describes a neutrally stable wave-like solution.

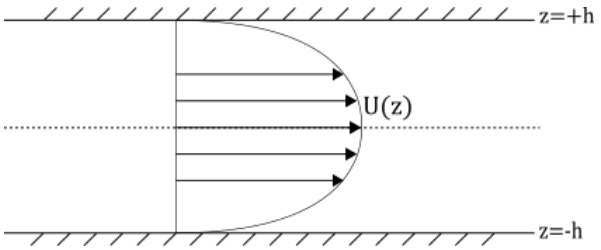


FIGURE. 2 Diagram of the parabolic velocity profile of pressure-driven flow plane Poiseuille flow between two parallel rigid boundaries.

Initially we can consider the three-dimensional Navier-Stokes and continuity equations which govern the motion of the fluid situated between the parallel boundaries.

$$\rho\left(\frac{\partial \mathbf{u}}{\partial t} + (\mathbf{u}\cdot\nabla)\,\mathbf{u}\right) = -\nabla p + \mu\nabla^2\mathbf{u}, \tag{3.1}$$

$$\nabla\cdot\mathbf{u} = 0, \tag{3.2}$$

where $\rho$ is the (constant) density of the fluid and $\mu$ is the kinematic viscosity. For convenience, this set of equations can be non-dimensionalised by introducing a characteristic length scale $h$, velocity scale $U$, pressure scale $\rho U^2$ and time scale $h/U$. Therefore we can define the following non-dimensionalised variables,

$$\mathbf{u}^* = \frac{\mathbf{u}}{U}, \quad \mathbf{x}^* = \frac{\mathbf{x}}{h}, \quad t^* = \frac{th}{U}, \quad p^* = \frac{p}{\rho U^2}, \quad \mathbf{U} = \frac{1}{U}\bar{\mathbf{U}}.$$

We arrive at the non-dimensionalised equations of motion and equation of continuity,

$$\frac{\partial \mathbf{u}^*}{\partial t^*} + (\mathbf{u}^* \cdot \nabla^*)\,\mathbf{u}^* = -\nabla^* p^* + \frac{1}{Re}\nabla^{*2}\mathbf{u}^*, \tag{3.3}$$

$$\nabla \cdot \mathbf{u}^* = 0, \tag{3.4}$$

where $Re = \rho U h/\mu$ is the Reynolds number. In the case of pressure driven flow through a parallel channel (plane Poiseuille flow) the function $U(z)$ must satisfy the following equation derived from the non-dimensionalised equations of motion,

$$\frac{1}{Re}\frac{\mathrm{d}^2 U}{\mathrm{d}z^2} = \frac{\mathrm{d}P}{\mathrm{d}x}, \tag{3.5}$$

Therefore in dimensionless form plane Poiseuille flow is given by,

$$U(z) = 1 - z^2, \quad z \in [-1, 1], \tag{3.6}$$

where,

$$\frac{\mathrm{d}P}{\mathrm{d}x} = \text{const.} \tag{3.7}$$

Now that we have derived the base flow describing plane Poiseuille flow, we perturb $U(z)$ to infinitesimal disturbances which take the form of normal modes. Therefore, perturbing the basic solution to search for wave-like solutions to the governing equations we have the following velocity and pressure fields,

$$\mathbf{u}^*(\mathbf{x}, \mathbf{t}) = \begin{pmatrix} U(z) \\ 0 \\ 0 \end{pmatrix} + \epsilon \begin{pmatrix} \hat{u}(z) \\ \hat{v}(z) \\ \hat{w}(z) \end{pmatrix} e^{i(\alpha x + \beta y - \omega t)}, \tag{3.8}$$

$$p^*(\mathbf{x}, t) = P(x) + \epsilon \hat{p}(z) e^{i(\alpha x + \beta y - \omega t)}), \tag{3.9}$$

where $\alpha$ and $\beta$ are wavenumbers that must be real, whereas the angular frequency $\omega = \omega_r + i\omega_i$ is considered to have both real and complex parts. Hence perturbing the solution in this way gives wave-like solutions to the governing equations that grow or decay as $t \to \infty$ like $e^{\omega_i t}$. As we have non-dimensionalised the equations the rigid boundaries of the flow are situated at $z = \pm 1$, the boundary conditions are $\hat{u} = \hat{v} = \hat{w} = 0$, at $z = \pm 1$. Substituting this solution into the governing equations, we clearly recover plane Poiseuille flow when considering $\mathcal{O}(\epsilon^0)$. Rewriting the complex frequency as $c = \omega/\alpha$ and letting $\mathrm{D} = d/dz$. Now, considering terms that are $\mathcal{O}(\epsilon)$ and neglecting all terms that are $\mathcal{O}(\epsilon^2)$ we obtain the following set of equations,

$$\{\mathrm{D}^2 - (\alpha^2 + \beta^2) + i\alpha Re(U - c)\}\hat{u} = i\alpha Re\hat{p} + Re\hat{w}U', \tag{3.10}$$

$$\{\mathrm{D}^2 - (\alpha^2 + \beta^2) + i\alpha Re(U - c)\}\hat{v} = i\beta Re\hat{p}, \tag{3.11}$$

$$\{\mathrm{D}^2 - (\alpha^2 + \beta^2) + i\alpha Re(U - c)\}\hat{w} = Re\mathrm{D}\hat{p}, \tag{3.12}$$

$$i\alpha\hat{u} + i\beta\hat{v} + \mathrm{D}\hat{w} = 0. \tag{3.13}$$

with the boundary conditions,

$$\hat{u} = \hat{v} = \hat{w} = 0, \quad z = \pm 1. \tag{3.14}$$

The general three-dimensional problem given by equations (3.10)-(3.13) with boundary conditions (3.14) can be reduced to a two-dimensional problem by using Squire's transformation (Squire, 1933). If we introduce the following relations,

$$\tilde{\alpha} = \sqrt{\alpha^2 + \beta^2}, \quad \tilde{\alpha}\tilde{u} = \alpha\hat{u} + \beta\hat{v}, \quad \tfrac{\tilde{p}}{\tilde{\alpha}} = \tfrac{\hat{p}}{\alpha},$$
$$\tilde{w} = \hat{w}, \quad \tilde{c} = c, \quad \tilde{\alpha}\widetilde{Re} = \alpha Re.$$

Then if we combine equation $\alpha\times$(3.10) and equation $\beta\times$(3.11) we obtain,

$$\{\mathrm{D}^2 - \tilde{\alpha}^2 + i\tilde{\alpha}\widetilde{Re}(U - \tilde{c})\}(\alpha\hat{u} + \beta\hat{v}) = i(\alpha^2 + \beta^2)\widetilde{Re}\tilde{p} + \tilde{\alpha}\widetilde{Re}\tilde{w}, \tag{3.15}$$

Thus we obtain the two-dimensional problem,

$$\{\mathrm{D}^2 - \tilde{\alpha}^2 - i\tilde{\alpha}\widetilde{Re}(U - c)\}\tilde{u} = i\tilde{\alpha}\widetilde{Re}\tilde{p} + \widetilde{Re}\tilde{w}U', \tag{3.16}$$
$$\{\mathrm{D}^2 - \tilde{\alpha}^2 - i\tilde{\alpha}\widetilde{Re}(U - c)\}\tilde{w} = \widetilde{Re}\mathrm{D}\tilde{p}, \tag{3.17}$$
$$i\alpha\tilde{u} + D\tilde{w} = 0. \tag{3.18}$$

The two-dimensional problem derived here is equivalent to the three-dimensional problem but with $\beta = \hat{v} = 0$. As $\tilde{\alpha} \geq \alpha$ and therefore $\widetilde{Re} \leq Re$, we have arrived at Squire's theorem which states in order to obtain the critical Reynolds number we need only consider two-dimensional disturbances. That is, if the flow is unstable three-dimensional infinitesimal disturbances for a particular Reynolds number, there exists a smaller Reynolds number where the flow is unstable to two-dimensional disturbances. As it is sufficient to consider the two-dimensional problem to compute the onset of instability as $Re$ is increased, we may restrict the problem so that only the components in $x$ and $z$ directions are considered. Now, we can combine (3.16) and (3.17) by differentiating (3.16) with respect to $z$ and multiplying (3.17) by $i\tilde{\alpha}$. Relabelling the Reynolds number and wavenumber corresponding to the two-dimensional problem as $Re$ and $\alpha$ respectively, as we will only consider the instability of the flow to two-dimensional disturbances from now on. Upon differentiating (3.16) with respect to $z$ one can make use of the continuity equation to demonstrate terms in (3.16) sum to zero. Rearranging to $i\alpha Re\mathrm{D}\hat{p}$, the two-dimensional problem becomes,

$$i\alpha Re\mathrm{D}\hat{p} = (\mathrm{D}^3 - \alpha^2\mathrm{D})\hat{u} - i\alpha Re(U - c)\mathrm{D}\hat{u} - ReU''\hat{w}, \tag{3.19}$$
$$i\alpha Re\mathrm{D}\hat{p} = i\alpha(\mathrm{D}^2 - \alpha^2)\hat{w} + \alpha^2 Re(U - c)\hat{w}. \tag{3.20}$$

Now that we have a two-dimensional problem, we can simply combine these two equations and express this problem in terms of a streamfunction $\psi = \psi(x, z, t)$ or its amplitude $\phi(z)$. Let,

$$\psi(x, z, t) = \phi(z)e^{i(\alpha x - \omega t)}, \tag{3.21}$$
$$\hat{u} = \psi_z, \tag{3.22}$$
$$\hat{w} = -\psi_x. \tag{3.23}$$

Substituting this stream function into our equation, we arrive at a fourth-order ordinary differential equation in the eigenfunction $\phi$. The result is the Orr-Sommerfeld equation,

$$(U - c)\left(\mathrm{D}^2 - \alpha^2\right)\phi - U''\phi + \frac{i}{\alpha Re}\left(\mathrm{D}^2 - \alpha^2\right)^2\phi = 0, \tag{3.24}$$

with boundary conditions

$$\phi = 0, \quad \phi' = 0, \quad \text{at} \quad z = \pm 1. \tag{3.25}$$

The famous Orr-Sommerfeld eigenvalue problem is given by (3.24) and (3.25). This significant equation with the accompanying boundary conditions forms the basis for hydrodynamic stability theory. Since the derivation of this equation, obtained independently in the early twentieth century by Orr (1907a,b) and Sommerfeld (1908), the study of solutions to this eigenvalue relation have been extensive. Numerous methods have been employed to solve this equation from asymptotic methods to numerical methods such as finite-difference schemes and spectral methods. In solving the Orr-Sommerfeld eigenvalue problem for a given Reynolds number $Re$ and wavenumber $\alpha$, we are solving for eigenvalues and eigenfunctions given by $c$ and $\phi$ respectively, where if $\mathbb{I}m(c) > 0$ for any eigenvalue $c$ one would conclude that plane Poiseuille flow is unstable to infinitesimal disturbances. Conversely if $\mathbb{I}m(c) < 0$ for all the eigenvalues we would conclude the flow is stable and neutrally stable if $\mathbb{I}m(c) = 0$. One of the most significant developments in solving this equation was achieved by Orszag (1971), where spectral methods were applied and were proven to be able to obtain solution of very high accuracy. It was found that plane Poiseuille flow was linearly unstable to infinitesimal disturbances above a critical Reynolds number of $Re = 5772.22$ with $\alpha = 1.02056$ as the level of disturbance (Orszag, 1971). In this report, a finite-difference scheme and an implementation of spectral methods will be used to solve the Orr-Sommerfeld eigenvalue equation, where the stability of the flow will be analysed for given values of the parameters $Re$ and $\alpha$.

# 4 A test problem - linear one-dimensional eigenvalue problem

In order to consolidate and clarify the methodology in solving such a system numerically, we begin first by constructing the numerical solution to a problem which has a known analytical solution. To do this we consider a simple linear harmonic one-dimensional problem. This problem is solved numerically using finite-difference methods, where these methods and formulation of the generalized eigenvalue problem will be analogous to section 5 where these methods will then be applied to the Orr-Sommerfeld eigenvalue equation.

In the construction of numerical schemes it is important to consider the accuracy and complexity of them, for instance a high-accuracy scheme will typically require more nodal points to approximate a derivative at one nodal point, this may become particularly complicated near the boundary where the numerical scheme may have to change as there will be an unequal number of points to left and right of near-boundary nodes. Therefore a compromise between complexity and accuracy can be made so that instead of using a complex numerical scheme of high order accuracy, one can make use of a less accurate scheme and increase the number of nodal points on the domain the equation is to be solved on. This means we are not required to use a specialised stencil at near boundary nodes.

In the analysis of our numerical solution obtained from using finite-difference methods, we can analyse the order of convergence, as well the error of the numerical solution compared with the exact solution. As the order of convergence can be predetermined in the construction of the finite-difference schemes used to solve an equation, conducting analysis on the numerical solution allows us to ensure the numerical method employed has worked as expected. For example, if we use a second-order scheme to solve an equation, increasing the number of nodal points by a factor of two, we can expect a logarithmic plot of the error results in a linear relationship where the gradient of the straight line is approximately two. The analysis conducted on the order of convergence will be analogous to section 5, where methods tested here will be applied to the Orr-Sommerfeld eigenvalue problem, furthermore in the following construction we will attempt to ensure second-order convergence of our numerical scheme. Now considering the following eigenvalue problem, with $\lambda$ unknown,

$$f'' + \lambda f = 0, \tag{4.1}$$

with the following boundary conditions,

$$f(0) = f(1) = 0. \tag{4.2}$$

We wish to approximate the function $f(z)$ over the interval $[0, 1]$ on a finite number of grid points.

$$\{z_j \in [0, 1] \quad | \quad j = 0, 1, ..., N-1\}, \tag{4.3}$$

We would like to find $\{f_j| \quad j = 0, 1, ...N-1\}$ such that,

$$f_j \approx f(z_j). \tag{4.4}$$

If we uniformly space the points over the interval $[0, 1]$ then the $N$ points are given by,

$$z_j = jh, \quad j = 0, 1, ..., N-1, \tag{4.5}$$

where $h = \frac{1}{N-1}$ is the grid spacing between adjacent points. Now we begin discretizing the problem by expressing terms in (4.1) in terms of a finite-difference scheme. We will make use of the following second-order central-difference scheme to approximate the second-order derivative,

$$f''(z_j) \approx \frac{f_{j+1} - 2f_j + f_{j-1}}{h^2}, \quad \text{for} \quad j = 1, 2, ...N-2. \tag{4.6}$$

Then, simply expressing $\lambda f = f_j$, the whole linear one-dimensional harmonic equation can be discretized to give the following,

$$\frac{f_{j+1} - 2f_j + f_{j-1}}{h^2} + \lambda f_j = 0, \quad \text{for} \quad j = 1, 2, \ldots, N-2, \tag{4.7}$$

with boundary conditions,

$$f_0 = 0, \quad f_{N-1} = 0. \tag{4.8}$$

Now, the system of equations given by (4.7)-(4.8) is formulated as a generalized eigenvalue problem, where the unknowns $f_0, f_1, ..., f_{N-1}, \lambda$ are solved for by implementing the eigenvalue problem in MATLAB. The resulting numerical solution consists of $N$ eigenvectors corresponding to the unknowns $f_0, f_1, ..., f_{N-1}$ and $N$ eigenvalues, which are approximately squared multiples of $\pi^2$. The generalized eigenvalue problem takes the form,

$$\mathrm{A}\mathbf{x} = \lambda \mathrm{B}\mathbf{x}. \tag{4.9}$$

The matrix $A$ is tridiagonal with entries determined from the numerical scheme for the second derivative and the matrix $B$ simply has entries only on the main diagonal. The first and last row correspond to the boundary conditions imposed. The system takes the form,

$$\begin{pmatrix} 1 & 0 & \cdots & \cdots & \cdots & 0 \\ \frac{1}{h^2} & \frac{-2}{h^2} & \frac{1}{h^2} & \cdots & \cdots & \vdots \\ 0 & \ddots & \ddots & \ddots & \cdots & \vdots \\ \vdots & \cdots & \ddots & \ddots & \ddots & 0 \\ \vdots & \cdots & \cdots & \frac{1}{h^2} & \frac{-2}{h^2} & \frac{1}{h^2} \\ 0 & \cdots & \cdots & \cdots & 0 & 1 \end{pmatrix} \begin{pmatrix} f_0 \\ f_1 \\ f_2 \\ \vdots \\ \vdots \\ f_{N-1} \end{pmatrix} = \lambda \begin{pmatrix} 0 & 0 & \cdots & \cdots & \cdots & 0 \\ 0 & -1 & \ddots & \cdots & \cdots & \vdots \\ \vdots & \ddots & \ddots & \ddots & \cdots & \vdots \\ \vdots & \cdots & \ddots & \ddots & \ddots & \vdots \\ \vdots & \cdots & \cdots & \ddots & -1 & 0 \\ 0 & \cdots & \cdots & \cdots & 0 & 0 \end{pmatrix} \begin{pmatrix} f_0 \\ f_1 \\ f_2 \\ \vdots \\ \vdots \\ f_{N-1} \end{pmatrix}. \tag{4.10}$$

The simple structure of the matrices in this problem will allow the problem to be solved relatively quickly as the matrices will increase in sparsity as the number of nodal points is increased.

## 4.1 Numerical results

By considering the analytical solution to the equation we can conduct an error analysis of the numerical solution to check the results obtained. The analytical solution to this linear one-dimensional problem is,

$$f_n(z) = B_n \sin(n\pi z), \quad \text{for} \quad n \in \mathbb{Z}, \tag{4.11}$$

where,

$$\lambda_n = n^2\pi^2, \quad \text{for} \quad n \in \mathbb{Z}. \tag{4.12}$$

Firstly, let us consider the numerical results obtained from solving the generalized eigenvalue problem on varying numbers of nodal points. Tabulated in table 1 are the approximations to the first five eigenvalues with the number of grid points they were found on. The approximate eigenvalues obtained in the numerical solution of the problem are denoted with a hat. As the number of nodal points used increases the approximate eigenvalues are expected to converge to the known true eigenvalues, which are squared multiples of $\pi^2$. Furthermore, we expect the approximate eigenvalues to converge to their respective true eigenvalues with second-order convergence.

| $N$ | $\hat{\lambda}_1$ | $\hat{\lambda}_2$ | $\hat{\lambda}_3$ | $\hat{\lambda}_4$ | $\hat{\lambda}_5$ |
|---|---|---|---|---|---|
| 8 | 9.7051 | 36.8980 | 76.1929 | 119.8071 | 159.1020 |
| 16 | 9.8336 | 38.9045 | 85.9424 | 148.8912 | 225.0000 |
| 32 | 9.8612 | 39.3435 | 88.1443 | 155.7631 | 241.5058 |
| 64 | 9.8676 | 39.4457 | 88.6609 | 157.3908 | 245.4645 |
| 128 | 9.8691 | 39.4704 | 88.7857 | 157.7849 | 246.4257 |
| 256 | 9.8695 | 39.4764 | 88.8163 | 157.8817 | 246.6621 |
| 512 | 9.8696 | 39.9057 | 88.8239 | 157.9057 | 246.7207 |
| 1024 | 9.8696 | 39.4783 | 88.8258 | 157.9117 | 246.7353 |

TABLE. 1 First five eigenvalues of the one-dimensional eigenvalue problem to (4.d.p) with increasing number of grid points $N$.

Considering numerical results in table 1, the approximations to the eigenvalues do indeed converge to their respective true eigenvalues $j^2\pi^2$ where the $j$-th approximation is given by $\lambda_j$. In the analysis of these results we should expect that more nodal points are required to obtain an accurate approximation to higher eigenvalues. This is demonstrated in the results in table 1. For example, if we consider $\hat{\lambda}_1$, we see that the approximation has converged up to an accuracy of four decimal places, for $N \geq 512$. Whereas, if we consider now $\hat{\lambda}_5$, we see that it has converged only to one decimal place for $N \geq 512$. Therefore we see that more nodal points are indeed required to obtain an accurate approximation to higher eigenvalues. In the error analysis of these results, we will see that the absolute error of the approximation of the first eigenvalue is far less than that of the fifth eigenvalue.

The eigenfunctions corresponding to the first harmonic and fifth harmonic are shown in figures 3a and 3b respectively, which have been obtained using $N = 512$ grid points. In figure 3b, we observe that the eigenfunction corresponding to the fifth harmonic is indeed much more oscillatory in comparison to the first harmonic in figure 3a. Therefore more nodal points are required to capture the detail of the eigenfunction. For the eigenfunctions corresponding to even higher harmonics there are more oscillations, hence a higher number of grid points over the interval are required to accurately describe the eigenfunctions.

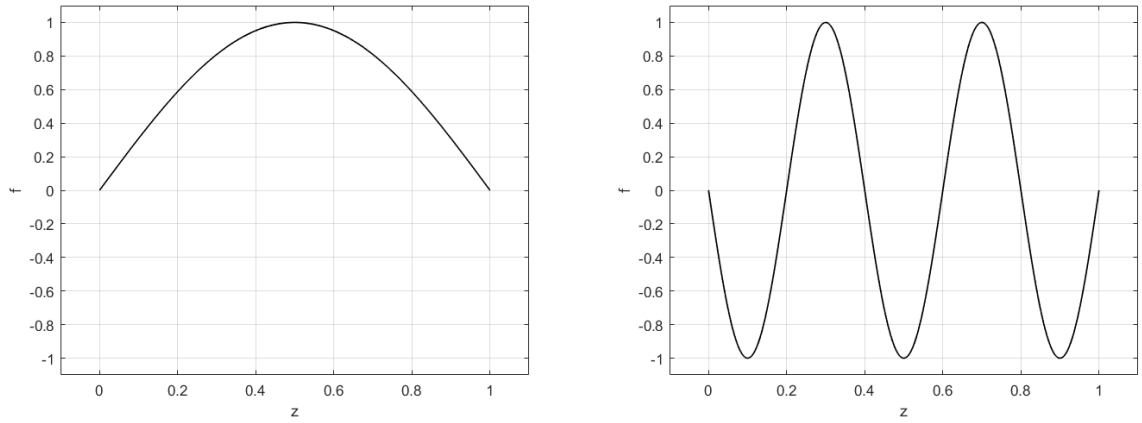


(a) (b)

FIGURE. 3 Eigenfunctions corresponding to (a) $\hat{\lambda}_1 = 9.8696$ and (b) $\hat{\lambda}_5 = 246.7207$ obtained with $N = 512$.

We see from figure 3a that the first harmonic is a much simpler curve, therefore only very few nodal points are required to obtain an accurate approximation to the true eigenvalue $\lambda_1$ and the eigenfunction. This is can be observed from table 1, where the difference in the approximation to the first eigenvalue for $N = 8$ and $N = 512$ is $\mathcal{O}(10^{-1})$. Whereas the same difference in the approximation to the fifth eigenvalue is $\mathcal{O}(10)$.

### 4.1.1 Error analysis of the eigenvalues

In considering the error of the numerical solution we consider the absolute error of the eigenvalues with respect to their analytic true values. The true eigenvalues of the problem are known to be $\lambda_j = j^2\pi^2, j \in \mathbb{Z}$, the error when compared with the true value of each eigenvalue found numerically is,

$$e_j = |\hat{\lambda}_j - j^2\pi^2|, \quad j \in \mathbb{Z}. \tag{4.13}$$

| $N$ | $e_1$ | $e_2$ | $e_3$ | $e_4$ | $e_5$ |
|---|---|---|---|---|---|
| 8 | 0.1646 | 2.5804 | 12.6335 | 38.1066 | 87.6381 |
| 16 | 0.0360 | 0.5739 | 2.8841 | 9.0224 | 21.7401 |
| 32 | 0.0084 | 0.1350 | 0.6821 | 2.1506 | 5.2343 |
| 64 | 0.0020 | 0.0327 | 0.1655 | 0.5229 | 1.2756 |
| 128 | 0.0005 | 0.0081 | 0.0408 | 0.1288 | 0.3144 |
| 256 | 0.0001 | 0.0020 | 0.0101 | 0.0320 | 0.0780 |
| 512 | 0.0000 | 0.0005 | 0.0025 | 0.0080 | 0.0194 |
| 1024 | 0.0000 | 0.0001 | 0.0006 | 0.0020 | 0.0048 |

TABLE. 2 Absolute error of the first five eigenvalues with varying number of nodal points $N$.

In table 2, the absolute error of the first five eigenvalues is shown. As expected the error in the approximation of the first eigenvalue is much smaller than the error in the fifth

eigenvalue and the order of the errors are $\mathcal{O}(10^{-1})$ and $\mathcal{O}(10)$ respectively. Furthermore, if we consider the factor of decrement for a given approximate eigenvalue, we see that the factor is approximately 4. For example, considering the column of errors $e_5$ corresponding to the fifth eigenvalue, we see that the factor of decrement between the final two rows is given by $\frac{0.0194}{0.0048} = 4.042$. Therefore in doubling the number of grid points, the magnitude of the error decreases by a factor of four, indicating the numerical scheme is working as intended with second-order convergence. Hence error of the numerical solution is useful not only in calculating the accuracy of the solution but also in confirming the order of convergence. The errors in table 2 are used in the next subsection in confirming that the numerical scheme employed in this example is indeed of second-order.

### 4.1.2 Convergence of the numerical scheme

In order to confirm the order of convergence of the numerical scheme, the error in the approximation to the eigenvalue for varying numbers of grid points is considered. The numerical scheme used in this example is of second-order, hence in a logarithmic plot of the error we should expect a linear relationship between the error and step-size $h$. Moreover as the numerical scheme has been constructed so that there is second-order convergence, the gradient of the linear plot should be approximately 2.

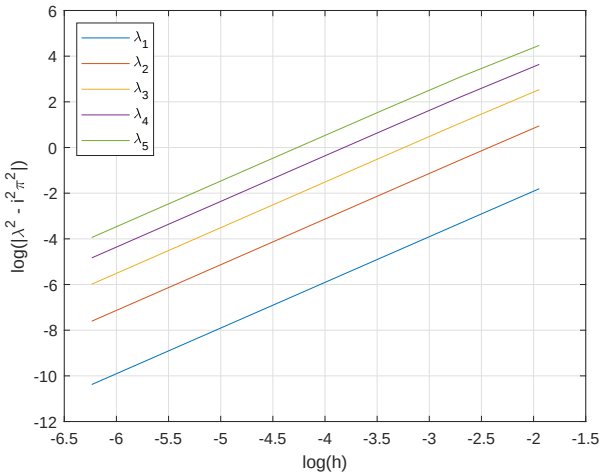


FIGURE. 4 Logarithmic plot of the absolute error of the first five eigenvalues with varying step-size $h$.

In figure 4, a logarithmic plot of the error of the approximations to the first five eigenvalues is shown for varying step-sizes $h$. We observe that there is indeed a linear relationship between the error and the step-size $h$. Moreover, the line corresponding to the first eigenvalue is located lower down the plane as the error in the first eigenvalue is smallest. Similarly the line corresponding to the fifth eigenvalue is located at the top of these five lines. Using a second-order finite-difference scheme we should expect to see quadratic convergence when computing the solution to this generalized eigenvalue problem on successively finer grids (as $h \to 0$). The gradients of each of the lines in figure 4 are shown in table 3.

| Eigenvalue | Gradient of line |
|---|---|
| $\lambda_1$ | 1.9984 |
| $\lambda_2$ | 1.9937 |
| $\lambda_3$ | 1.9860 |
| $\lambda_4$ | 1.9751 |
| $\lambda_5$ | 1.9611 |

TABLE. 3 Gradients of lines in figure corresponding to the first five eigenvalues.

From table 3 we can confirm that the order of convergence of the numerical scheme implemented to solve the one-dimensional eigenvalue problem is of second-order. The gradient of the line corresponding to the first eigenvalue is, as expected, the closest to a value of 2. This method confirming the order of convergence of the numerical scheme is only possible as we are simply comparing the numerical solution with the analytic solution. If there were no analytic formula for the eigenvalues then one would not be able to compute the absolute error in this way.

# 5 The Orr-Sommerfeld eigenvalue problem

Now we consider the Orr-Sommerfeld equation derived previously as a generalized eigenvalue problem and formulate the problem in a similar manner to the one-dimensional harmonic test problem. The Orr-Sommerfeld equation is a fourth-order equation therefore discretizing such an equation will require a fourth-order finite-difference scheme. As we can write any fourth-order problem as two second-order problems we can define a function $\psi(z)$ such that it is sufficient to consider at most a second-order finite difference scheme. This now simplifies the problem however there are now two unknowns to be determined for each nodal point across the flow. We write $\psi(z)$ as,

$$\psi(z) = (\mathrm{D}^2 - \alpha^2)\phi(z). \tag{5.1}$$

Therefore rewriting the Orr-Sommerfeld equation as,

$$(U - c)\psi - \phi U'' + \frac{i}{\alpha Re}(\mathrm{D}^2 - \alpha^2)^2\phi = 0, \tag{5.2}$$

with boundary conditions,

$$\phi = 0, \quad \phi' = 0 \quad \text{at} \quad z = \pm 1. \tag{5.3}$$

The parameters of the above equation are $Re$, $\alpha$ and $c$, where $\alpha$ and $Re$ are considered to be real and $c$ is the complex eigenvalue. To investigate temporal stability, we can therefore vary the quantities $Re$ and $\alpha$ and then solve the following generalized eigenvalue problem for a discrete set of eigenvalues $c_j$,

$$U\psi - \phi U'' + \frac{i}{\alpha Re}(\mathrm{D}^2 - \alpha^2)^2\psi = c\psi. \tag{5.4}$$

In the case of plane Poiseuille flow $U(z) = 1 - z^2$ represents a laminar parabolic flow profile across the channel.

## 5.1 Formulating the discretized equations

The boundary conditions imposed at the channel walls are,

$$\phi = 0, \quad \phi' = 0 \quad \text{at} \quad z = \pm 1, \tag{5.5}$$

The first condition corresponds to the no-penetration condition ($\hat{w} = 0$ and $\phi = 0$) and the second condition corresponds to the no-slip condition ($\hat{u} = 0$ implies $\phi' = 0$). When discretizing the first equation we find that $\phi_0 = 0$ and $\phi_{N-1} = 0$, however a second-order one-sided finite-difference scheme is required to discretize the boundary condition $\phi' = 0$ in order to ensure quadratic convergence of the discretized scheme. To construct the one-sided finite-difference scheme at the boundary at $z = 1$ we begin by considering the two closest points to the boundary, and using the Taylor series expansion of $\phi$,

$$\phi'(z) = a\phi(z) + b\phi(z + h) + c\phi(z + 2h), \tag{5.6}$$

where $h$ represents the step-size and $a, b$ and $c$ are constants to be found. Now, using Taylor series, we obtain

$$\phi' = a\phi + b\left(\phi + h\phi' + \frac{h^2}{2}\phi''\right) + c\left(\phi + 2h\phi' + 2h^2\phi''\right) + (b + c)\mathcal{O}(h^3), \tag{5.7}$$

$$\phi'(z) = (a + b + c)\phi + h(b + 2c)\phi' + h^2\left(\frac{b}{2} + 2c\right)\phi'' + (b + c)\mathcal{O}(h^3). \tag{5.8}$$

In order to have second-order convergence to be consistent with our discretized system, we set the coefficients of $\phi$ and $\phi''$ to zero and the coefficient of $\phi'$ equal to 1. The result is the following system of equations,

$$\begin{aligned} a + b + c &= 0, \\ b + 2c &= \frac{1}{h}, \\ \frac{b}{2} + 2c &= 0. \end{aligned}$$

Solving this system of equations by rearranging the second equation for $b$ and then substituting into the third equation, we obtain,

$$a = \frac{-3}{2h}, \quad b = \frac{2}{h}, \quad c = \frac{-1}{2h}.$$

The discretized boundary condition at the lower boundary $\phi'(-1) = 0$ is therefore given by,

$$\frac{1}{2h}\left(-3\phi_0 + 4\phi_1 - \phi_2\right) = 0.$$

By a similar argument the discretized boundary condition at the upper boundary $\phi'(1) = 0$ is given by,

$$\frac{1}{2h}\left(3\phi_{N-1} - 4\phi_{N-2} + \phi_{N-3}\right) = 0.$$

Thus including the one-sided second-order finite difference scheme at the walls and the no-slip condition the discretized boundary conditions are,

$$\phi_0 = 0, \tag{5.9}$$
$$\phi_{N-1} = 0, \tag{5.10}$$
$$-3\phi_0 + 4\phi_1 - \phi_2 = 0, \tag{5.11}$$
$$3\phi_{N-1} - 4\phi_{N-2} + \phi_{N-3} = 0. \tag{5.12}$$

There are two unknowns in $\phi_j$ and $\psi_j$ at each nodal point so we have two equations that need to be solved, these are Orr-Sommerfeld Equation written in terms of $\psi$ and $\phi$, and the equation for $\psi$.

$$U\psi - \phi U'' + \frac{i}{\alpha Re}\left(\mathrm{D}^2 - \alpha^2\right)\psi = c\psi, \tag{5.13}$$
$$\psi = \left(\mathrm{D}^2 - \alpha^2\right)\phi. \tag{5.14}$$

Discretizing the Orr-Sommerfeld equation with $\psi(z) = (\mathrm{D}^2 - \alpha^2)\phi(z)$ we can use the same second-order finite-difference scheme to approximate $\mathrm{D}^2\psi$ in the Orr-Sommerfeld Equation. Furthermore we can write,

$$\begin{aligned} \phi(z_j) &\approx \phi_j, \quad j = 0, 1, ..., N-1, \\ U(z_j) &= 1 - z_j^2, \quad z_j \in [-1, 1]. \end{aligned}$$

Noting that $U'' = -2$ the equations to be solved at each nodal point are,

$$\left(U_j - \left(\frac{2}{h^2} + \alpha^2\right)\frac{i}{\alpha Re}\right)\psi_j + 2\phi_j + \frac{i}{\alpha Re}\left(\frac{\psi_{j+1} + \psi_{j-1}}{h^2}\right) = c\psi_j, \tag{5.15}$$

$$\psi_j - \frac{\phi_{j+1} - 2\phi_j + \phi_{j-1}}{h^2} + \alpha^2\phi_j = 0. \tag{5.16}$$

The unknowns $\phi_j$ and $\psi_j$ at each nodal point from the vector of unknowns corresponding to the eigenvector in the generalized eigenvalue problem of the following form,

$$A\mathbf{\Psi} = cB\mathbf{\Psi}, \tag{5.17}$$

where the eigenvector $\mathbf{\Psi} = (\psi_0, \phi_0, \psi_1, \phi_1, ..., \psi_{N-1}, \phi_{N-1})^T$. The generalized eigenvalue problem therefore takes the following form,

$$\begin{pmatrix} 0 & \frac{-3}{2h} & 0 & \frac{4}{2h} & 0 & \frac{-1}{2h} & \cdots & 0 \\ 0 & 1 & 0 & \cdots & \cdots & \cdots & \cdots & 0 \\ \frac{i}{\alpha Re h^2} & \alpha_1 & 2 & \frac{i}{\alpha Re h^2} & 0 & \cdots & \cdots & 0 \\ 0 & \frac{-1}{h^2} & 1 & \frac{2}{h^2} & 0 & \frac{-1}{h^2} & \cdots & 0 \\ \vdots & \ddots & \ddots & \ddots & \ddots & \ddots & \cdots & \vdots \\ \vdots & \cdots & \ddots & \ddots & \ddots & \ddots & \ddots & \vdots \\ \vdots & \cdots & \cdots & \frac{1}{2h} & 0 & \frac{-4}{2h} & 0 & \frac{3}{2h} \\ 0 & \cdots & \cdots & \cdots & \cdots & \cdots & 0 & 1 \end{pmatrix} \begin{pmatrix} \psi_0 \\ \phi_0 \\ \psi_1 \\ \phi_1 \\ \vdots \\ \vdots \\ \psi_{N-1} \\ \phi_{N-1} \end{pmatrix} = c \begin{pmatrix} 1 & 0 & \cdots & \cdots & \cdots & 0 \\ 0 & 0 & 0 & \cdots & \cdots & \vdots \\ 0 & 0 & 1 & 0 & \cdots & \vdots \\ \vdots & \cdots & \ddots & \ddots & \ddots & \vdots \\ \vdots & \cdots & \cdots & \ddots & 1 & 0 \\ 0 & \cdots & \cdots & \cdots & 0 & 0 \end{pmatrix} \begin{pmatrix} \psi_0 \\ \phi_0 \\ \psi_1 \\ \phi_1 \\ \vdots \\ \psi_{N-1} \\ \phi_{N-1} \end{pmatrix}, \tag{5.18}$$

where $\alpha_j = U_j - \left(\frac{2}{h^2} + \alpha^2\right)\frac{i}{\alpha Re}$.

## 5.2 Numerical results

The parameters of the generalized eigenvalue problem $\alpha$ and $Re$ are real quantities which can be varied to give eigenvalues which have real and complex parts $c = c_r + ic_i$. A mode is unstable if it grows exponentially in time, that is $c_i > 0$, and neutrally stable if $c_i = 0$. The onset of instability corresponds to when $c_i$ first becomes non-negative for a given wave number $\alpha$ and Reynold's number $Re$, hence in this case the onset of instability corresponds to the first eigenvalue that has complex part $c_i = 0$. For the case of plane Poiseuille flow the theoretical critical Reynolds number is given by $Re_c = 5772.22$ with wavenumber $\alpha_c = 1.02056$ (Orszag, 1971). As the first neutrally stable mode is said to appear with these particular $Re$ and $\alpha$, in computing the eigenvalues we expect to see the presence of an eigenvalue $\mathbb{I}m(c) \approx 0$ corresponding to the first neutrally stable mode. Below are the eigenvalues corresponding to the most unstable mode, along with the number of grid points used to find them and the corresponding run time in seconds.

| $N$ | $c$ | Factor of decrement of $\mathbb{I}m\,(c)$ | Run time |
|---|---|---|---|
| 32 | $0.22161247 - 0.09269740i$ | 0.1246 | 0.017 |
| 64 | $0.27508173 - 0.01191992i$ | 7.7767 | 0.030 |
| 128 | $0.26716897 - 0.00385179i$ | 3.0946 | 0.191 |
| 256 | $0.26483885 - 0.00112813i$ | 3.4143 | 1.459 |
| 512 | $0.26421471 - 0.00030822i$ | 3.6601 | 14.108 |
| 1024 | $0.26405519 - 0.00008075i$ | 3.8170 | 145.233 |
| 2048 | $0.26401511 - 0.00002067i$ | 3.9066 | 1498.054 |

TABLE. 4 Eigenvalue corresponding to the least stable mode found by solving the generalized eigenvalue problem on $N$ grid points with $(Re, \alpha) = (5772.22, 1.02056)$, with associated run time in seconds.

From table 4 we can see that the complex part of the most unstable mode associated for $(Re, \alpha) = (5772.22, 1.02056)$ converges to zero quadratically. This can be observed from the third column of table 4 which demonstrates that doubling the number of grid points $N$ reduces the complex part by roughly a factor of four. From the analysis of the second-order finite-difference scheme in the case of the one-dimensional test problem, this demonstrates the second-order convergence of the finite-difference scheme used in solving the Orr-Sommerfeld eigenvalue problem. Initially for small $N$ the factor of decrement of $\mathrm{Im}(c)$ fluctuates by a large amount, however we cannot expect the scheme to be very accurate as the number of grid points over the domain is relatively small. After $N = 128$ however, we begin to observe the quadratic convergence of the scheme, because the factor of decrement appears to converge to a factor of four. Unlike the linear one-dimensional harmonic eigenvalue problem we do not have an analytical solution and therefore we cannot calculate the error of each eigenvalue. The time taken to obtain the approximation to the least stable eigenvalue for a given $N$ appears to increase by approximately a factor of ten when the number of nodal points $N$ is doubled.

In solving the generalized eigenvalue problem on $N$ nodal points in the formulation derived above, there are two unknowns at each nodal point. An important consequence of this is that for $N$ nodal points the matrices in the generalized eigenvalue system have dimensions of $2N \times 2N$. Hence the computational expense of calculating all eigenvalues and eigenvectors for potentially a very large system of discretized equations is very high. This is observed in table 4, as the increase in run time for solving the generalized eigenvalue problem on $N$ nodal points becomes very large once $N \geq 512$. Moreover, after solving the generalized eigenvalue problem, in order to determine the stability of the flow for given parameters $(Re, \alpha)$, we are required to sort through the eigenvalues to obtain the eigenvalue corresponding to the least stable mode. Therefore a drawback of solving the generalized eigenvalue problem is that we are required to solve the whole system and calculate potentially thousands of eigenvalues and eigenvectors, when we are truly only concerned with one eigenvalue when determining stability.

The physical interpretation of the eigenvalue $c$ is seen more clearly seen when decomposed into its real and imaginary parts in the perturbation wave. The real part of $c$, given by $\mathbb{R}e\,(c) = c_r$ is interpreted as the phase speed of the perturbation wave, as a proportion of the maximum velocity in the channel, where as the imaginary part of $\mathbb{I}m\,(c) = c_i$ is interpreted as the growth rate of the mode. Naturally the value of the growth rate is very significant as it determines whether or not a mode grows, decays or remains the same

with time, in turn classifying the stability of mode. If we consider the real part of the eigenvalues $c$ in table 4, we see that the wave speed of the least stable mode converges to a value of $c_r = 0.26402$ to 5 decimal places. Therefore that the perturbation wave propagates along the channel at a speed $0.26402\times$ the velocity taken at the centreline of the channel.

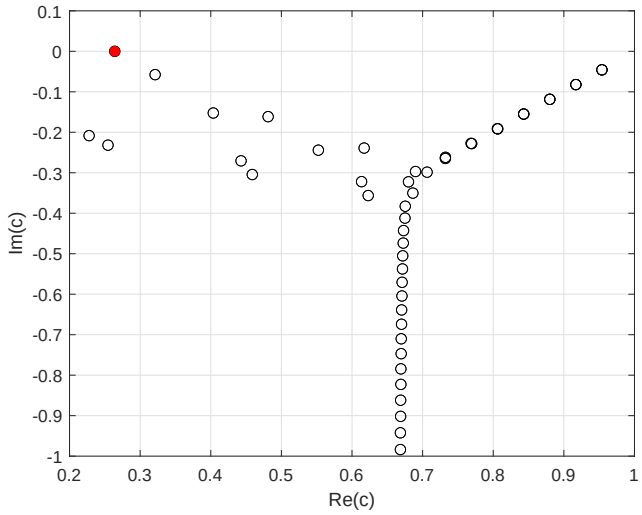


FIGURE. 5 Eigenvalue spectrum for $\mathbb{I}m\,(c_j) > -1$, obtained from solving the generalized eigenvalue problem for $Re = 5772.22$, $\alpha = 1.02056$. The eigenvalue coloured red signifies the least stable eigenvalue.

The spectrum of the eigenvalues $c_j$ for which $\mathbb{I}m\,(c_j) > -1$ in the complex plane is shown in figure 5. We observe that the eigenvalue spectrum has a clear structure which forms three distinct groups in three branches in the complex plane. Two of these groups have very regular structure and form almost straight lines. The group that includes the eigenvalue corresponding to the least stable mode has a much more scattered spread out structure in comparison to the regular structure of the other two groups. We note that although the eigenvalue corresponding to the least stable mode is found in the upper left region of the plot in figure 5, the eigenvalues forming the branch in the upper right region of the plot also have a small imaginary part. The eigenvalues in this region correspond to slowly decaying modes, as they are still stable.

In solving the generalized eigenvalue problem on $N = 2048$ we obtain the set of eigenvalues $\{c_0, c_1, ..., c_{4095}\}$, with the set of eigenvectors $\{\mathbf{\Psi_0}, \mathbf{\Psi_1}, ..., \mathbf{\Psi_{4095}}\}$, where the $j$th eigenvector is given by $\mathbf{\Psi}_j = \left(\psi_0^j, \phi_0^j, \psi_1^j, \phi_1^j, ..., \psi_{2047}^j, \phi_{2047}^j\right)^T$. An approximation to the eigenfunctions $\phi_j$ associated with the eigenvalues $c_j$ is therefore given by the vector $\phi_j = \left(\phi_0^j, \phi_1^j, ..., \phi_{2047}^j\right)^T$. Below in figure 6 are plots of three different eigenfunctions. Figure 6a is a plot of the eigenfunction corresponding to the least stable mode with both real and imaginary parts over $z \in [-1, 1]$ where the corresponding eigenvalue is $c_4 = 0.26402 - 0.00002i$. The eigenfunction associated with the least stable eigenvalue shown in figure 6a is symmetric about the line $z = 0$, whereas the eigenfunctions in figures 6b and 6c are anti-symmetric about the line $z = 0$. Furthermore, this eigenfunction describes a symmetric mode, as the eigenfunction itself is symmetric on the domain $z \in [-1, 1]$. In figure 6a, we note that to obtain a reasonably accurate approximation to this rather simple curve, we require 2048 nodal points across the channel. Furthermore,

we observe that near the boundary the real part of the eigenfunction appears to meet the boundaries almost perpendicular to $z = \pm 1$.

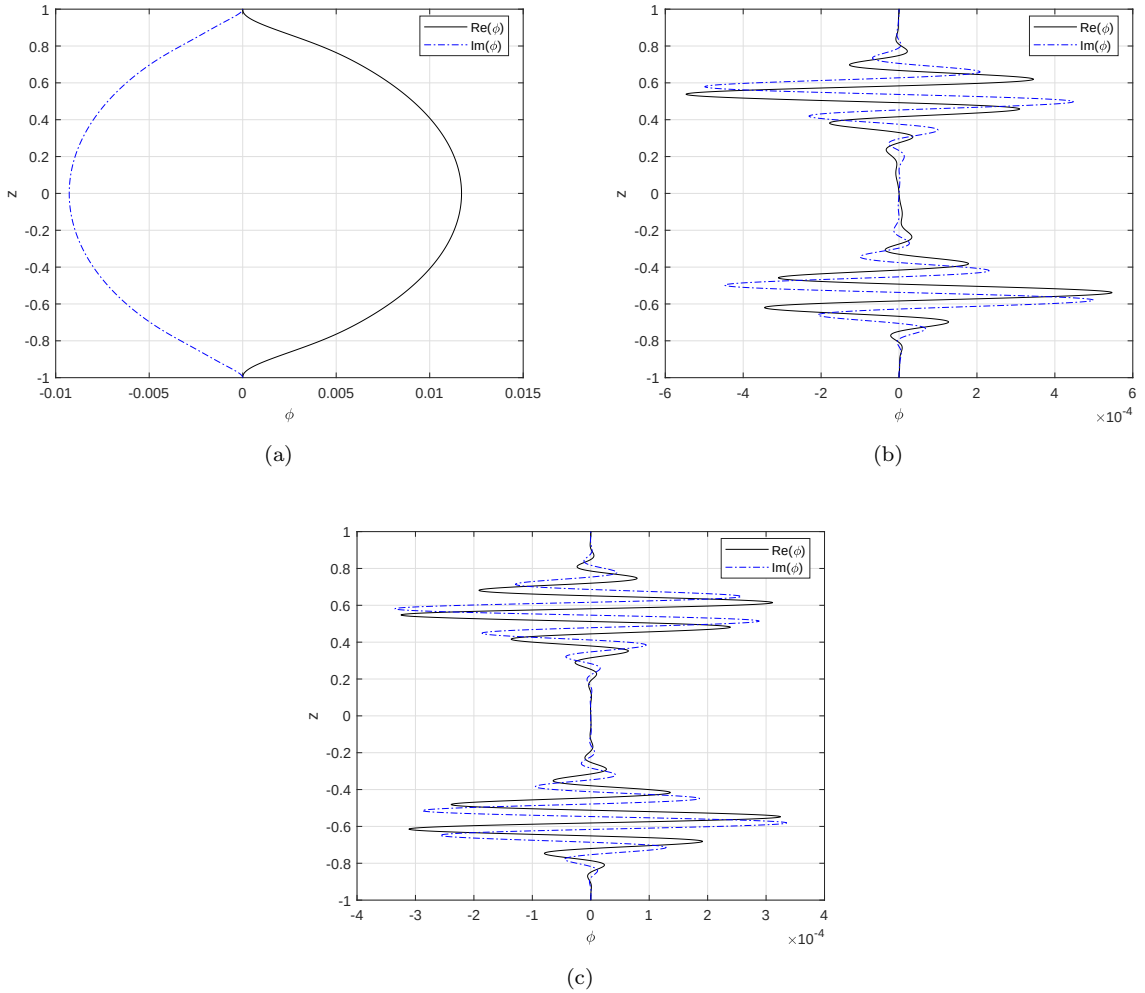


(a) (b)

(c)

FIGURE. 6 Eigenfunctions $\phi(z)$ with both real and imaginary parts with corresponding eigenvalues (a) $c_4 = 0.26402 - 0.00002i$ (the least stable eigenvalue) (b) $c_{30} = 0.70631 - 0.29852i$ (c) $c_{35} = 0.67501 - 0.41198i$, obtained with $N = 2048$ nodal points for $Re = 5772.22$, $\alpha = 1.02056$.

In comparison, the other two plots of eigenfunctions in figure 6b and 6c correspond to anti-symmetric modes, that is instead of the curve being a simple reflection about the $z = 0$ axis, the eigenfunction is also reflected in the $\phi = 0$ axis. The eigenfunction in figure 6b has corresponding eigenvalue $c_{30} = 0.70631 + 0.29852i$ and for the eigenfunction in figure 6c the corresponding eigenvalue is $c_{35} = 0.67501 + 0.41198i$. Although both eigenfunctions in figures 6b and 6c are anti-symmetric about the line $z = 0$, we note that the anti-symmetry is more easily seen in the eigenfunction in figure 6b. This is because the eigenfunction in figure 6c corresponds to an eigenvalue in the lower branch of the eigenvalue spectrum, whereas the eigenfunction in figure 6b corresponds to an eigenvalue situated in the upper right branch of the eigenvalue spectrum as described in figure 5. As the eigenfunction is both real and complex, the imaginary part of the eigenfunctions is simply the complex amplitude of the perturbation wave.

The eigenfunctions in figure 6b and 6c are much more oscillatory in comparison to the eigenfunction in figure 6a. Therefore in order to obtain a highly accurate approximation for the functions $\hat{u}$ and $\hat{w}$, which describe the perturbation wave in the $x$-$z$ plane, we require a large number of nodal points to capture all the detail of the highly oscillatory eigenfunctions. If we were to use even half the number of nodal points used to calculate the eigenfunctions here, we will most likely fail to capture much of the detail of the eigenfunctions.

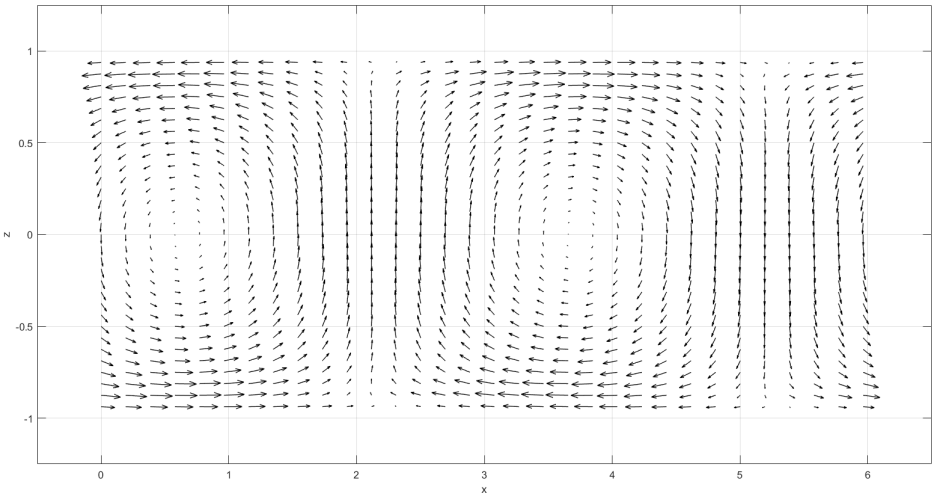


FIGURE. 7 Vector field plot of the perturbation wave with the eigenfunction corresponding to the least stable eigenvalue $c_4 = 0.26402 - 0.00002i$ obtained using $N = 2048$ nodal points, with $Re = 5772.22$, $\alpha = 1.02056$.

In order to gain a physical interpretation of perturbation wave, we can plot the vector field in the $x$-$z$ plane. Considering the eigenfunction shown in figure 6a which corresponds to the least stable mode, we can compute the vector field given by the perturbation wave,

$$\begin{pmatrix} \hat{u} \\ \hat{w} \end{pmatrix} = \begin{pmatrix} \phi'(z) \\ -i\alpha\phi(z) \end{pmatrix} e^{i\alpha(x-ct)}, \tag{5.19}$$

Discretizing this vector equation, we obtain a vector field that can be plotted using the eigenfunction found from computing the solution to the generalized eigenvalue problem. A second-order central-difference scheme is used to approximate the first derivative of $\phi'$ for the nodal points not on the boundaries.

$$\begin{pmatrix} \hat{u}_i \\ \hat{w}_i \end{pmatrix} = \begin{pmatrix} \frac{\phi_{j+1}-\phi_{j-1}}{2h} \\ -i\alpha\phi_j \end{pmatrix} e^{i\alpha(x_j-ct)}, \tag{5.20}$$

where the approximations to $\phi'$ at the boundary have been constructed using the previously derived second-order finite-difference scheme for the first derivative at the boundary.

$$\phi'(z_0) \approx \frac{1}{2h}\left(-3\phi_0 + 4\phi_1 - \phi_2\right), \tag{5.21}$$

$$\phi'(z_{N-1}) \approx \frac{1}{2h}\left(3\phi_{N-1} - 4\phi_{N-2} + \phi_{N-3}\right). \tag{5.22}$$

Figure 7 was created using the MATLAB function `quiver`, which in this case plots arrows with directional components given by the discretized vector field constructed from solving the generalized eigenvalue problem. The matrices are created which hold values of components $\hat{u}_j$ and $\hat{w}_j$ for $z_j \in [-1, 1]$ and $x_j \in [0, \frac{2\pi}{\alpha}]$; that is, the vector field is plotted over one cycle of the perturbation wave. As the generalized eigenvalue problem is solved on a very fine grid with a high number of nodal points, we require a plot which we are able to interpret. Hence for this reason, we can take every $k$-th point to construct an approximate visualisation of the vector field. As the number of nodal points is $N = 2048$, we can take $k = 64$ to give the plot shown in figure 7. The value for $k$ can be adjusted to give the most interpretive and informative visualisation of the vector field.

In figure 7, plotted for $t = 0$, we observe that the vector field corresponding to the least stable mode exhibits roll cells in the $x$-$z$ plane. The perturbation wave given by the least stable mode has been plotted for one cycle here and propagates in the $x$-direction with wave speed that is $0.26402\times$ the velocity taken at the centreline of the channel. As the $x$-coordinate of the vector field is simply a multiple of the derivative at the $z$-coordinate, we know that the $x$-coordinate will be zero when the $z$-coordinate takes its maximum or minimum at a peak or trough respectively. This is illustrated in the vector field plot, for example when the $z$-coordinate takes its maximum, the arrows are nearly vertical directed upwards away from the $x$-axis as there is almost no direction from the $x$-coordinate. Moreover when the $z$-coordinate takes its minimum, the arrows are pointed directly downwards towards the $x$-axis. Alternatively the maxima and minima of the $x$-coordinate are shown by the near horizontal arrows near the boundaries, whereby a similar argument the direction of the arrow is given almost entirely by the $x$-coordinate. Furthermore as the $z$-coordinate is periodic with period $2\pi/\alpha$, we observe the arrows rotating about the point which corresponds to $z$-coordinate is equal to zero.

We can also consider the vector field when the eigenfunction from figure 6c is used. The differences from the eigenfunction corresponding to the least stable mode are that this function is anti-symmetric and highly oscillatory. Therefore we can expect to see a very different plot of the vector field in the $x$-$z$ plane, the vector field corresponding to this particular eigenfunction is shown in figure 8. The plot of the vector field in the $x$-$z$ plane in figure 8 is clearly very different from that in figure 7. Due to the fact that the eigenfunction in this case is anti-symmetric, we have the $x$ and $z$ coordinates are zero or very close to zero around the centre of the channel. Furthermore the eigenfunction takes the value zero near the boundaries and at the boundaries. However, the characteristic feature of the eigenfunction is its highly oscillatory nature which shows how the function rapidly changes sign and magnitude over the channel. As the eigenfunction is highly oscillatory, a small incremental change in $z$ leads to sign change in the $z$-coordinate resulting in the arrows in the vector field plot changing to the opposite direction. As one approaches the boundary, the effect of viscosity becomes important as the fluid velocity is always reduced to zero due to the no-slip condition. This is manifested in the flow by the existence of a thin layer near the boundary where viscous effects are important and in which the velocity varies rapidly to fulfill the no-slip condition. In the $x$-$z$ plane we observe that the adjacent layers pass over each other in different directions, in the regions where the eigenfunction is non-zero. The vector field in figure 8 demonstrates that in solving the Orr-Sommerfeld problem we are required to resolve many boundary layers travelling opposite adjacent to each other close to the boundaries. The more oscillatory an eigenfunction is near the boundaries, the more layers we are required to resolve. The eigenmode corresponding to the least stable mode shown in 6a, with vorticity strongly

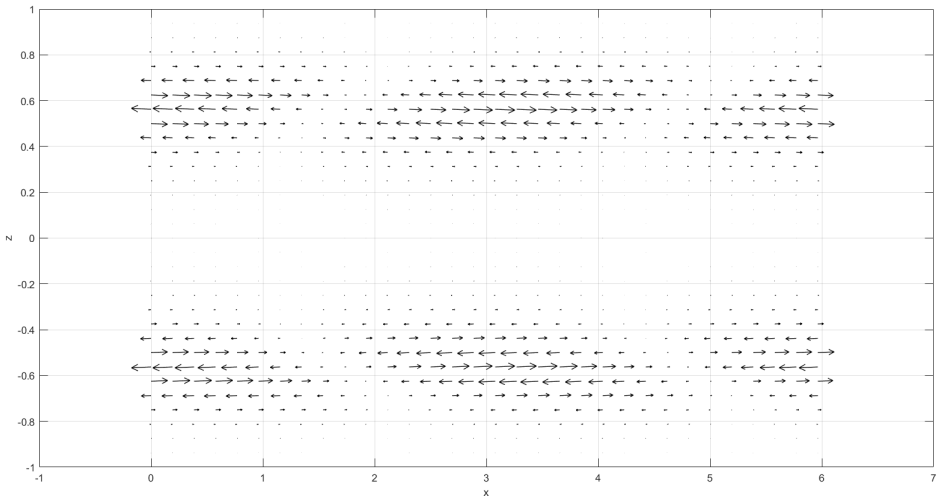


FIGURE. 8 Vector field showing regions of rapid change near the boundaries, also known as boundary layers. The corresponding eigenfunction to this vector field is shown in figure 6c with $c_{35} = 0.67501 - 0.41198i$ obtained for $Re = 5772.22$, $\alpha = 1.02056$.

concentrated near $z = \pm 1$ is known as a Tollmien-Schlichting wave. The presence of these boundary layers in the flow, is a demonstration of the complications that arise when solving the Orr-Sommerfeld equation. The high number of nodal points required to obtain an accurate solution to the Orr-Sommerfeld equation are needed as we are resolving these layers which have rapid change near the boundaries, as viscous forces reduce the velocity to zero close to the boundary. We are required to use more nodal points over the channel in order to gain better resolution of the boundary layers, and therefore a solution with higher accuracy.

In this section we have solved the Orr-Sommerfeld eigenvalue problem, by solving the generalized eigenvalue problem constructed using finite-difference methods. From the literature, the values of the parameters $\alpha$ and $Re$ corresponding to the onset of instability are $\alpha = 1.02056$ and $Re = 5772.22$. If we wish to vary these parameters to obtain another set of values $(Re, \alpha)$, for which the Orr-Sommerfeld equation is solved and the least stable mode has associated eigenvalue with $\mathrm{Im}(c) = 0$, then we are required to solve the generalized eigenvalue problem on a very fine grid for each desired combination of $(Re, \alpha)$. The run time demonstrates how computationally expensive it is to solve the generalized eigenvalue problem on a very fine grid. Hence as we are only concerned with the eigenvalue associated with the least stable mode for each combination of $(Re, \alpha)$, we can develop a methodology for approximating such an eigenvalue.

# 6 One-dimensional boundary value problem and an iterative method

Returning to the one-dimensional harmonic problem discussed in section 4, we aim to use Newton's iterative method to converge to a given eigenvalue more quickly. With the Orr-Sommerfeld eigenvalue problem we are only concerned with finding the least stable mode given by the eigenvalue $c$ with the smallest imaginary part. Therefore using an iterative method to converge to this eigenvalue would be advantageous as it would vastly reduce the computational time and cost of finding the least stable mode. As seen previously in section 4, computing all eigenvalues and eigenvectors of the generalized eigenvalue problem and then sorting the eigenvalues to find the corresponding least stable mode is very computationally expensive.

As is discussed below in formulating the iterative method our problem is transformed from an initial-value problem into a nonlinear boundary value problem which means in most cases our iterative method is only locally convergent. This means we require a guess which is sufficiently accurate so that the local iterative scheme does not diverge away from the solution. The aim of using the local iterative method in this sense is to calculate the solution on a coarser grid (to give a sufficiently accurate guess with a reduced computational cost), then use the eigenvalue corresponding to the least stable mode as our guess for $c$ and the corresponding eigenvector $\mathbf{\Psi}$. This constructed guess is then used on a finer grid to solve the equations formulated using the local iterative method for a correction term which is driven down close to zero in only a few iterations.

Firstly we will use our iterative method in the context of our one-dimensional test problem. The guess defining where we will start our local iterative method, can be obtained by using any function that satisfies the boundary conditions and setting our guess for the eigenvalue we wish to converge to, to a value arbitrarily close to the exact value. Then the iterative method will be performed, updating the guess at each pass of the algorithm, until a threshold is reached for the correction terms, in which case we will conclude that the scheme has converged to the approximate solution. The methodology will be applied to the Orr-Sommerfeld eigenvalue problem in section 7. We begin by recalling our original equation and the following boundary conditions,

$$f'' + \lambda f = 0, \quad with \quad f(0) = 0, \quad f(1) = 0. \tag{6.1}$$

Now treating $\lambda$ as an unknown quantity just like the discretized values of the function at nodal points, we have the complete set of unknowns $\{f_0, f_1, ..., f_{N-1}, \lambda\}$. The problem is now no longer a linear initial-value problem but rather a nonlinear boundary value problem. As we are now treating $\lambda$ as an unknown we are required to add an arbitrary normalisation condition. The additional boundary condition will be taken at the wall to be,

$$f'(0) = 1,$$

Thus now we have the following nonlinear boundary value problem with $\lambda$ unknown,

$$f'' + \lambda f = 0, \quad with \quad f(0) = f(1) = 0, \quad f'(0) = 1. \tag{6.2}$$

In comparison to the initial-value problem, the nonlinear boundary value problem has the additional boundary condition $f'(0) = 1$. This condition could equally have been taken at $z = 1$ at the other boundary, however taking the normalisation condition at the

midpoint between the boundaries is not as straight forward as it is unclear where the curve achieves its maximum. Adding the normalisation condition simply means we are selecting one of the eigenfunctions $f$ which has a gradient of 1 at $z = 0$.

## 6.1 Establishing the iterative scheme

Formulating this problem with an iterative method, at each iteration we wish to solve for the unknowns $\{f_0, f_1, ..., f_{N-1}, \lambda\}$. We begin with an initial guess for the unknowns for the first iteration the aim is to solve for a set of correction terms each corresponding to an unknown, then on repeated iterations the correction term corrects the guess and drives the magnitude of the correction terms down to a predetermined threshold. As the correction term is driven down close to zero the corrected guess will converge to the exact values of the unknowns $\{f_0, f_1, ..., f_{N-1}, \lambda\}$. Formulating this problem with our iterative method we begin by letting,

$$f = f^G + \tilde{f}, \tag{6.3}$$

$$\lambda = \lambda^G + \tilde{\lambda}, \tag{6.4}$$

where the terms with $\tilde{}$ denote the correction terms and terms with a raised $G$ denote the terms representing the initial guess. Substituing this into the nonlinear differential equation we obtain,

$$f^{(G)''} + \tilde{f}'' + (\lambda^G + \tilde{\lambda})(f^G + \tilde{f}) = 0, \tag{6.5}$$

Expanding out the brackets,

$$f^{(G)''} + \tilde{f}'' + \lambda^G f^G + \lambda^G \tilde{f} + \tilde{\lambda} f^G + \tilde{\lambda}\tilde{f} = 0. \tag{6.6}$$

Neglecting the nonlinear term $\tilde{\lambda}\tilde{f}$ we obtain the following formulation,

$$\tilde{f}'' + \lambda^G \tilde{f} + \tilde{\lambda} f^G = -[f^{(G)''} + \lambda^G f^G]. \tag{6.7}$$

where the left hand side of the equation represents the Jacobian and the right hand side of the equation represents the residuals. As this iterative scheme will be derived from the finite-difference approach taken previously, we will discretize the equation and boundary conditions using a second-order central-scheme. A system of equations is formed from the discretized equations, where the correction terms will be solved for at each iteration and the guess updated. We note that if the initial guess for the function $f$ is of high accuracy, then the right-hand side of the equation is approximately zero. Constructing a second-order finite-difference scheme for the additional boundary condition $f'(0) = 1$, we have the following discretized boundary conditions,

$$\tilde{f}_0 = -f_0^G, \tag{6.8}$$

$$\tilde{f}_{N-1} = -f_{N-1}^G, \tag{6.9}$$

$$\frac{-3\tilde{f}_0 + 4\tilde{f}_1 - \tilde{f}_2}{2h} = 1 - \frac{-3f^G + 4f_1^G - f_2^G}{2h}. \tag{6.10}$$

Discretizing (6.7) using a second order central-difference scheme to approximate the derivatives at the nodal points over the domain,

$$\frac{\tilde{f}_{j+1} - 2\tilde{f}_j + \tilde{f}_{j-1}}{h^2} + \lambda^G \tilde{f}_j + \tilde{\lambda} f_j^G = -\left[\frac{f_{j+1}^G - 2f_j^G + f_{j-1}^G}{h^2} + \lambda^G f_j^G\right], \tag{6.11}$$

Thus,

$$\Rightarrow \frac{1}{h^2}(\tilde{f}_{j+1} + \tilde{f}_{j-1}) + (\lambda^G - \frac{2}{h^2})\tilde{f}_j + \tilde{\lambda} f_j^G = -\left[\frac{f_{j+1}^G + f_{j-1}^G}{h^2} + \left(\lambda^G - \frac{2}{h^2}\right) f_j^G\right]. \tag{6.12}$$

Now, from the discretized equation we formulate the system of equations in matrix form. The matrix is then inverted to obtain the correction terms which are then added to the previous guesses for the function $f$ and the eigenvalue we are approximating $\lambda$. In the algorithm, this updated guess is calculated iteratively until the correction term reaches a predetermined threshold which concludes that the iterative algorithm has converged. The matrix formulation is given by $A\mathbf{x} = \mathbf{b}$ where the matrix $A$ and vectors $\mathbf{x}$, $\mathbf{b}$ are given by,

$$\begin{pmatrix} 0 & \frac{-3}{2h} & \frac{4}{2h} & \frac{-1}{2h} & \cdots & \cdots & 0 \\ 0 & 1 & 0 & 0 & \cdots & \cdots & 0 \\ f_1^G & \frac{1}{h^2} & \frac{-2}{h^2} & \frac{1}{h^2} & \cdots & \cdots & 0 \\ f_2^G & 0 & \frac{1}{h^2} & \frac{-2}{h^2} & \frac{1}{h^2} & \cdots & 0 \\ \vdots & \cdots & \cdots & \ddots & \ddots & \ddots & \vdots \\ f_{N-2}^G & \cdots & \cdots & \cdots & \frac{1}{h^2} & \frac{-2}{h^2} & \frac{1}{h^2} \\ 0 & \cdots & \cdots & \cdots & \cdots & 0 & 1 \end{pmatrix} \begin{pmatrix} \tilde{\lambda} \\ \tilde{f}_0 \\ \tilde{f}_1 \\ \vdots \\ \vdots \\ \vdots \\ \tilde{f}_{N-1} \end{pmatrix} = \begin{pmatrix} 1 - \frac{-3f_0^G + 4f_1 - f_3^G}{2h} \\ -f_0^G \\ -\frac{f_2^G - 2f_1^G + f_0^G}{h^2} - \lambda^G f_1^G \\ \vdots \\ \vdots \\ -\frac{f_{N-2}^G - 2f_{N-3}^G + f_{N-4}^G}{h^2} - \lambda^G f_{N-3}^G \\ -f_{N-1}^G \end{pmatrix}.$$

## 6.2 Numerical results

The advantage in using the local iterative method employed here is that we are able to obtain a highly accurate approximation to a desired eigenvalue (and eigenfunction) at reduced computational expense. It is known that solving the generalized eigenvalue problem for all eigenvalues and eigenvectors is very computationally expensive if we are only concerned with one eigenvalue. The local iterative method is expected to converge in only a few iterations, if the guess is sufficiently accurate. If the guess is of high accuracy then we will most likely require fewer iterations to achieve a desired accuracy when compared with a guess of poor accuracy. The matrix A formed from the linear system of equations only needs to be inverted at each iteration, therefore as the iterative method will usually converge in $\mathcal{O}(1)$ steps (generally three or four) this is the most significant computational expense. Although inverting the matrix is potentially very computationally expensive, it will be significantly less expensive when compared with solving the generalized eigenvalue problem.

In order to compare the method used in section 4 with our local iterative method, we can approximate the same eigenvalue on the same number of grid points and observe the difference in run times for both methods. From section 4, it is known that the eigenvalues of the one-dimensional test problem are simply squared multiples of $\lambda_1 = \pi^2$. Tabulated below is analysis on how run time varies with the number of grid points $N$ for both the

method used in section 4 and the iterative method formulated above. For our iterative method employed we start with a guess of $\lambda_1^G = 8.5$ and iterate on $N$ grid points until the correction term corresponding to the approximation of the eigenvalue $< 10^{-8}$. That is, if the correction term is $< 10^{-8}$, we will assume that we have converged on $N$ grid points.

| $N$ | $\lvert\lambda - \pi^2\rvert$ | Run time (GEVP) | Run time (Iterative method) |
|---|---|---|---|
| 8 | 0.16455346 | 0.014 | 0.015 |
| 16 | 0.03602473 | 0.012 | 0.017 |
| 32 | 0.00844396 | 0.010 | 0.018 |
| 64 | 0.00204504 | 0.011 | 0.017 |
| 128 | 0.00050327 | 0.020 | 0.018 |
| 256 | 0.00012483 | 0.082 | 0.026 |
| 512 | 0.00003109 | 0.775 | 0.039 |
| 1024 | 0.00000776 | 9.167 | 0.139 |
| 2048 | 0.00000019 | 113.508 | 0.496 |

TABLE. 5 Error of the approximation to the first eigenvalue $\pi^2$ with the run time in seconds for both methods.

The run time for obtaining the eigenvalues by solving the generalized eigenvalue problem in section 4 is tabulated with the run time for obtaining the approximation to the first eigenvalue by the local iterative method. From table 5 we observe that for $N \leq 128$, there is negligible difference in run time between the methods; in fact, obtaining an approximation to the eigenvalues by solving the generalized eigenvalue problem for $N \leq 64$ has a smaller run time when compared to the run time for iterative method. However this may be due to the fact that the iterative method will continue to iterate until the threshold for the magnitude of the correction term for the eigenvalue is reached. Therefore unless the initial guess is very close to the true value, we are almost guaranteed to perform a few iterations.

The benefit of using the iterative method to obtain an approximation to the first eigenvalue is seen for $N \geq 512$, where for $N = 2048$ the run time for our local iterative method is 0.496 seconds and 113.508 when solving the generalized eigenvalue problem. For obtaining an approximation of one eigenvalue, the method of solving the generalized eigenvalue problem clearly becomes intractable for $N \geq 2048$. Hence formulating the iterative method in this way allows us to calculate a highly accurate approximation to a particular eigenvalue.

# 7 Orr-Sommerfeld boundary value problem

In this case we treat $c$ as our additional unknown just as $\lambda$ was in our test problem. In applying an iterative method to the Orr-Sommerfeld, there are a few minor differences when compared with the formulation for the test problem. Firstly instead of simply defining a function that satisfies our boundary conditions, we will calculate our guess by solving the generalized eigenvalue problem once on a coarser grid. The coarseness of the grid is defined such that the solution to the generalized eigenvalue problem is again sufficiently accurate so that our local iterative scheme doesn't diverge from the solution we are looking for.

As we have established solving the generalized eigenvalue problem using the formulation in section 4, we have achieved quadratic convergence. Hence in this case fewer nodal points are required to achieve a desired accuracy than would be for linear convergence for example. Therefore we can achieve a more accurate guess more quickly with reduced computational cost, meaning the coarseness does not need to be reduced in order to obtain a workable guess for our local iterative scheme. Secondly our normalisation condition is given by,

$$\psi(-1) = 1. \tag{7.1}$$

which is also equivalent to $\phi''(-1) = 1$ as $\psi(-1) = (\mathrm{D}^2 - \alpha^2)\phi(-1) = \phi''(-1) = 1$. However it is easier to impose $\psi(-1) = 1$ as our normalisation condition rather than $\phi''(-1) = 1$ as we do not need to construct a second-order finite-difference scheme for $\phi''$ at the boundary. Similar to our one-dimensional test problem we have the set of unknowns $\{\psi_0, \phi_0, ..., \psi_{N-1}, \phi_{N-1}, c\}$ which define our nonlinear boundary value problem for the Orr-Sommerfeld equation.

The local iterative method employed is performed on our initial guess until the correction term corresponding to the eigenvalue we wish to approximate is less than a predetermined threshold. As the rate of convergence of the iterative method is at least quadratic if suitable conditions are satisfied, we can expect there to be a small number of iterations before the eigenvalue is less than the threshold. The following subsection establishes the local iterative scheme.

## 7.1 Establishing the iterative scheme

We begin by recalling the Orr-Sommerfeld equation,

$$U\psi - \phi U'' + \frac{i}{\alpha Re}\left(\mathrm{D}^2 - \alpha^2\right)\psi = c\psi, \tag{7.2}$$

$$\psi = \left(\mathrm{D}^2 - \alpha^2\right)\phi. \tag{7.3}$$

In order to construct our iterative scheme we begin by decomposing the unknowns $c$, $\phi$ and $\psi$ into a guess for the unknown and a correction term, which we aim to drive down close to zero. These decompositions are then substituted into the equations above and are rearranged so that the Jacobian part of the iterative method is on the left-hand side of the equation and the residuals are on the right-hand side of the equation. Formulating the equations this way we iteratively solve for the correction terms $\tilde{c}$, $\tilde{\phi}$ and $\tilde{\psi}$ and then update the guess component of each unknown. We start by decomposing our unknowns

into guess component and correction term,

$$\psi = \psi^G + \tilde{\psi}, \tag{7.4}$$
$$\phi = \phi^G + \tilde{\phi}, \tag{7.5}$$
$$c = c^G + \tilde{c}. \tag{7.6}$$

Substituting this into the Orr-Sommerfeld equation and our equation for $\psi$ we obtain,

$$(U - (c^G + \tilde{c}))(\psi^G + \tilde{\psi}) + 2(\phi^G + \tilde{\phi}) + \frac{i}{\alpha Re}\left(\mathrm{D}^2 - \alpha^2\right)\left(\psi^G + \tilde{\psi}\right) = 0, \tag{7.7}$$
$$\psi^G + \tilde{\psi} = (\mathrm{D}^2 - \alpha^2)(\phi^G + \tilde{\phi}). \tag{7.8}$$

Neglecting the nonlinear term $\tilde{c}\tilde{\psi}$, we obtain the following

$$\begin{aligned}\left(U - c^G\right)\tilde{\psi} + 2\tilde{\phi} + \frac{i}{\alpha Re}\left(\mathrm{D}^2 - \alpha^2\right)\tilde{\psi} - \tilde{c}\psi^G \\ = -\left[(U - c^G)\psi^G + 2\phi^G + \frac{i}{\alpha Re}\left(\mathrm{D}^2 - \alpha^2\right)\psi^G\right],\end{aligned} \tag{7.9}$$

$$\tilde{\psi} - (\mathrm{D}^2 - \alpha^2)\tilde{\phi} = -\left[\psi^G - (\mathrm{D}^2 - \alpha^2)\phi^G\right]. \tag{7.10}$$

with boundary conditions,

$$\phi(-1) = \phi(1) = 0, \quad \phi'(-1) = \phi'(1) = 0, \quad \psi(-1) = 1. \tag{7.11}$$

where the left-hand side of (7.9) and (7.10) represent the jacobian and the right-hand side represents the residuals. As we iterate and drive down the size of the correction term, the residuals will converge to zero as our guesses for the unknowns converge to their true values. We now discretize the equations and formulate the numerical problem to be solved, this results in a system of equations in which we are solving for the correction terms by multiplying an inverted matrix by a vector of discretized residuals. Discretizing both equations we have,

$$\begin{aligned}(U_j - c^G)\tilde{\psi}_j + 2\tilde{\phi}_j + \frac{i}{\alpha Re}\left(\frac{\tilde{\psi}_{j+1} - 2\tilde{\psi}_j + \tilde{\psi}_{j-1}}{h^2} - \alpha^2\tilde{\psi}_j\right) - \tilde{c}\psi_j^G = \\ -\left[(U_j - c^G)\psi_j^G + 2\phi_j^G + \frac{i}{\alpha Re}\left(\frac{\psi_{j+1}^G - 2\psi_j^G + \psi_{j-1}^G}{h^2} - \alpha^2\psi_j^G\right)\right]\end{aligned}$$

$$\tilde{\psi}_j - \frac{\tilde{\phi}_{j+1} - 2\tilde{\phi}_j + \tilde{\phi}_{j-1}}{h^2} + \alpha^2\tilde{\phi}_j = -\left[\psi_j^G - \frac{\phi_{j+1}^G - 2\phi_j^G + \phi_{j-1}^G}{h^2} + \alpha^2\phi_j^G\right]. \tag{7.12}$$

After discretizing and rearranging the equations, we obtain the jacobian on the left-hand side of the equation and the residuals on the right-hand side of the equation. The discretized system takes the form $\mathrm{A}\mathbf{x} = \mathbf{b}$ where the vector $\mathbf{x}$ is a vector of correction terms. This vector of discretized correction terms is found at each iteration by inverting the matrix A and right multiplying the vector $\mathbf{b}$. The structure and sparsity of the matrix A obviously plays a huge role in being able to best utilise this local iterative method as

we aim to use this on a large number of nodal points. The discretized system takes the form,

$$\begin{aligned}\alpha_j\tilde{\psi}_j + 2\tilde{\phi}_j + \frac{i}{\alpha Re}\left(\frac{\tilde{\psi}_{j+1}+\tilde{\psi}_{j-1}}{h^2}\right) - \tilde{c}\psi_j^G \\ = -\left[\alpha_j\psi_j^G + 2\phi_j^G + \frac{i}{\alpha Re}\left(\frac{\psi_{j+1}^G+\psi_{j-1}^G}{h^2}\right)\right],\end{aligned} \tag{7.13}$$

$$\tilde{\psi}_j - \frac{\tilde{\phi}_{j+1}+\tilde{\phi}_{j-1}}{h^2} + \left(\alpha^2+\frac{2}{h^2}\right)\tilde{\phi}_j = -\left[\psi_j^G - \frac{\phi_{j+1}^G+\phi_{j-1}^G}{h^2} + \left(\alpha^2+\frac{2}{h^2}\right)\phi_j^G\right]. \tag{7.14}$$

where $\alpha_j = U_j - c^G - \frac{i}{\alpha Re}\left(\alpha^2+\frac{2}{h^2}\right)$ with boundary conditions,

$$\begin{aligned}\phi(-1)=0 &\implies \tilde{\phi}_0 = -\phi_0^G,\\ \phi(1)=0 &\implies \tilde{\phi}_{N-1} = -\phi_{N-1}^G,\\ \phi'(-1)=0 &\implies \frac{-3\tilde{\phi}_0+4\tilde{\phi}_1-\tilde{\phi}_2}{2h} = -\frac{-3\phi_0^G+4\phi_1^G-\phi_2^G}{2h},\\ \phi'(1)=0 &\implies \frac{3\tilde{\phi}_{N-1}-4\tilde{\phi}_{N-2}+\tilde{\phi}_{N-3}}{2h} = -\frac{3\phi_{N-1}^G-4\phi_{N-2}^G+\phi_{N-3}^G}{2h},\\ \psi(-1)=1 &\implies \tilde{\psi}_0 = 1-\psi_0^G.\end{aligned} \tag{7.15}$$

Now we formulate the matrix equation $A\mathbf{x}=\mathbf{b}$ from our discretized equations and boundary conditions derived above,

$$\begin{pmatrix} 0 & 1 & 0 & 0 & 0 & 0 & 0 & \cdots & 0\\ 0 & 0 & \frac{-3}{2h} & 0 & \frac{4}{2h} & 0 & \frac{-1}{2h} & \cdots & 0\\ 0 & 0 & 1 & 0 & 0 & 0 & 0 & \cdots & 0\\ \psi_1^G & \frac{i}{\alpha Reh^2} & 0 & \alpha_1 & 2 & \frac{i}{\alpha Reh^2} & 0 & \cdots & 0\\ 0 & 0 & \frac{-1}{h^2} & 1 & \frac{2}{h^2}+\alpha^2 & \frac{1}{h^2} & 0 & \cdots & 0\\ \vdots & \cdots & \cdots & \ddots & \ddots & \ddots & \ddots & \ddots & \vdots\\ 0 & \cdots & \cdots & \cdots & \frac{1}{2h} & 0 & \frac{-4}{2h} & 0 & \frac{3}{2h}\\ 0 & \cdots & \cdots & \cdots & 0 & 0 & 0 & 0 & 1 \end{pmatrix} \begin{pmatrix} \tilde{c}\\ \tilde{\psi}_0\\ \tilde{\phi}_0\\ \tilde{\psi}_1\\ \tilde{\phi}_1\\ \vdots\\ \vdots\\ \tilde{\phi}_{N-1}\end{pmatrix}$$

$$= \begin{pmatrix} 1-\psi_0^G\\ -\frac{-3\phi_0^G+4\phi_1-\phi_3^G}{2h}\\ -\phi_0^G\\ \alpha_1\psi_1^G + 2\phi_1^G + \frac{i}{\alpha Re}\left(\frac{\psi_2^G+\psi_0^G}{h^2}\right)\\ \psi_1^G - \frac{\phi_2^G+\phi_0^G}{h^2} + \left(\alpha^2+\frac{2}{h^2}\right)\phi_1^G\\ \vdots\\ \vdots\\ -\frac{3\phi_{N-1}^G-4\phi_{N-2}^G+\phi_{N-3}^G}{2h}\\ -\phi_{N-1}^G\end{pmatrix}. \tag{7.16}$$

This system of discretized equations returns the correction terms in the vector when the matrix A is inverted and multiplied by the vector **b**. This is performed iteratively in the algorithm and the guess terms are updated by adding the corresponding correction term to its corresponding guess term. This is performed until the algorithm converges and the correction terms have a magnitude below a predetermined threshold.

## 7.2 Numerical Results

The analysis done here is analogous to the analysis done in the previous section, as we wish to compare the performance of our iterative method employed with solving the generalized eigenvalue problem, when obtaining an approximation to one eigenvalue. In this case the local iterative method is formulated such that we obtain an approximation to the eigenvalue corresponding to the least stable mode. In order to do this, on a coarse grid we solve the generalized eigenvalue problem once to find an approximation to this eigenvalue. Then using the formulation derived above in this section, we iterate on a finer grid to obtain an approximation of higher accuracy.

When computing an approximation to the eigenvalue corresponding to the least stable mode using the iterative method, the most computationally expensive operation is inverting the matrix A in the linear system of equations given by the formulation above. Since the set of equations corresponding to the iterative scheme differ from the one-dimensional test problem, the structure of the matrix A is different. This matrix is less sparse than the matrix A associated with the test problem as we have more terms in our equations. Whereby the matrix A associated with the Orr-Sommerfeld boundary value problem formulation is a pentadiagonal matrix with one column with non-zero entries corresponding to the approximation to the eigenvalue. As the number of grid points required to obtain an approximation of high accuracy is large, a pentadiagonal matrix does not mean there are considerably more non-zero entries, as proportionally the number of non-zero entries to the number of zero entries is very small.

| $N$ | $c$ | Factor of decrement of $\mathbb{I}m(c)$ | Run time |
|---|---|---|---|
| 32 | $0.29604092 - 0.03031998i$ | 0.5536 | 0.047 |
| 64 | $0.27508173 - 0.01191992i$ | 2.5436 | 0.049 |
| 128 | $0.26716897 - 0.00385179i$ | 3.0946 | 0.073 |
| 256 | $0.26483885 - 0.00112814i$ | 3.4143 | 0.164 |
| 512 | $0.26421471 - 0.00030822i$ | 3.6602 | 0.591 |
| 1024 | $0.26405519 - 0.00008075i$ | 3.8169 | 3.011 |
| 2048 | $0.26401511 - 0.00002068i$ | 3.9048 | 20.893 |
| 4096 | $0.26400508 - 0.00000524i$ | 3.9501 | 162.666 |

TABLE. 6 Least stable eigenvalue obtained using a local iterative method, on $N$ grid points with $(Re, \alpha) = (5772.22, 1.02056)$ with corresponding run time in seconds. The decrement of the imaginary part is also shown to demonstrate the second-order convergence of the method. These values were obtained with an initial guess for the least stable eigenvalue of $0.49150981 - 0.00246467i$ (obtained by solving the generalized eigenvalue problem on $N = 8$ grid points).

In order to evaluate the performance of the local iterative method in obtaining an approximation to the least stable eigenvalue, we can compare the run time taken using method with solving the generalized eigenvalue problem on $N$ grid points. As stated previously, the local iterative method employed here requires an educated guess of the quantities we are aiming to approximate, in this case the guess is obtained on a coarser grid. If we are to use a guess of high accuracy, this means that when solving the generalized eigenvalue problem a very fine grid is required, this is known to have a much higher run time, see table 4. Therefore there is trade-off in the accuracy of the guess and run time of the iterative method. In obtaining the values in table 6 an initial guess of $0.49150981 - 0.00246467i$ is used for the least stable eigenvalue, this is the approximation

found using only 8 grid points.

The advantage of using a guess of high accuracy, not only for the least stable eigenvalue but also in the approximation to the eigenfunction $\phi(z)$ and to $\psi(z) = (\mathrm{D}^2 - \alpha)\phi(z)$, is that the computation to generate a result with a high degree of accuracy is achieved more quickly. For example, using this local iterative method, it is known that using the rather poor guess of $0.49150981 - 0.00246467i$ for the least stable eigenvalue the time taken to achieve the approximation of $0.26400508 - 0.00000524i$ is approximately 162.666 seconds. Now, in contrast, if the guess is made with 128 grid points, that is the approximation to the least stable eigenvalue is $0.26716897 - 0.00385179i$, then the time taken is approximately 72.374 seconds. Therefore in using a guess obtained on sixteen times more grid points, the run time to achieve the same accuracy is more than halved.

However, if one is to increase the accuracy of the initial guess for the local iterative method, a generalized eigenvalue problem of greater computational expense must be solved. The cost in run time of solving the generalized eigenvalue problem has been discussed previously and it is known that the run time increases by a factor of ten as the number of grid points $N$ is doubled. Therefore the computational cost of achieving a highly accurate approximation to the least stable eigenvalue is quickly dominated by obtaining an initial guess of high accuracy. For example, from previously discussed results the run time associated with solving the generalized eigenvalue problem on $N = 512$ grid points is approximately 14.108 seconds. Although this guess is significantly more accurate than the guess used to obtain the values obtained in table 5, if this initial guess were to be used to generate an approximation on $N = 1024$ grid points the run time would be greater than if a guess of lower accuracy was used. This example demonstrates the trade-off in accuracy for the initial guess that allows us to best utilise the benefit of the local iterative scheme, that is obtaining a highly accurate approximation to the least stable eigenvalue in a shorter run time. We note that using a guess of $0.26483885 - 0.00112814i$ the local iterative method converged to a value of $0.26400257 - 0.00000132i$ on $N = 8192$ grid points. This had an associated run time of approximately 938 seconds. This is due to the large matrix that needs to be inverted at each iteration of the method.

The order of convergence of the local iterative scheme it demonstrated by the third column in table 6. In using the critical values for the parameters $(Re, \alpha) = (5772.22, 1.02056)$ it is known that the imaginary part of the least stable eigenvalue will converge to zero. The factor of decrement of the imaginary part shown in the third column of table 6 shows that the local iterative method employed here exhibits second-order convergence as doubling the number of grid points results in a decrease by approximately a factor of four. The threshold, which determines the stopping condition for the local iteration, is the magnitude of the correction term associated with the eigenvalue we are approximating. The threshold has been set as $10^{-8}$, therefore when the magnitude of the correction term is less than this threshold, we will assume that the local iterative scheme has converged. Generally if the initial guess substituted into the local iterative scheme derived is sufficiently accurate, the iterative method converges in only four or five iterations. Even with a very small threshold of $10^{-8}$ this was observed in the implementation of the iterative scheme derived for obtaining the eigenvalue and eigenfunction corresponding to the least stable mode.

From these two sections on the formulation of this local iterative method, we have gained a means of more quickly obtaining the eigenvalue corresponding to the least stable mode for given values of the parameters $(Re, \alpha)$. Since we are only concerned about the set of values of $(Re, \alpha)$ which correspond to instability, this local iterative method allows

us to test combinations of the parameters to obtain the values of $(Re, \alpha)$ which correspond to neutral stability. Ultimately varying the parameters $(Re, \alpha)$ changes the wave speed at which perturbation wave corresponding to the least stable mode propagates along the channel. Physically increasing the Reynolds number means we are driving the flow at a higher rate through the channel, and varying the wavenumber $\alpha$ means that we are varying the frequency of waves per unit distance.

# 8 Computation of the neutral stability curve

The values of the parameters $(Re, \alpha)$ are defined to be on the curve of neutral stability, if the eigenvalue $c$ corresponding to the least stable mode has $\text{Im}(c) = 0$. The significance of the neutral stability curve is that it illustrates the relationship between varying values of the parameters Reynolds number, wavenumber. In plotting the neutral stability curve we map out two regions, one in which the imaginary part of the eigenvalue associated with the least stable mode is negative, and one in which the imaginary part is positive. Thus in plotting the neutral curve, we map out regions of stability and instability in the $Re$-$\alpha$ plane. The neutral stability curve is shown in figure 9. Furthermore for a given set of parameters $(Re, \alpha)$ on the neutral curve, there is an associated wave speed (expressed as a proportion of the maximum velocity in the channel) with which the perturbation wave corresponding to the least stable mode propagates along the channel. This wave speed is clearly important in characterising the instability. The relationship between the phase speed of the perturbation wave and the given $(Re, \alpha)$ that lies on the neutral curve can be illustrated from the data obtained in computing the neutral curve. This relationship is shown in figure 10.

For the Orr-Sommerfeld equation we are required to solve the generalized eigenvalue problem numerically for a given set of $(Re, \alpha)$ and determine if $\text{Im}(c) \approx 0$ for the least stable mode. This can be performed over a set range of $(Re, \alpha)$, therefore all the values of the parameters that correspond to neutral stability map out the neutral stability curve. As we have seen in previous sections, obtaining an approximation to the eigenvalue by solving the generalized eigenvalue problem fully is computationally expensive and has a very high run time. To verify that a given set of values of $(Re, \alpha)$ does indeed correspond to neutral stability, we require an approximation to the eigenvalue with sufficient accuracy and suitably short run time. Therefore we will make use of the formulation of the local iterative method derived previously in section 7. We know the onset of instability is given by the values of the parameters $(Re, \alpha) = (5772.22, 1.02056)$ (Orszag, 1971), hence rather than testing all combinations of $(Re, \alpha)$ over a set range, we can begin in the neighbourhood of this point and then test neighbouring points in the $Re$-$\alpha$ plane.

The region enclosed by the curve in figure 9 is defined as the unstable region, where for a given $(Re, \alpha)$ the eigenvalue associated with the least stable mode has $\text{Im}(c) > 0$. The region outside the curve is the stable region, where $\text{Im}(c) < 0$. Now we begin formulating our naive parameter search in the $Re$-$\alpha$ plane. To plot the curve of neutral stability, we begin in the region of the onset of instability, as this corresponds to a set of values for the parameters which are known to be on the curve of neutral stability, namely $(Re, \alpha) = (5772.22, 1.02056)$. In obtaining values of $(Re, \alpha)$ that lie on the neutral stability curve, we can consider the curve as two branches. The upper and lower branches are split at the onset of instability. The values of the parameters which are found to lie on the neutral curve, by the naive parameter search, are then plotted in $\alpha$-$Re$ plane up to $Re < 40,000$.

In order to produce this curve, the local iterative method was performed on different values of the parameters $(Re, \alpha)$ to obtain an approximation to the least stable eigenvalue. As we have seen in section 5, on $N = 2048$ grid points the eigenvalue corresponding to the least stable mode was found to be $0.26401511 - 0.00002067i$, therefore we are required to introduce a threshold for the imaginary part of the eigenvalue to determine the stability it constitutes. In computing the neutral curve, the iterative method was used on $N = 512$ grid points to reduce the computational expense, and a given set of values $(Re, \alpha)$ is

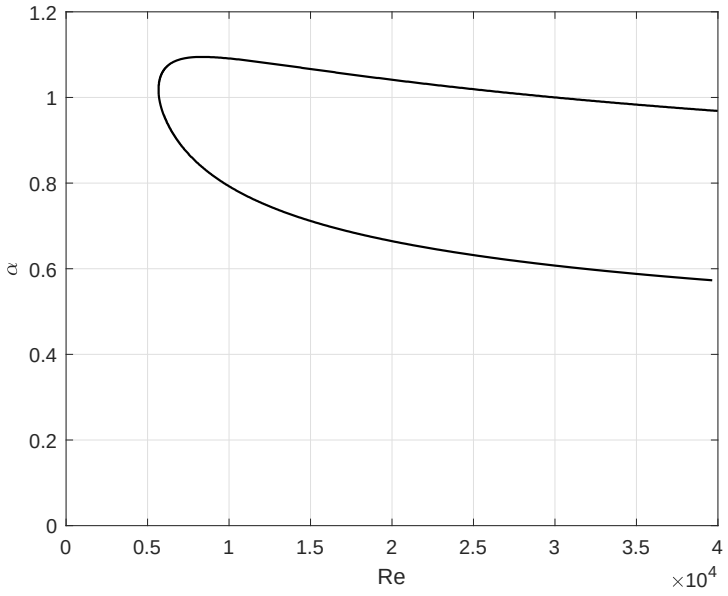


FIGURE. 9 Curve of neutral stability for $Re < 40,000$.

defined to be on the curve of neutral stability if $|\mathrm{Im}(c)| < 0.0005$. From table 6, it is known that on $N = 512$ grid points, local iterative method converges in 0.039 seconds giving an eigenvalue $0.26421471 - 0.00030822i$. The total run time to compute the neutral curve for $Re < 40,000$ was found to be approximately 551.486 seconds. As the shape of the neutral curve changes dramatically over a small range of $\alpha$ for $Re < 10,000$, a finer grid is used to accurately approximate the neutral curve in these regions close to the peak of the upper branch and the set of $(Re, \alpha)$ corresponding to the onset of instability. Overall in the computation of the neutral curve for $Re < 40,000$, the iterative method is performed on 3187 different combinations of Reynolds numbers and wavenumbers.

Physically, increasing the Reynolds number corresponds to driving flow through the channel at higher velocities. We observe from the neutral curve in figure 9, that the range of wavenumbers defining the unstable region for a given Reynolds number appears to remain the same, that is the distance between the two branches does not seem to increase. At the onset of instability located at the left most point on the curve, the combination of $(Re, \alpha)$ corresponds to the lowest theoretical speed at which we can drive the fluid through the channel and observe instability. The interpretation of real part of the least stable eigenvalue is also of interest as it defines the phase speed at which the perturbation wave propagates through the channel. The relationship of this phase speed is illustrated by the the curve in figure 10.

In figure 10, the phase speed of the perturbation wave is shown with Reynolds number $Re$, when the growth rate is zero. The plot illustrates the implicit relationship between the values of the parameters $(Re, \alpha)$ and phase speed at which the perturbation wave propagates. In the naive parameter search used here, the real part of the eigenvalue is recorded if a combination $(Re, \alpha)$ lies on the neutral curve. We observe that the curve of the phase speed with Reynolds number has a similar structure to the neutral curve, that is, it has two branches which originate from the phase speed corresponding to the onset of instability at the left most point on the curve. The value of $c_r$ in $Re$-$c_r$ plane that corresponds to the onset of instability is approximately $c_r = 0.26408235$. Furthermore, we

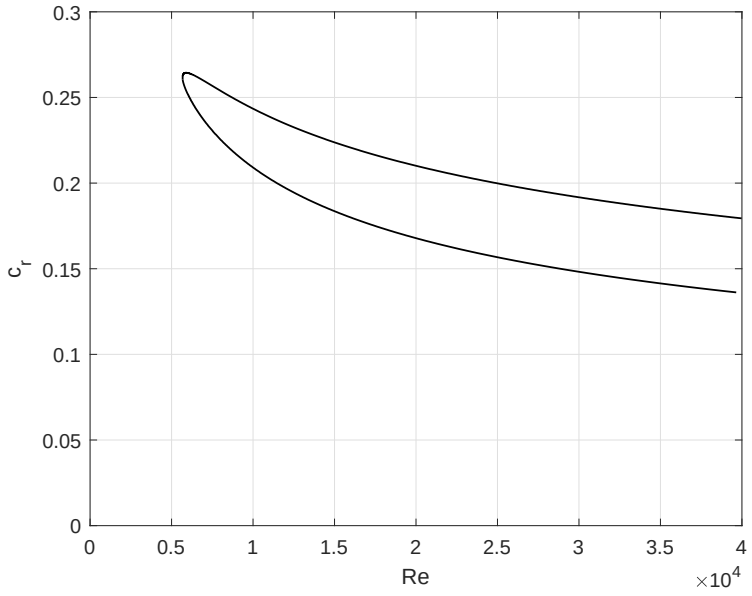


FIGURE. 10 Wave speed $c_r$ for $Re < 40,000$.

also observe that the phase speed corresponding to the boundaries of stability decreases as the Reynolds number increases. Hence if we drive the flow through the channel at higher velocities, the phase speed at which the perturbation wave propagates through the fluid decreases as a function of the wavenumber and Reynolds number.

The phase speed $c_r$ can be shown to be bounded between the minimum and maximum values of the parabolic velocity profile given by $U(z)$, by a result known as Howard's semi-circle theorem. The theorem states that the complex eigenvalues of a neutral or amplified modes lie inside or on a semi-circle centred at $(\frac{U_{max}+U_{min}}{2}, 0)$ in the complex plane, where $U_{max}$ and $U_{min}$ are the maximum and minimum values of the velocity respectively (Howard, 1961). Moreover, demonstrating the phase speed $c_r$ is indeed bounded $U_{min} < 0 < U_{max}$. As a result of non-dimensionalising the governing equations we have the result that the phase velocity must lie in the interval $[0, 1]$. Considering the curve in figure 10, we observe that the phase speed of the perturbation wave for given values of the parameters, is indeed bounded between 0 and 1.

As the Reynolds number is increased and the flow is driven through the channel at higher velocities, one can consider the inviscid limit as the correction term that characterises viscous effects decreases. In the case of plane Poiseuille flow, the flow can be shown to be stable in the inviscid approximation. The fourth-order differential equation we were required to solve is replaced by a second-order differential equation known as Rayleigh's equation, with two boundary conditions. We can consider a result found by Rayleigh (1880) to determine whether the inviscid approximation is in agreement with experimental results, where the flow is turbulent above a critical Reynolds number. Rayleigh's inflection point criterion states that a necessary condition for inviscid instability of a base velocity profile $U(z)$ is that $U(z)$ has a point of inflection in the domain, that is $U''(z_I) = 0$ for some $z_I \in [z_1, z_2]$. Rayleigh's equation characterises the flow in the inviscid approximation, that is viscous effects which are accounted for in the Orr-Sommerfeld equation, are disregarded in Rayleigh's equation. Rayleigh's equation

with the two boundary conditions is given by,

$$(U-c)\left(\mathrm{D}^2-\alpha^2\right)\phi - U''\phi = 0, \tag{8.1}$$

with,

$$\phi(1) = 0, \quad \phi(-1) = 0, \tag{8.2}$$

where the two boundary conditions correspond to the no-penetration condition as the no-slip condition is not applicable in the inviscid flow approximation. Now if we consider the following simple bookwork, if we assume the existence of an unstable mode that is $\mathrm{Im}(c) > 0$ then $U - c \neq 0$. Then, multiplying Rayleigh's equation by the complex conjugate of the eigenfunction (denoted by $\bar{\phi}$),

$$\bar{\phi}\frac{\mathrm{d}^2\phi}{\mathrm{d}z^2} - \alpha^2\bar{\phi}\phi - \frac{U''\bar{\phi}\phi}{U-c} = 0. \tag{8.3}$$

Integrating over the domain and dividing by $(U-c)$,

$$\int_{-1}^{1}\left(\bar{\phi}\frac{\mathrm{d}^2\phi}{\mathrm{d}z^2} - \alpha^2\bar{\phi}\phi - \frac{U''\bar{\phi}\phi}{U-c}\right)dz = 0,$$

Integrating the first term by parts,

$$\left[\bar{\phi}\phi\right]_{-1}^{1} - \int_{-1}^{1}\frac{\mathrm{d}\bar{\phi}}{\mathrm{d}z}\frac{\mathrm{d}\phi}{\mathrm{d}z}dz - \int_{-1}^{1}\frac{U''\bar{\phi}\phi}{U-c}dz - \alpha^2\int_{-1}^{1}\bar{\phi}\phi dz = 0, \tag{8.4}$$

then multiplying by $-1$,

$$\int_{-1}^{1}\left|\frac{\mathrm{d}\phi}{\mathrm{d}z}\right|^2 dz + \int_{-1}^{1}\frac{U''(U-c)\phi^2}{|U-c|^2}dz + \alpha^2\int_{-1}^{1}|\phi|^2 dz = 0, \tag{8.5}$$

then taking the imaginary part gives,

$$c_i\int_{-1}^{1}\frac{U''(U-c)\phi^2}{|U-c|^2}dz = 0. \tag{8.6}$$

Hence, since the integral is zero, the integrand must change sign (at least once) over the domain $[-1,1]$. Therefore, we arrive at Rayleigh's inflection point criterion which states there must exist $z_I \in [-1,1]$ such that $U(z_I) = 0$. In the case of plane Poiseuille flow, the base flow has a parabolic profile, therefore there is no inflection point over the domain.

$$U(z) = 1 - z^2, \quad \Rightarrow \quad U''(z) = -2,$$

Hence we have that plane Poiseuille flow is inviscidly stable. That is in the inviscid limit ($Re \to \infty$, with wavelength of disturbance $\alpha$ and the eigenfunction remaining of finite order), plane Poiseuille flow is stable. We note that the viscous term may remain $\mathcal{O}(1)$ for values of $(\mathrm{D}^2-\alpha^2)\psi$ that are $\mathcal{O}(Re)$. However plane Poiseuille flow is known to be unstable and undergoes a transition to turbulent flow for high Reynolds numbers. Therefore it would appear that viscosity may play a role in inducing the instability in the flow. The conclusion drawn from considering the inviscid limit, that plane Poiseuille flow is stable, contradicts that observed in experiments, where plane Poiseuille flow is

unstable above a critical Reynolds number. For very large Reynolds numbers, the term in the Orr-Sommerfeld equation which accounts for viscosity is given by a small correction which is a decreasing function of $Re$. In some situations, the role of viscosity in the flow may be one of damping, this is often the case for flows that are characterised by low Reynolds numbers.

In order to understand the contradiction arrived at by considering the inviscid approximation, we can consider the physical interpretation given by Taylor (1915) for the condition of instability. As summarised by Drazin and Howard (1966), Taylor noted that when $U''$ is always of one sign over the channel, the frictionless slipping of the fluid at the boundaries prevented the transfer of $x$-momentum necessary to maintain an unstable disturbance. Moreover Taylor explained that viscosity allowed momentum to be diffused from the boundaries. The assumption of frictionless boundaries prevents the transfer of momentum, which is a necessary accompaniment of a disturbance of a fluid for which $U''$ is everywhere negative (as it is in plane Poiseuille flow) (Taylor, 1915). Thus for a given base flow, the flow may be stable for the inviscid fluid but unstable for the viscous fluid. The role of viscosity can be one of dissipation or damping and therefore contributes to stabilizing the flow, however viscosity may also be destabilizing as the no-slip condition enforced at the boundaries leads to rapid variations of the velocity in the form of boundary layers that must be resolved.

## 8.1 Discussion of some experimental results

It has been found in numerous experiments that the theoretical value for the critical Reynolds number $Re_{crit} = 5772.22$ is not as physically important as was first thought. In figure 11, an illustration is shown of the experimental setup used by Reynolds to observe the transition from laminar to turbulent flow. Since Reynolds carried out his experiments in the late nineteenth century, many further experiments have been done in order to accomplish agreement between experimental and theoretical results. Firstly we may note that Reynolds conducted his experiments with Hagen-Poiseuille flow or Poiseuille flow in a pipe which, in contrast to plane Poiseuille flow, is linearly stable to infinitesimal disturbances (Davey, 1973). Hence the transition to turbulence observed by Reynolds in pipe flow appears contradict the lack of a theoretical prediction for transition from the linear theory. Some experimental results with regard to the theoretical prediction of the transition for plane Poiseuille flow are discussed here.

In many experimental settings the critical Reynolds number has been found to be far lower than the theoretical value predicted. For example, in one particular study the transition from laminar flow to the observation of turbulent spots in the flow was found to occur for $Re > 2200$ (Alavyoon *et al.*, 1986). The phenomena of turbulent spots was observed by Reynolds himself in his series of experiments and it is a critical feature often observed in plane Poiseuille flow right before the flow is considered to be fully turbulent (Reynolds, 1883). We note that the subcritical transition to turbulent flow may even occur for Reynolds numbers almost a magnitude lower than that of the critical Reynolds number. These experimental results are said to demonstrate the importance of nonlinear effects, consequently this subverts the assumption that the transition to turbulent flow is the result of the growth of infinitesimal (linear) disturbances (Alavyoon *et al.*, 1986). Hence the linear stability analysis may not be sufficient to predict the transition to turbulence, thus discrepancies between the theoretical prediction and experimental results highlight the importance of the nonlinear theory.

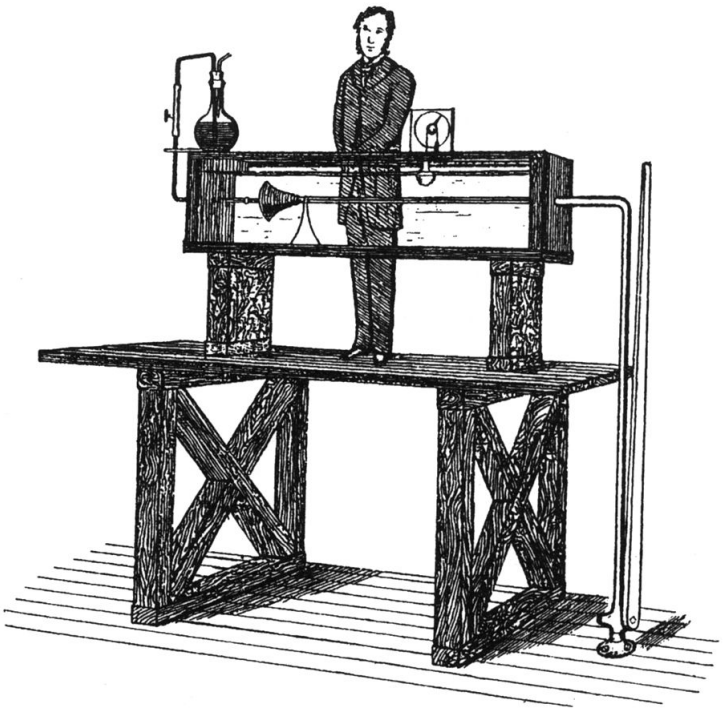

FIGURE. 11 Illustration of the apparatus used by Reynolds to observe the nature of the transition from laminar to turbulent flow in plane Poiseuille flow (Reynolds, 1883).

In experimental settings the effect of background turbulence in the flow is found to influence the value of the Reynolds number at which the flow undergoes the transition from laminar to turbulent flow. In experiments conducted by Nishioka *et al.* (1975) the background turbulence was reduced to 0.05% which allowed for the flow to remain laminar for Reynolds numbers up to $Re = 8000$, far greater than the critical Reynolds number $Re_{crit} = 5772.22$. Sinusoidal disturbances can be introduced into the base flow to excite waves of finite amplitude downstream. It was found that without artificial excitations in the flow (brought about by a vibrating ribbon in the flow) it was sometimes possible to achieve laminar flow up to $Re = 9000$ (Nishioka *et al.*, 1975). However this was attributed to the low background turbulence of 0.05% in the flow, in addition small disturbances require a large distance (which exceeded the length of the channel) to allow them to grow in amplitude sufficient for the triggering of the transition to turbulence (Nishioka *et al.*, 1975). The conclusions of this experiment were that the small disturbance introduced by means of of vibrating ribbon behave as predicted by the linear theory, that is a Reynolds number of approximately 6000 (Nishioka *et al.*, 1975).

In contrast we can again consider the subcritical transition from laminar to turbulent flow in plane Poiseuille flow. Such a transition is often of practical importance, as evidently there are fine experimental settings (such as reducing the background turbulence to 0.05%) required to achieve experimental results that are in complete agreement with the critical transition $Re$ predicted from the linear theory. In a similar experiment conducted by Nishioka and Asai (1985), the minimum transition Reynolds number was found to be approximately 1000, which is less than 20% of the critical Reynolds number predicted by the linear theory. In the estimation of the nonlinear critical Reynolds number, through numerical simulations it was found that the two-dimensional wave motion of the Orr-Sommerfeld mode is unstable to infinitesimal three-dimensional disturbances, when the

amplitude exceeds a certain threshold (Orszag and Patera, 1983). This three-dimensional linear instability has been described as a key mechanism for the subcritical transition to turbulence, hence it was termed as a secondary instability. The critical Reynolds number of the secondary instability was found to be approximately 1000, this is roughly where viscous effects become important, in that they may be destabilizing.

# 9 Chebyshev polynomials and the spectral-tau method

In this section we outline the methodology that will be used in solving the Orr-Sommerfeld eigenvalue problem by utilising the spectral approach instead of finite-differences methods. In spectral methods the tau method is one of the most widely used techniques in solving differential equations. Alternatively the other methods that may used are Galerkin and collocation. The Galerkin method is discussed as a possible method of solving the Orr-Sommerfeld eigenvalue problem by Orszag (1971), however the tau method was the method of choice used to obtain numerical results. Chebyshev spectral tau methods provide a powerful technique in solving ordinary differential equations and have been extensively used in fluid dynamics to obtain a numerical solution to the governing equations. Furthermore spectral methods often provide a numerical solution with great accuracy at far less of a computational expense, hence the techniques used in spectral methods give a superior alternative to the finite-difference approach. In the Chebyshev spectral-tau method the unknown function is approximated by a series of Chebyshev polynomials with coefficients to be determined, where in order to make this approximation computationally tractable the series is truncated at $N$ terms. The $n$-th degree Chebyshev polynomial is defined in the following way,

$$T_n(z) = \cos(n\theta), \quad \text{where} \quad z = \cos(\theta). \tag{9.1}$$

Chebyshev polynomials can be expressed as a function of $z$ by using standard trigonometric manipulations, the first few are shown below.

$$\begin{aligned} T_0(z) &= 1, \\ T_1(z) &= z, \\ T_2(z) &= 2z^2 - 1, \\ T_3(z) &= 4z^3 - 3z, \\ &\vdots \end{aligned}$$

A graph of the first six Chebyshev polynomials is shown below in figure 12, this graph demonstrates that a linear combination of these polynomials can simulate highly oscillatory behaviour of a solution. The Chebyshev polynomials listed are of the first kind, the $n$-th Chebyshev polynomial of the second kind is given by,

$$U_n(\cos\theta)\sin\theta = \sin(n+1)\theta.$$

Chebyshev polynomials of the second kind are not used here in the formulation of the spectral-tau method. This is because the derivative of the $n$-th degree Chebyshev polynomial of the first kind can be equated to other Chebyshev polynomials of the first kind by a particularly useful recurrence relation. Among the many properties of Chebyshev polynomials, one unique property is that on the interval $-1 \leq z \leq 1$ all of the polynomials take their maxima at either 1 or $-1$. Chebyshev polynomials are the most common basis functions to be used in a series expansion to approximate the solution using the spectral method.

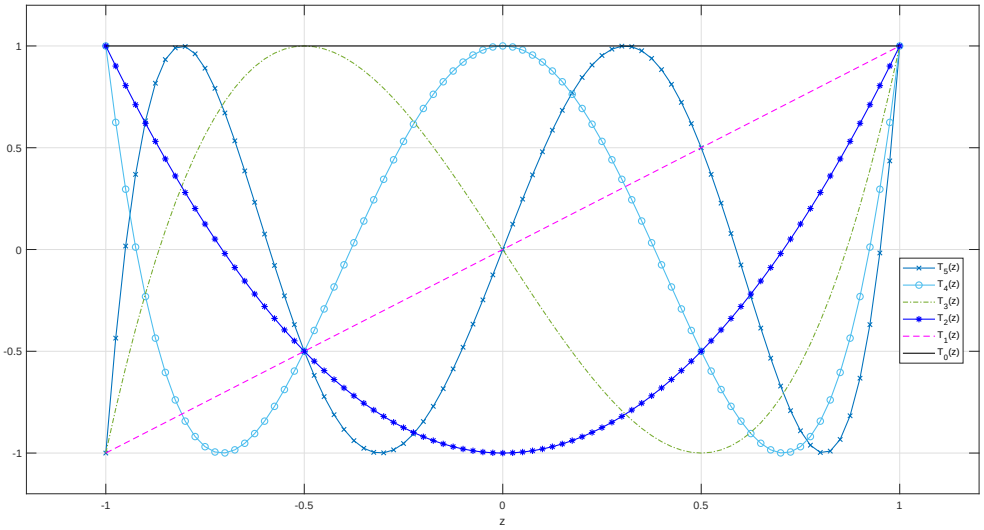


FIGURE. 12 First six Chebyshev polynomials of the first kind on the domain $-1 \leq z \leq 1$.

If we suppose that we wish to approximate a function by a series of Chebyshev polynomials truncated at $N$.

$$\phi(z) \approx \phi_N(z) = \sum_{n=0}^{N} \phi_n T_n(z). \tag{9.2}$$

The idea of the tau method is to add constants to the series expansion given by (9.2) so that a trial function need not satisfy the boundary conditions. The number of constants added to the series expansion is equivalent to the number of boundary conditions in the problem. If $N$ is the dimension of the domain and there are $k$ boundary conditions, there are now $N + k$ coefficients to be solved for. The $k$ additional equations required to solve for the coefficients added arise from the boundary conditions. Therefore we obtain a complete set of equations where the number of coefficients is equal to the number of equations.

In solving the Orr-Sommerfeld eigenvalue problem, the tau method is the simpler of the two methods proposed by Orszag (1971). Although the Galerkin method is discussed the tau method is used to obtain the numerical results. A disadvantage of using the tau method is that two unstable eigenvalues arise that are artifacts of the discretization of the numerical scheme. Therefore in the analysis of the numerical results of the implementation of this method we should expect there to be two spurious unstable eigenvalues in the solution to the problem. The magnitudes of these artifacts increase rapidly as more terms are added to the series expansion. Although these eigenvalues can be disregarded as non-physical, it is possible to eliminate them from the solution by implementing a modified tau method (McFadden *et al.*, 1990). In the following implementation of the spectral-tau method here, the spurious eigenvalues are not eliminated before solving the Orr-Sommerfeld eigenvalue problem. We will analyse the magnitude of these spurious eigenvalues as the number of Chebyshev polynomials used is varied.

Firstly we can take the inner product of $\phi$ with the $m$-th degree Chebyshev polynomial,

$$\langle \phi_N \, , T_m \rangle = \left\langle \sum_{n=0}^{N} \phi_n T_n(z) \, , T_m \right\rangle = \sum_{n=0}^{N} \phi_n \langle T_n \, , T_m \rangle = \phi_m \langle T_m \, , T_m \rangle,$$

$$\Rightarrow \phi_m = \frac{\langle \phi_N \, , T_m \rangle}{\langle T_m \, , T_m \rangle}. \tag{9.3}$$

We can derive an expression for the coefficients of the polynomials in the Chebyshev series.

$$\langle T_m \, , T_m \rangle = \int_{-1}^{1} T_m^2 \frac{dz}{\sqrt{1-z^2}} = -\int_{\pi}^{0} \cos^2(m\theta) d\theta = \frac{1}{2}\left[\theta + \frac{\sin(2m\theta)}{2m}\right]_0^{\pi}. \tag{9.4}$$

We note that by L'Hôpital's rule,

$$\lim_{m\to 0} \frac{\sin(2m\pi)}{2m} = \lim_{m\to 0} \frac{2\pi\cos(2\pi m)}{2} = \pi \lim_{m\to 0} \cos(2\pi m) = \pi. \tag{9.5}$$

Therefore, if we consider the two cases where $m = 0$ and $m > 0$, we have,

$$m = 0, \quad \langle T_m \, , T_m \rangle = \pi, \tag{9.6}$$

$$m > 0, \quad \langle T_m \, , T_m \rangle = \frac{\pi}{2}. \tag{9.7}$$

Hence the coefficients $\phi_n$ can be expressed by the following equation,

$$\phi_n = \frac{2}{\pi c_n} \int_{1}^{-1} \phi(z) T_n(z) \frac{dz}{\sqrt{1-z^2}}, \quad c_n = \begin{cases} 1 & \text{if } n = 0 \\ 2 & \text{if } n > 0 \end{cases} \tag{9.8}$$

and we observe that,

$$\int_{1}^{-1} T_m(z) T_n(z) \frac{dz}{\sqrt{1-z^2}} = \frac{\pi}{2} c_n \delta_{nm}. \tag{9.9}$$

Now if we consider the derivative of the function we are approximating $\phi(z)$ we notice the series of Chebyshev polynomials can be rewritten with different coefficients $\phi_n^{(1)}$,

$$\phi_N'(z) = \sum_{n=1}^{N} \phi_n T_n'(z) = \sum_{n=0}^{N-1} \phi_n^{(1)} T_n(z). \tag{9.10}$$

Now we will manipulate the following trigonometric identity to find a relationship between $\phi_n$ and $\phi_n^{(1)}$.

$$2\sin(r\theta)\cos(p\theta) = \sin((p+r)\theta) - \sin((p-r)\theta), \tag{9.11}$$

$$2\cos(p\theta) = \frac{\sin((p+r)\theta) - \sin((p-r)\theta)}{\sin(r\theta)}, \tag{9.12}$$

Letting $p = n$, $r = 1$ and $z = \cos\theta$ we obtain the following recurrence relation relating the first derivatives of Chebyshev polynomials of the first kind to a multiple of a Chebyshev polynomial of the first kind,

$$2T_n(z) = \frac{\sin((n+1)\theta)}{\sin\theta} - \frac{\sin((n-1)\theta)}{\sin\theta}, \tag{9.13}$$

$$2T_n(z) = \frac{1}{n+1}\frac{\mathrm{d}}{\mathrm{d}z}\left(T_{n+1}(z)\right) - \frac{1}{n-1}\frac{\mathrm{d}}{\mathrm{d}z}\left(T_{n-1}(z)\right). \tag{9.14}$$

Now we can use this reccurence relation in the definition of $\phi'_N(z)$,

$$\begin{aligned}
\phi'_N(z) = \sum_{n=0}^{N} \phi_n T_n(z) &= \frac{1}{2}\sum_{n=0}^{N-1} \phi_n \left( \frac{1}{n+1} T'_{n+1}(z) - \frac{1}{n-1} T'_{n-1}(z) \right), \\
\Rightarrow \quad \sum_{n=1}^{N} \phi_n T'_n(z) &= \frac{\mathrm{d}}{\mathrm{d}z} \left[ \frac{1}{2}\sum_{n=0}^{N-1} \phi_n \left( \frac{1}{n+1} T'_{n+1}(z) - \frac{1}{n-1} T'_{n-1}(z) \right) \right], \\
2\sum_{n=1}^{N} \phi_n T'_n(z) &= \sum_{n=0}^{N-1} \phi_n^{(1)} \left( \frac{1}{n+1} T'_{n+1}(z) - \frac{1}{n-1} T'_{n-1}(z) \right). \qquad (9.15)
\end{aligned}$$

Equating the coefficients of the derivatives of Chebyshev polynomials of the first kind and noting that $T'_k = T'_{-k}$,

$$\begin{aligned}
\phi_0^{(1)} - \phi_2^{(1)} &= 2\phi_1, \\
\frac{1}{2}\phi_1^{(1)} - \frac{1}{2}\phi_3^{(1)} &= 2\phi_2, \\
\frac{1}{3}\phi_2^{(1)} - \frac{1}{3}\phi_4^{(1)} &= 2\phi_3, \\
&\vdots \\
\frac{1}{N+1}\phi_{N-1}^{(1)} - \frac{1}{N+1}\phi_{N+1}^{(1)} &= 2\phi_N. \qquad (9.16)
\end{aligned}$$

More generally, we have the relation,

$$c_k \phi_k^{(q)} - \phi_{k+2}^{(q)} = 2(k+1)\phi_{k+1}^{(q-1)}, \quad \text{for} \quad 0 \le k \le N-q, \qquad (9.17)$$

$$\text{where} \quad c_n = \begin{cases} 1 & \text{if } n = 0 \\ 2 & \text{if } n > 0 \end{cases} \qquad (9.18)$$

If we consider the case where $q = 1$ and $\phi_n^{(0)} = \phi_n$. Starting with $k = N-1$,

$$\begin{aligned}
c_{N-1}\phi_{N-1}^{(1)} - \phi_{N+1}^{(1)} &= 2N\phi_N, \\
&\vdots \\
c_2\phi_2^{(1)} - \phi_4^{(1)} &= 2(3)\phi_3, \\
c_1\phi_1^{(1)} - \phi_3^{(1)} &= 2(2)\phi_2, \\
c_0\phi_0^{(1)} - \phi_2^{(1)} &= 2(1)\phi_1, \qquad (9.19)
\end{aligned}$$

Formulating this system of equations in matrix form we can begin to develop the numerical scheme which allows us easily relate the coefficients of the derivatives $\phi_n^{(q)}, (q > 0)$ to the coefficients of the Chebyshev series $\phi_n$. This results in a matrix equation of the form,

$$\mathrm{C}\boldsymbol{\Phi}^{(1)} = \mathrm{A}\boldsymbol{\Phi}, \qquad (9.20)$$

where the matrix C and A are defined below from the system of equations above.

$$\begin{pmatrix} 2 & 0 & -1 & 0 & 0 & \cdots & 0 \\ 0 & 1 & 0 & -1 & 0 & \cdots & 0 \\ 0 & 0 & 1 & 0 & -1 & \cdots & 0 \\ 0 & 0 & 0 & 1 & 0 & \ddots & 0 \\ \vdots & \cdots & \cdots & \ddots & \ddots & \ddots & \vdots \\ 0 & \cdots & \cdots & \cdots & 0 & 1 & 0 \\ 0 & \cdots & \cdots & \cdots & 0 & 0 & 1 \end{pmatrix} \begin{pmatrix} \phi_0^{(1)} \\ \phi_1^{(1)} \\ \phi_2^{(1)} \\ \vdots \\ \vdots \\ \phi_{N-2}^{(1)} \\ \phi_{N-1}^{(1)} \end{pmatrix} = \begin{pmatrix} 0 & 2 & 0 & \cdots & \cdots & 0 \\ 0 & 0 & 4 & \cdots & \cdots & 0 \\ 0 & 0 & 0 & \cdots & \cdots & 0 \\ \vdots & \cdots & \ddots & \ddots & \ddots & \vdots \\ 0 & \cdots & \cdots & \cdots & 2(N-1) & 0 \\ 0 & \cdots & \cdots & \cdots & 0 & 2N \end{pmatrix} \begin{pmatrix} \phi_0 \\ \phi_1 \\ \phi_2 \\ \vdots \\ \vdots \\ \phi_{N-1} \\ \phi_N \end{pmatrix}. \tag{9.21}$$

Since the matrix C is non-singular $\mathrm{C}^{-1}$ exists, therefore we can define another matrix E formed by left multiplying A by $\mathrm{C}^{-1}$.

$$\mathbf{\Phi}^{(1)} = \mathrm{C}^{-1}\mathrm{A}\mathbf{\Phi} = \mathrm{E}\mathbf{\Phi}. \tag{9.22}$$

Moreover for the $q$-th derivative we have,

$$\mathbf{\Phi}^{(q)} = \mathrm{E}\mathbf{\Phi}^{(q-1)} = \mathrm{E}\ldots\mathrm{E}\mathbf{\Phi} = \mathrm{E}^k\mathbf{\Phi}. \tag{9.23}$$

If we consider the system of equations given by (9.18) we can express the coefficients of the first derivative in summation form. Recalling the definition for the coefficient $c_n, \quad for \quad n \geq 0$, we have the following for $n = 0$ in the case where we have considered an infinite expansion,

$$\begin{aligned} 2\phi_0^{(1)} &= 2\phi_1 + \phi_2^{(1)}, \\ &= 2\phi_1 + 6\phi_3 + \phi_4^{(1)}, \\ &= 2\phi_1 + 6\phi_3 + 10\phi_5 + \phi_6^{(1)}, \\ &= 2\phi_1 + 6\phi_3 + 10\phi_5 + 14\phi_7 + \ldots, \\ &= 2(\phi_1 + 3\phi_3 + 5\phi_5 + \ldots), \\ 2\phi_0^{(1)} &= 2\sum_{\substack{k=1 \\ k\equiv 1 \bmod 2}}^{\infty} k\phi_k, \end{aligned} \tag{9.24}$$

A more general relation can be derived using the recurrence relation (9.16), where for the first derivative,

$$c_n\phi_n^{(1)} = 2\sum_{\substack{k=n+1 \\ k+n\equiv 1 \bmod 2}}^{\infty} k\phi_k, \tag{9.25}$$

and more generally for the $q$-th derivative,

$$c_n\phi_n^{(q)} = 2\sum_{\substack{k=n+1 \\ k+n\equiv 1 \bmod 2}}^{\infty} k\phi_k^{(q-1)}. \tag{9.26}$$

The summation form for the coefficients of the second and fourth derivative, which will be useful in formulating the Orr-Sommerfeld problem, are found to be ,

$$\begin{aligned} c_n\phi_n^{(2)} &= 2 \sum_{\substack{k=n+1 \\ k+n\equiv 1 \bmod 2}}^{\infty} k\phi_k^{(1)} = \sum_{\substack{k=n+1 \\ k+n\equiv 1 \bmod 2}}^{\infty} k \left[ \frac{2}{c_k} \sum_{\substack{m=k+1 \\ m+k\equiv 1 \bmod 2}}^{\infty} m\phi_m \right], \\ &= 4 \sum_{\substack{k=n+2 \\ k\equiv n \bmod 2}}^{\infty} k\phi_k \sum_{\substack{m=k+1 \\ m+k\equiv 1 \bmod 2}}^{k-1} m, \\ \Rightarrow \quad c_n\phi_n^{(2)} &= \sum_{\substack{k=n+2 \\ k\equiv n \bmod 2}}^{\infty} k(k^2-n^2)\phi_k. \end{aligned} \tag{9.27}$$

Furthermore for the fourth derivative,

$$c_n\phi_n^{(4)} = \frac{1}{24} \sum_{\substack{k=n+4 \\ k\equiv n \bmod 2}}^{\infty} k\left(k^2(k^2-4)^2 - 3n^2k^4 + 3n^4k^2 - n^2(n^2-4)^2\right)\phi_k. \tag{9.28}$$

Although the matrix formulation will be used in formulating the Orr-Sommerfeld eigenvalue problem, it is worth noting the forms of derivative coefficients $\phi_n^{(q)}$ for $q > 0$ as they are simply a summation of the coefficients. If we truncate to $N$ terms, as both formulations coincide, one can check that these summations are correct by raising the matrix E to the appropriate power and analysing the entries of the resulting matrix. The simple relationship between the derivative coefficients and coefficients of the zero-th derivative in the matrix formulation allows us to easily set up the computational problem.

## 9.1 Formulation of the Orr-Sommerfeld problem with the spectral-tau method

Now we will apply the spectral tau method to the Orr-Sommerfeld equation and formulate the numerical scheme. The Orr-Sommerfeld eigenvalue problem will be formulated as a generalized eigenvalue problem as it was in previous sections, where the wavenumber $\alpha$ is taken to be purely real and $c$ complex. In this case instead of solving for the eigenfunctions directly, the eigenvectors obtained from the resulting system will be coefficients of a Chebyshev polynomial series truncated at $N$ terms. Therefore in order to obtain the eigenfunctions we are required to substitute these coefficients back into the Chebyshev series. The numerical approximations of the eigenfunctions are therefore simply expressed in terms of a linear combination of trigonometric functions. We begin by recalling the Orr-Sommerfeld equation,

$$(U-c)\left(\mathrm{D}^2-\alpha^2\right)\phi - U''\phi + \frac{i}{\alpha Re}\left(\mathrm{D}^2-\alpha^2\right)^2\phi = 0, \tag{9.29}$$

with boundary conditions

$$\phi = 0, \quad \phi' = 0, \quad \text{at} \quad z = \pm 1. \tag{9.30}$$

Then expressing the function $\phi$ as an infinite series of Chebyshev polynomials with coefficients $\phi_n$,

$$\phi(z) = \sum_{n=0}^{\infty} \phi_n T_n(z). \tag{9.31}$$

Now substituting this into the Orr-Sommerfeld equation we obtain,

$$(U-c)\left(\frac{\mathrm{d}^2}{\mathrm{d}z^2} - \alpha^2\right)\sum_{n=0}^{\infty}\phi_n T_n - U''\sum_{n=0}^{\infty}\phi_n T_n + \frac{i}{\alpha Re}\left(\frac{\mathrm{d}^2}{\mathrm{d}z^2} - \alpha^2\right)^2 \sum_{n=0}^{\infty}\phi_n T_n = 0. \tag{9.32}$$

Expanding and applying the differential operators,

$$\begin{aligned}(1-z^2)\sum_{n=0}^{\infty}\phi_n^{(2)}T_n - c\sum_{n=0}^{\infty}\phi_n^{(2)}T_n + c\alpha^2\sum_{n=0}^{\infty}\phi_n T_n - \alpha^2(1-z^2)\sum_{n=0}^{\infty}\phi_n T_n + 2\sum_{n=0}^{\infty}\phi_n T_n \\ + \frac{i}{\alpha Re}\left[\sum_{n=0}^{\infty}\phi_n^{(4)}T_n - 2\alpha^2\sum_{n=0}^{\infty}\phi_n^{(2)}T_n + \alpha^4\sum_{n=0}^{\infty}\phi_n T_n\right] = 0.\end{aligned} \tag{9.33}$$

Now we can rearrange the terms in (9.33) to begin formulating the generalized eigenvalue problem,

$$\begin{aligned}(1-z^2)\sum_{n=0}^{\infty}\phi_n^{(2)}T_n - \alpha^2(1-z^2)\sum_{n=0}^{\infty}\phi_n T_n + 2\sum_{n=0}^{\infty}\phi_n \\ + \frac{i}{\alpha Re}\left[\sum_{n=0}^{\infty}\phi_n^{(4)}T_n - 2\alpha^2\sum_{n=0}^{\infty}\phi_n^{(2)}T_n + \alpha^4\sum_{n=0}^{\infty}\phi_n T_n\right]T_n \\ = c\left[\sum_{n=0}^{\infty}\phi_n^{(2)}T_n - \alpha^2\sum_{n=0}^{\infty}\phi_n T_n\right].\end{aligned} \tag{9.34}$$

Now, we are required to calculate the form of the coefficients of the terms $(1-z^2)\mathrm{D}^2\phi$ and $(1-z^2)\phi$. Firstly we can rewrite the base flow, given by $U(z)$, in terms of Chebyshev polynomials,

$$U(z) = 1 - z^2 = \frac{1}{2}\left(T_0 - T_2\right). \tag{9.35}$$

This gives,

$$U\phi = \frac{1}{2}\left(T_0 - T_2\right)\sum_{n=0}^{\infty}\phi_n T_n. \tag{9.36}$$

In order to express The products of the Chebyshev polynomials emerging from the product of the base flow with the function $\phi(z)$, can be expressed as sum of Chebyshev polynomials by making use of the following recurrence relation. For integers $n$ and $m$ we have,

$$2T_n(z)T_m(z) = T_{n+m}(z) + T_{|n-m|}(z), \tag{9.37}$$

Using the recurrence relation to obtain a form for the coefficients when the term $U(z)\phi$ is expressed in terms of Chebyshev polynomials we have,

$$U\phi = \frac{1}{2}\sum_{n=0}^{\infty}\phi_n(T_0T_n - T_2T_n) = \frac{1}{2}\sum_{n=0}^{\infty}\phi_n\left(T_n - \frac{1}{2}\left(T_{n+2} + T_{|n-2|}\right)\right), \tag{9.38}$$

$$= \frac{1}{2}\sum_{n=0}^{\infty}\phi_nT_n - \frac{1}{4}\sum_{n=0}^{\infty}\phi_n\left(T_{n+2} + T_{|n-2|}\right), \tag{9.39}$$

$$= \frac{1}{2}\sum_{n=0}^{\infty}\phi_nT_n - \frac{1}{4}\sum_{n=0}^{\infty}\phi_nT_{n+2} - \frac{1}{4}\sum_{n=0}^{\infty}\phi_nT_{|n-2|}. \tag{9.40}$$

In order to obtain the form of the coefficients in terms of the zeroth derivative coefficients, we can expand the summations in (9.40) and group the coefficients of the $n$-th degree Chebyshev polynomial. The first few terms are given by the following,

$$\begin{aligned} U\phi = \left(\frac{1}{2}\phi_0 - \frac{1}{4}\phi_2\right)T_0 + \left(\frac{1}{4}\phi_1 - \frac{1}{4}\phi_3\right)T_1 + \left(\frac{1}{2}\phi_2 - \frac{1}{2}\phi_0 - \frac{1}{4}\phi_4\right)T_2 \\ + \left(\frac{1}{2}\phi_3 - \frac{1}{4}\phi_1 - \frac{1}{4}\phi_5\right)T_3 + \ldots. \end{aligned} \tag{9.41}$$

If we again make use of the coefficient $c_n$, where $c_0 = 2$ and $c_n = 1$ for $n > 0$, then the coefficient of the $n$-th Chebyshev polynomial can be written in the following form in the series,

$$U\phi = \sum_{n=0}^{\infty}\left[\phi_n - \frac{1}{4}\left(c_{n-2}\phi_{n-2} + \phi_n\left(c_n + c_{n-1}\right) + \phi_{n+2}\right)\right]T_n, \tag{9.42}$$

where $c_n = 0$ for $n < 0$. Similarly,

$$U\phi'' = \phi'' - z^2\phi'' = \sum_{n=0}^{\infty}\left[\phi_n^{(2)} - \frac{1}{4}\left(c_{n-2}\phi_{n-2}^{(2)} + \phi_n^{(2)}\left(c_n + c_{n-1}\right) + \phi_{n+2}^{(2)}\right)\right]T_n. \tag{9.43}$$

We must also express the boundary conditions in terms of Chebyshev polynomials. Here we use the important fact that Chebyshev polynomials take their extrema at either $-1$ or 1 on the interval $-1 \leq z \leq 1$, that is $T_n(1) = 1$ and $T_n(-1) = (-1)^n$.

$$\phi(1) = 0 \quad \Rightarrow \quad \sum_{n=0}^{\infty}\phi_n = 0, \tag{9.44}$$

$$\phi(-1) = 0 \quad \Rightarrow \quad \sum_{n=0}^{\infty}(-1)^n\phi_n = 0, \tag{9.45}$$

$$\phi'(1) = 0 \quad \Rightarrow \quad \sum_{n=0}^{\infty}n^2\phi_n = 0, \tag{9.46}$$

$$\phi'(-1) = 0 \quad \Rightarrow \quad \sum_{n=0}^{\infty}n^2(-1)^{n-1}\phi_n = 0, \tag{9.47}$$

Now in order to have computationally feasible numerical scheme we truncate at $N$ terms. We approximate the function $\phi(z)$ by,

$$\phi_N(z) = \sum_{n=0}^{N}\phi_nT_n. \tag{9.48}$$

Substituting this into the Orr-Sommerfeld equation, and using the facts obtained from the previous section e.g. there are $N-q$ terms for the $q$-th derivative where the coefficients are given by $\phi_n^{(q)}$.

$$\begin{aligned}(1-z^2)\sum_{n=0}^{N-2}\phi_n^{(2)}T_n - \alpha^2(1-z^2)\sum_{n=0}^{N}\phi_n T_n \\ +\frac{i}{\alpha Re}\Big[\sum_{n=0}^{N-4}\phi_n^{(4)}T_n - 2\alpha^2\sum_{n=0}^{N-2}\phi_n^{(2)}T_n + \alpha^4\sum_{n=0}^{N}\phi_n T_n\Big] + 2\sum_{n=0}^{N}\phi_n T_n \\ = c\left[\sum_{n=0}^{N-2}\phi_n^{(2)}T_n - \alpha^2\sum_{n=0}^{N}\phi_n T_n\right].\end{aligned} \tag{9.49}$$

The coefficients corresponding to the product of the base velocity with the eigenfunction and its second derivative may be rewritten in the form (9.42) and (9.43) respectively. Thus,

$$\begin{aligned}\sum_{n=0}^{N-2}\left[\phi_n^{(2)} - \frac{1}{4}\left(c_{n-2}\phi_{n-2}^{(2)} + \phi_n^{(2)}\left(c_n + c_{n-1}\right) + \phi_{n+2}^{(2)}\right)\right]T_n \\ -\alpha^2\sum_{n=0}^{N}\left[\phi_n - \frac{1}{4}\left(c_{n-2}\phi_{n-2} + \phi_n\left(c_n + c_{n-1}\right) + \phi_{n+2}\right)\right]T_n \\ +\frac{i}{\alpha Re}\left[\sum_{n=0}^{N-4}\phi_n^{(4)}T_n - 2\alpha^2\sum_{n=0}^{N-2}\phi_n^{(2)}T_n + \alpha^4\sum_{n=0}^{N}\phi_n T_n\right] + 2\sum_{n=0}^{N}\phi_n T_n \\ = c\left[\sum_{n=0}^{N-2}\phi_n^{(2)}T_n - \alpha^2\sum_{n=0}^{N}\phi_n T_n\right].\end{aligned} \tag{9.50}$$

The final step in forming our numerical scheme is to take the inner product $N-4$ times. This gives us the system of equations which will be put into matrix formulation and solved as a generalized eigenvalue problem. By taking the inner product $N-4$ times, we obtain $N-3$ equations in $N-1$ unknowns. However in the series expansion there are $N+1$ unknowns given by $\phi_0, \phi_1, \ldots, \phi_N$. Therefore by the spectral-tau method, the remaining unknowns are determined by adding the boundary conditions to the system of equations. This gives a complete system of $N+1$ equations for $N+1$ unknowns which can be solved.

$$\begin{aligned}\phi_n^{(2)} - \frac{1}{4}\big(c_{n-2}\phi_{n-2}^{(2)} + \phi_n^{(2)}(c_n + c_{n-1}) + \phi_{n+2}^{(2)}\big) \\ -\alpha^2\big[\phi_n - \frac{1}{4}\big(c_{n-2}\phi_{n-2} + \phi_n(c_n + c_{n-1}) + \phi_{n+2}\big)\big] \\ +2\phi_n + \frac{i}{\alpha Re}\big(\phi_n^{(4)} - 2\alpha^2\phi_n^{(2)} + \alpha^4\phi_n\big) = c\big[\phi_n^{(2)} - \alpha^2\phi_n\big], \\ \text{for} \quad n = 0, 1, 2, \ldots, N-4.\end{aligned} \tag{9.51}$$

Now formulating the coefficients of the Chebyshev polynomial and the coefficients corresponding to the derivatives in matrix notation, we can first note that the terms involving

$U(z)$ can be expressed in the form $\mathrm{Q}\mathbf{\Phi}$. The matrix Q is defined as follows,

$$\begin{pmatrix} \frac{1}{2} & 0 & -\frac{1}{4} & 0 & 0 & \cdots & 0 & 0 & 0 & 0 \\ 0 & \frac{1}{4} & 0 & -\frac{1}{4} & 0 & \cdots & 0 & 0 & 0 & 0 \\ -\frac{1}{2} & 0 & \frac{1}{2} & 0 & -\frac{1}{4} & \cdots & 0 & 0 & 0 & 0 \\ 0 & -\frac{1}{4} & 0 & \frac{1}{2} & 0 & \ddots & 0 & 0 & 0 & 0 \\ \vdots & \cdots & \ddots & \ddots & \ddots & \ddots & \ddots & \vdots & 0 & 0 \\ 0 & \cdots & \cdots & -\frac{1}{4} & 0 & \frac{1}{2} & 0 & -\frac{1}{4} & 0 & 0 \\ 0 & \cdots & \cdots & \cdots & \cdots & 0 & 0 & 0 & 0 & 0 \\ 0 & \cdots & \cdots & \cdots & \cdots & 0 & 0 & 0 & 0 & 0 \\ 0 & \cdots & \cdots & \cdots & \cdots & 0 & 0 & 0 & 0 & 0 \\ 0 & \cdots & \cdots & \cdots & \cdots & 0 & 0 & 0 & 0 & 0 \end{pmatrix} \begin{pmatrix} \phi_0 \\ \phi_1 \\ \phi_2 \\ \vdots \\ \vdots \\ \vdots \\ \phi_{N-1} \\ \phi_N \end{pmatrix} = \mathrm{Q}\mathbf{\Phi}. \tag{9.52}$$

Moreover formulating the product of the second derivative of $\phi$ with the base flow $U(z)$ we have,

$$\phi_n^{(2)} - \frac{1}{4}\left(c_{n-2}\phi_{n-2}^{(2)} + \phi_n^{(2)}\left(c_n + c_{n-1}\right) + \phi_{n+2}^{(2)}\right), \quad n = 0, 1, 2, \ldots, N-4, \tag{9.53}$$

which in matrix formulation takes the form,

$$\mathrm{QE}^2\mathbf{\Phi}. \tag{9.54}$$

In summary, we have the following system of equations defining our generalized eigenvalue problem $\mathrm{A}\mathbf{\Phi} = c\mathrm{B}\mathbf{\Phi}$, where the matrices are defined by the equations for the coefficients.

$$\left[\mathrm{QE}^2 - \alpha^2\mathrm{Q} + 2\mathrm{I} + \frac{i}{\alpha Re}\left(\mathrm{E}^4 - 2\alpha^2\mathrm{E}^2\mathrm{I} + \alpha^4\mathrm{I}\right)\right]\mathbf{\Phi} = c\left(\mathrm{E}^2 - \alpha^2\mathrm{I}\right)\mathbf{\Phi}, \tag{9.55}$$

where I is the identity matrix with the final four rows filled with zeros only. The boundary conditions complete the entries in final four rows,

$$\phi(1) = 0 \quad \Rightarrow \quad \sum_{n=0}^{N}\phi_n = 0, \tag{9.56}$$

$$\phi(-1) = 0 \quad \Rightarrow \quad \sum_{n=0}^{N}(-1)^n\phi_n = 0, \tag{9.57}$$

$$\phi'(1) = 0 \quad \Rightarrow \quad \sum_{n=0}^{N}n^2\phi_n = 0, \tag{9.58}$$

$$\phi'(-1) = 0 \quad \Rightarrow \quad \sum_{n=0}^{N}n^2(-1)^{n-1}\phi_n = 0. \tag{9.59}$$

The complete generalized eigenvalue problem to be solved is given by (9.55)-(9.59). The structure of the matrix on the right-hand side of (9.55) is well ordered as it is upper triangular. On the left-hand side of (9.55) it is not surprising the structure is somewhat more complicated as there are a range of derivatives and cross products involving those derivatives. Overall the left-hand side of (9.55) is a linear combination of pentadiagonal matrices from the matrix Q and upper triangular matrices from the matrix E. This generalized eigenvalue problem will solve for the complex eigenvalues given by $c$ and the eigenvectors $\mathbf{\Phi}$ which are vectors of coefficients of the truncated Chebyshev series. In the next section the numerical results from solving this generalized eigenvalue problem are discussed.

# 10 Numerical results of the spectral-tau method

The key difference in using spectral methods to solve the Orr-Sommerfeld eigenvalue problem is that spectral methods have far superior error properties when compared with simple finite-difference schemes. In the formulation of the Orr-Sommerfeld eigenvalue problem with finite-difference methods, the numerical scheme was constructed so that it had second-order convergence. Finite-difference methods take the local approach of approximation, whereas spectral methods take the global approach of approximation. For this reason the error properties improve rapidly as the number of Chebyshev polynomials used increases. In this section we will analyse and discuss the numerical results of implementation of the spectral-tau method to the Orr-Sommerfeld eigenvalue problem formulated in the previous section.

We can begin by first demonstrating the high accuracy achieved by spectral methods at very little computational cost. The table below shows the least stable eigenvalue for $(Re, \alpha) = (5772.22, 1.02056)$ with increasing number of Chebyshev polynomials used in the series expansion.

| $N$ | c | Run time (secs) |
|---|---|---|
| 38 | $0.26400095 + 4.3i(-7)$ | 0.000894 |
| 50 | $0.26400174 - 3.1i(-9)$ | 0.001465 |
| 64 | $0.26400174 - 3.0i(-9)$ | 0.002613 |
| 86 | $0.26400174 - 3.1i(-9)$ | 0.004942 |
| 100 | $0.26400174 - 3.2i(-9)$ | 0.009740 |
| 120 | $0.26400174 - 6.6i(-10)$ | 0.013643 |

TABLE. 7 Least stable eigenvalue for $Re = 5772.22$ and $\alpha = 1.02056$ with the number of Chebyshev polynomials $N$ used and the run time in seconds.

The high accuracy gained from using the spectral-tau formulation to solve the Orr-Sommerfeld problem is evident from the approximation to the least stable eigenvalue in table 7. For $N > 38$ the real part of least stable eigenvalue is accurate to eight decimal places with the value $\mathbb{R}e(c_{crit}) = 0.26400174$, thus demonstrating the rapid convergence of spectral methods. Furthermore it turns out the spectral-tau method gives an accurate approximation to ten decimal places for $N > 50$. Moreover the computational expense is clearly very small since the run time is so short. The main reason for this is that the matrices in the generalized eigenvalue problem are relatively small therefore this reduces the number of operations required to solve the problem. In general it takes of order $N^3$ operations to solve an eigenvalue problem and the consistent structure of the matrices arising from the recurrence relations for Chebyshev polynomials allows the system of equations to be solved much more quickly.

In the formulation of the spectral-tau method one can confine the search of the least stable mode to symmetric modes only. This means that in the Chebyshev series expansion approximating the solution contains only even order Chebyshev polynomials, that is the coefficients $\phi_n = 0$ for $n$ odd. This approach was taken by Orszag (1971). In the formulation of the spectral-tau method discussed here, this fact was not used to confine the search for the least stable mode. However the orders of the coefficients obtained by

solving the generalized eigenvalue problem for $(Re, \alpha) = (5772.22, 1.02056)$, are found to be $\mathcal{O}(10^{-10})$ for $\phi_n$ where $n$ is odd. Whereas the magnitude of the coefficients $\phi_n$ for even $n$ is $\mathcal{O}(10^{-1})$. Hence, as expected, the contributions to the sum of Chebyshev polynomials are dominated by even order Chebyshev polynomials.

## 10.1 Analysis of spurious eigenvalues

The values of the spurious eigenvalues obtained as artifacts in the solution to the Orr-Sommerfeld equation are shown in table 8 with a varying number of Chebyshev polynomials. The values corresponding to the two spurious eigenvalues for $N = 38$ and $N = 50$ are in agreement with those found by McFadden *et al.* (1990). As the accuracy of the non-spurious most unstable eigenvalue increases (to a value $0.237526489 + 0.003739671i$ for $N = 80$), we observe that the magnitudes of the spurious eigenvalues have increased significantly. Therefore the spurious eigenvalues increase rapidly in magnitude as the number of Chebyshev polynomials retained in the solution is increased. The Orr-Sommerfeld equation is not a time-dependent system, however for systems which involve time derivatives, these non-physical eigenvalues cause severe numerical instability (McFadden *et al.*, 1990). The presence of these spurious eigenvalues in the numerical results means that more care is required when selecting the least stable eigenvalue from the eigenvalue spectrum generated.

| $N$ | First three unstable eigenvalues |
|---|---|
| 38 | 0.054299574 + 178.0472006i |
| | 0.057820287 + 158.7554783i |
| | 0.237526758 + 0.003734266i |
| 50 | 0.040926078 + 563.5511540i |
| | 0.042880923 + 517.4762544i |
| | 0.237526481 + 0.003739669i |
| 80 | 0.025353499 + 3934.202516i |
| | 0.026076848 + 3734.835654i |
| | 0.237526489 + 0.003739671i |

TABLE. 8 First three unstable eigenvalues for $Re = 10,000$ and $\alpha = 1.0$ with the number of Chebyshev polynomials $N$ used.

As reported by McFadden *et al.* (1990) the removal of these eigenvalues can be achieved by employing the vorticity-stream-function formulation of the Orr-Sommerfeld equation, or by modifying the Galerkin approach. However a more direct modification of the usual Chebyshev-tau formulation can be made to eliminate the spurious eigenvalues. We may begin by considering the $N - 3$ equations for the coefficients produced by the Chebyshev-tau method. Thus, recalling the system of equations given by (9.51) with the

four boundary conditions,

$$\begin{aligned}\phi_n^{(2)} - \frac{1}{4}\big(c_{n-2}\phi_{n-2}^{(2)} + \phi_n^{(2)}(c_n + c_{n-1}) + \phi_{n+2}^{(2)}\big) \\ -\alpha^2\big[\phi_n - \frac{1}{4}\big(c_{n-2}\phi_{n-2} + \phi_n(c_n + c_{n-1}) + \phi_{n+2}\big)\big] \\ +2\phi_n + \frac{i}{\alpha Re}\big(\phi_n^{(4)} - 2\alpha^2\phi_n^{(2)} + \alpha^4\phi_n\big) = c\big[\phi_n^{(2)} - \alpha^2\phi_n\big], \\ \text{for} \quad n = 0, 1, 2, \ldots, N-4.\end{aligned} \tag{10.1}$$

The modification to the Chebyshev-tau method described by McFadden *et al.* (1990) is as follows. While the left-hand side of the equation is left unchanged, the term corresponding to the second derivative on the right-hand side is altered. The normal form of the second derivative of the infinite sum truncated at $N$ is given by,

$$c_n\phi_n^{(2)} = \sum_{\substack{k=n+2 \\ k\equiv n \bmod 2}}^{N} k(k^2 - n^2)\phi_k. \tag{10.2}$$

However, the summation is modified so that the final two columns representing the matrix representing the second derivative are set to zero. In other words the second derivative is represented in the following way,

$$c_n\hat{\phi}_n^{(2)} = \sum_{\substack{k=n+2 \\ k\equiv n \bmod 2}}^{N-2} k(k^2 - n^2)\phi_k. \tag{10.3}$$

Hence the modified form system of equations given by the coefficients is given by,

$$\begin{aligned}\phi_n^{(2)} - \frac{1}{4}\big(c_{n-2}\phi_{n-2}^{(2)} + \phi_n^{(2)}(c_n + c_{n-1}) + \phi_{n+2}^{(2)}\big) \\ -\alpha^2\big[\phi_n - \frac{1}{4}\big(c_{n-2}\phi_{n-2} + \phi_n(c_n + c_{n-1}) + \phi_{n+2}\big)\big] \\ +2\phi_n + \frac{i}{\alpha Re}\big(\phi_n^{(4)} - 2\alpha^2\phi_n^{(2)} + \alpha^4\phi_n\big) = c\big[\hat{\phi}_n^{(2)} - \alpha^2\phi_n\big], \\ \text{for} \quad n = 0, 1, 2, \ldots, N-4.\end{aligned} \tag{10.4}$$

The result of this modification is that the spurious eigenvalues that were present in the normal Chebyshev-tau method are eliminated. Moreover this modification to the numerical scheme, produced from the spectral-tau implementation, results in essentially no loss in accuracy of the truely physical eigenvalues (McFadden *et al.*, 1990). In the numerical results reported by McFadden *et al.* (1990), it was found that in the approximation to the most unstable eigenvalue the modified Chebyshev-tau method $0.23752676 + 0.00373427i$ was less accurate than the unmodified Chebyshev-tau method $0.23752985 + 0.00373031i$ (to 8 d.p.), for $N = 38$ Chebyshev polynomials. However, for $N = 50$ Chebyshev polynomials, the approximation to the most unstable eigenvalue obtained by the modified method is found to coincide with that obtained with the unmodified method, giving a value $0.23752648 + 0.00373967i$ (McFadden *et al.*, 1990). Therefore, the simple modification outlined by McFadden *et al.* (1990) to the Chebyshev-tau method demonstrates that the spurious eigenvalues which are clearly non-physical can be eliminated from the numerical solution obtained via spectral-tau implementation. Moreover, this modification essentially does not result in any loss of accuracy.

## 10.2 Analysis of eigenvalue spectrum and most unstable eigenmodes

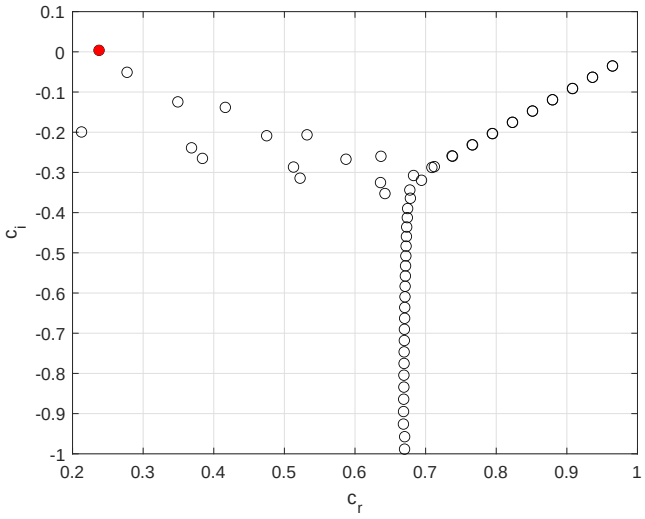


FIGURE. 13 Eigenvalue spectrum obtained by solving the Orr-Sommerfeld eigenvalue problem using the Spectral-tau method, using values $Re = 10,000$ and $\alpha = 1.0$. The least stable eigenvalue highlighted in red is $c_{crit} = 0.23752649 + 0.00373967i$ found using 120 Chebyshev polynomials.

The eigenvalue spectrum is shown in figure 13 with values $Re = 10,000$ and $\alpha = 1.0$, which has a value for the least stable eigenvalue of $c_{crit} = 0.23752649 + 0.00373967i$ which has been highlighted in red. The calculation and accuracy of this eigenvalue has been extensively discussed in the literature as a critical means of comparing methods of solving the Orr-Sommerfeld eigenvalue problem. Moreover it has been found that results are accurate to eight decimal places up to at least $Re = 50,000$ when more than 25 even-degree Chebyshev polynomials are used (Orszag, 1971). This has also been confirmed in the analysis of the results of this implementation of the spectral-tau method. In this case both odd and even order Chebyshev polynomials were used, where it was found that using all Chebyshev polynomials up to and including $T_{51}(z)$ the approximation to $c_{crit}$ was found to be $0.23752648 + 0.00373967i$, where 25 even-order Chebyshev polynomials exactly have been used. The approximation to the eigenvalue found using all Chebyshev polynomials up to and including $T_{52}(z)$ was found to be $0.23752649 + 0.00373967i$, which is indeed accurate to eight decimal places. Thus confirming a key inference from the study of the accuracy of the eigenvalues.

The structure of the eigenvalue spectrum, as expected, is similar to that seen before for values $Re = 5772.22$ and $\alpha = 1.02056$. However in this case more Chebyshev polynomials were required to capture the detail of the spectrum as the Reynolds number $Re = 10,000$ used was much higher. The eigenvalue spectrum shown in figure 13 was created using 120 Chebyshev polynomials, it was also found that to obtain the known structure of the eigenvalue spectrum for $Re = 5772.22$ and $\alpha = 1.02056$ at least 93 Chebyshev polynomials are required. When 93 Chebyshev polynomials were used to create the eigenvalue spectrum for $Re = 10,000$ and $\alpha = 1.0$ the structure of the spectrum had the distinctive branches close to the line $c_i = 0$, however there was a lack of detail in the lower branch that extends down the plane parallel with $c_r = 0$. Although the least stable eigenvalue

(highlighted in red) has been found in the upper left branch of the spectrum, we note that there are fast modes (where $c_r$ is close to 1) in the upper right branch. These fast modes have a corresponding phase speed $c_r$ which is close to that of the velocity taken at the centreline of the channel. Although they are stable (as $c_i < 0$), the closer $c_i$ is to zero the more weakly damped the fast mode is. Below a table of the ten least stable eigenvalues is shown.

| Mode number | Eigenvalue |
|---|---|
| 1 | $0.23752649 + 0.00373967i$ |
| 2 | $0.96463092 - 0.03516728i$ |
| 3 | $0.96464251 - 0.03518658i$ |
| 4 | $0.27720434 - 0.05089873i$ |
| 5 | $0.93631654 - 0.06320150i$ |
| 6 | $0.93635178 - 0.06325157i$ |
| 7 | $0.90798305 - 0.09122274i$ |
| 8 | $0.90805633 - 0.09131286i$ |
| 9 | $0.87962729 - 0.11923285i$ |
| 10 | $0.87975570 - 0.11937073i$ |

TABLE. 9 Ten least stable eigenvalues for $\alpha = 1.0$ and $Re = 10,000$.

The table above showing the ten least stable eigenvalues show the distribution of the eigenvalues close to the line $c_i = 0$ in the complex plane. The least stable eigenvalue is always found to be in the upper left branch of eigenvalue spectrum, this is demonstrated by the neutral stability curve of the phase speed. That is the phase speed of the least stable mode for any given Reynolds number $Re$ and wavenumber $\alpha$ does not exceed a value of approximately 0.264, which is a fraction of the maximum velocity in the channel taken at the centreline. From table 9 we observe that for the ten least stable eigenvalues all mode numbers except 1 and 4 correspond to a modal pair. Therefore the ten least stable eigenvalues are dominated by fast modes with eigenvalues in the upper right branch of the eigenvalue spectrum. It is difficult to see the modal pairs in figure 13, however towards the lower part of the upper right branch one can observe there are two eigenvalues where much of their circles overlap. The values of these eigenvalues are approximately $0.7089 - 0.2877i$ and $0.7123 - 0.2855$. The modal pairs of 2 and 3 are the least stable of all the modals pairs in the spectrum and the fastest with phase speeds of $c_r = 0.96463092$ and $c_r = 0.96464251$ for the mode 2 and 3 respectively.

In figures 14-16 the eigenfunctions, contour plots of the normal velocity and the vector field plots corresponding to the three least stable eigenvalues are shown. We may recall the form of the vector field of the perturbation wave,

$$\begin{pmatrix} \hat{u} \\ \hat{w} \end{pmatrix} = \begin{pmatrix} \phi'(z) \\ -i\alpha\phi(z) \end{pmatrix} e^{i\alpha(x-ct)}. \tag{10.5}$$

The derivative coefficients are easily obtained numerically by making use of the matrix formulation derived in section 9. The eigenfunction in figure 14a corresponding to the least stable eigenvalue $c_{crit} = 0.23752649 + 0.00373967i$ is symmetric as expected. The

contour plot of the normal velocity $\hat{w}$, in figure 14b shows the locations in the channel where the magnitude of $z$-coordinate is at its largest. In this case these locations are found at the centre of the channel, where in figure 14c the arrows are parallel to the $z$-axis directed downwards or upwards.

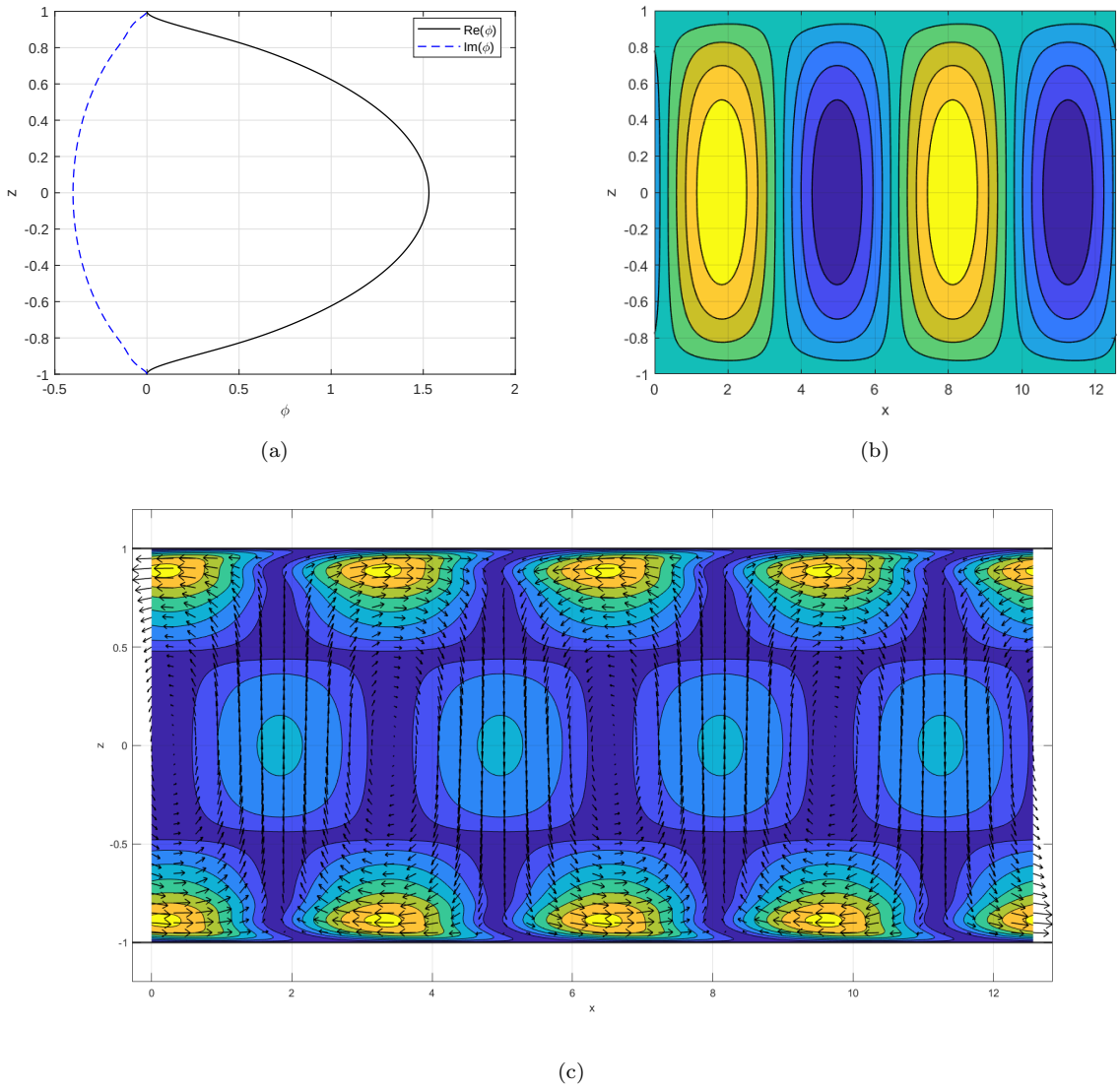


(a) (b)

(c)

FIGURE. 14 (a) Eigenfunction; (b) Contours of the normal velocity $\hat{w}$; (c) Vector field with contours over two cycles of the perturbation wave, corresponding to the least stable eigenvalue $c_{crit} = 0.23752649 + 0.00373967i$ found with $Re = 10000$ and $\alpha = 1.0$.

The contour plot displayed underneath the vector field in figure 14c is a contour of the magnitude of the vectors. We observe around the centreline of the channel, that the magnitude of the $z$-coordinate given by $\hat{w}$ is much larger when compared with the $x$ coordinate $\hat{u}$. Conversely, near the boundaries at $z = \pm 1$ the vector field almost parallel with the $x$-axis. It is known from Howard's semicircle theorem that the complex phase speed $c$ for any unstable mode must lie within a semicircle in the upper half-plane (Howard, 1961). The size of the semicircle is determined by the range of the base flow $U(z)$, which is $[0, 1]$ since the problem has been non-dimensionalised. Hence for the fast modes which form modal pairs, the phase speed are very close to the maximum velocity

in the channel taken at the centreline. In figures 15 and 16, there are similar plots to figure 14, however the second and third least stable eigenvalues are used respectively.

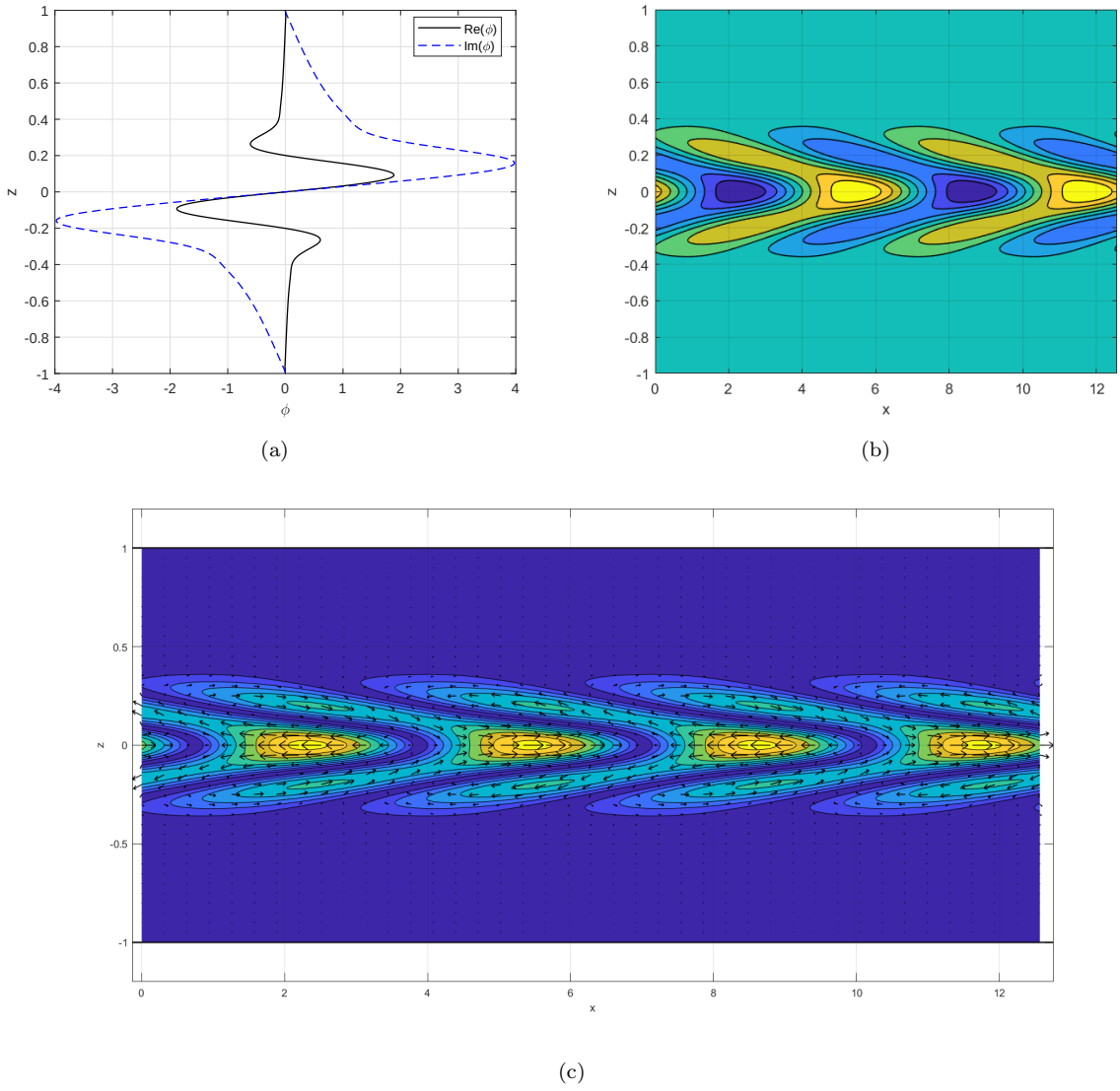


(a) (b)

(c)

FIGURE. 15 (a) Eigenfunction; (b) Contours of the streamwise velocity $\hat{u}$; (c) Vector field with contours over two cycles of the perturbation wave, corresponding to the second least stable eigenvalue $c = 0.96463092 - 0.03516728i$ found with $Re = 10,000$ and $\alpha = 1.0$.

The second and third least stable eigenvalues give rise to a pair of antisymmetric and symmetric eigenfunctions. Clearly from figure 15a, the eigenfunction with corresponding eigenvalue $c = 0.96463092 - 0.03516728i$ is antisymmetric and from figure 15a the eigenfunction is symmetric, where the corresponding eigenvalue is $c = 0.96464251 - 0.03518658i$. In figure 15c the structure of the contour plot of the streamwise velocity in the channel is related to the magnitude of the derivative of the eigenfunction. The normal component in the vector field given by $\hat{w}$ has values that are only $\mathcal{O}(1)$, whereas the streamwise component $\hat{u}$ has values that are $\mathcal{O}(10)$. This explains why the shape of the contours in the vector field is much more similar to that in the streamwise velocity contour in comparison to the normal velocity contour. Furthermore in figure 15c the plot of the vector field demonstrates the antisymmetry of the eigenfunction as all

arrows on the centreline $z = 0$ are parallel with the $x$-axis.

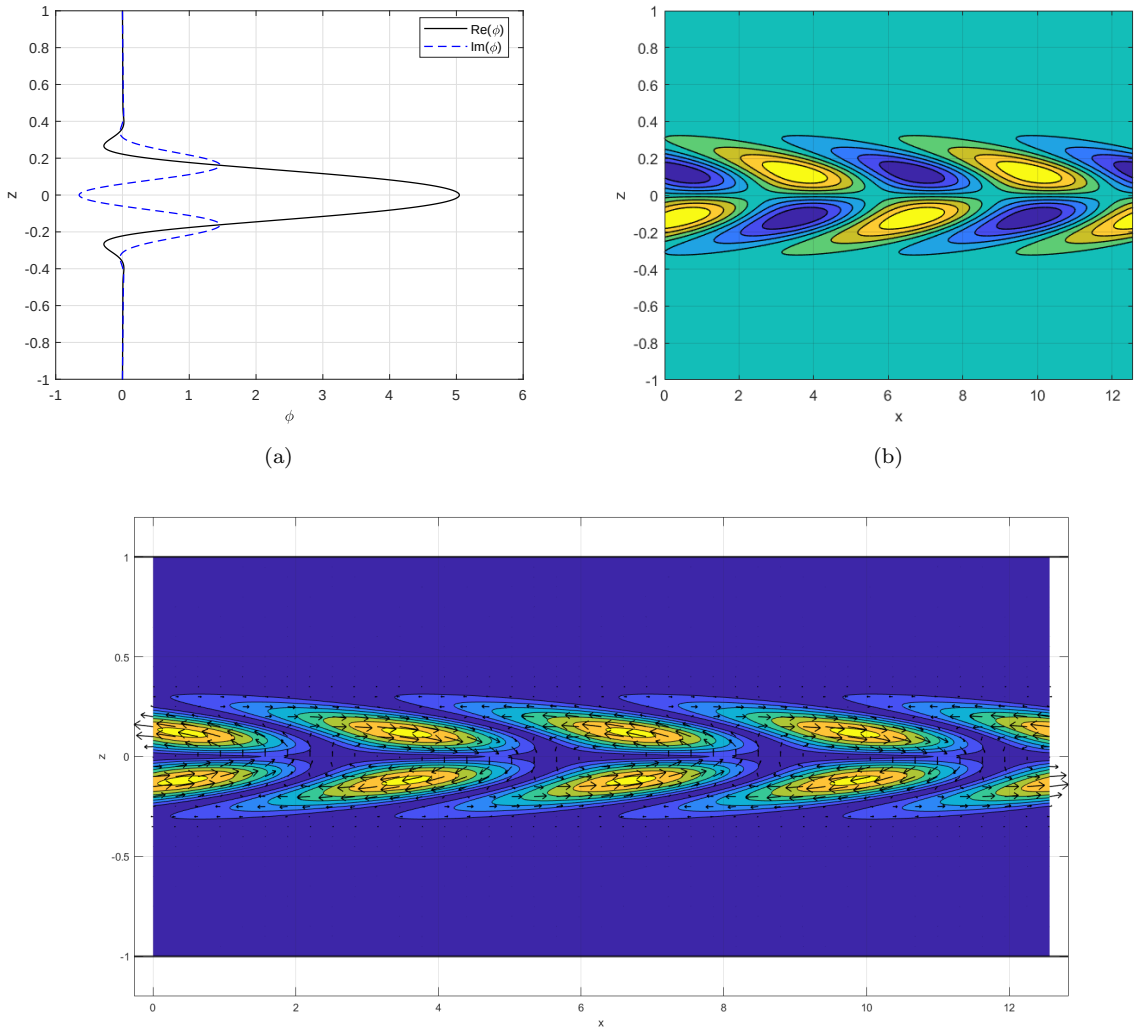


(a) (b)

(c)

FIGURE. 16 (a) Eigenfunction; (b) Contours of the streamwise velocity $\hat{u}$; (c) Vector field with contours over two cycles of the perturbation wave, corresponding to the second least stable eigenvalue $c = 0.96464251 - 0.03518658i$ found with $Re = 10,000$ and $\alpha = 1.0$.

The symmetry in the eigenfunction shown in figure 16a is also seen in the contour plot of the streamwise velocity $\hat{u}$ in figure 16b. Since the eigenfunction is symmetric the magnitude of the derivative is independent of the sign of $z$, however the sign of the derivative of is dependent on the sign of $z$. Hence there is an antisymmetric relationship in the streamwise velocity, resulting in the difference in colours of the contours in figure 16b. Similar to figure 15, the magnitude of the values in the streamwise direction are much larger in comparison to the magnitude of the values in the normal direction. This is again why the dominant feature of the contours in figure 16c is the shape of the contours from the streamwise velocity.

The study surrounding the coalescence of modes and degeneracies in eigenvalues has been discussed as a possible mechanism of understanding the transition from laminar to turbulent flow. It has been shown previously that the transition Reynolds number

depends strongly on the initial disturbance level in the flow, thus demonstrating the importance of nonlinear effects in some experimental settings. A direct resonance in a physical system occurs when two (or more) wave modes coalesce (Koch, 1986). The physical importance of these resonances has been the subject of many studies in the literature as a means of attempting to understand the importance of mode coalescence in the transition to turbulence.

We may recall that the subcritical transition to turbulence that was termed as a secondary instability by Orszag and Patera (1983), where the critical Reynolds number corresponding to this instability is approximately $Re = 1000$. In a study conducted by Gustavsson (1981), it was found that the critical Reynolds numbers corresponding to resonances found were all much smaller than 1000, approximately the smallest Reynolds number for which transition has been observed experimentally. The resonances presented by Gustavsson (1981) were exact, however for a resonant-like behaviour to occur, it is sufficient to find eigenvalues that are close. Although the modal pairs for close eigenvalues do not exhibit resonance in the exact sense, they may still produce large amplitudes for some wavenumber combinations (Gustavsson, 1981). Gustavsson (1981) concluded that this suggests that nonlinear interactions between different resonances and/or secondary instabilities triggered by the resonances could play a role in the transition to turbulence. This again highlights the need to appeal to nonlinear theory, as the linear theory is not sufficient to understand the subcritical transition. The damping rate associated with the coalescence of two (or more) wave modes is important as it locally dictates the nature in which the mode grows. The modes will ultimately decay, however the algebraic growth may dominate the exponential decay locally if the coalescing modes are nearly neutral. This algebraic growth can lead to potentially large amplitudes and may initiate the nonlinear solution long before the exponentially growing mode does (Koch, 1986). It was concluded from Koch (1986) that spatial direct resonances between Orr-Sommerfeld modes are possible in plane Poiseuille flow, however turbulence is observed to set in before this response becomes large enough. In this sense then, the spatial degeneracy mechanism plays a passive role in transition in plane Poiseuille flow.

The temporal development of the responses among degeneracies in stable temporal Orr-Sommerfeld eigenmodes has also been studied to analyse if it could contribute to the transition mechanism. By analysing only six of the infinitely many degeneracies of plane Poiseuille flow, it was found that some degeneracies do exhibit temporal growth in amplitude (Shanthini, 1989). Degeneracy among higher eigenmodes with higher damping rates were also discussed, these correspond to a higher Reynolds number at which they contribute to the transition mechanism. Therefore these degeneracies may be of marginal importance from the transition viewpoint (Shanthini, 1989). Another conclusion drawn from the study carried out by Shanthini (1989) was that the time for which the degeneracy-response is in the growing phase is shown to be stretched for larger Reynolds numbers, meaning that the degeneracies are active for longer periods of time the larger the Reynolds number. The mathematically correct observation of Squire's theorem eliminates the requirement to consider the three-dimensional problem in search of the critical Reynolds to which plane Poiseuille flow becomes unstable. However it would appear that in order to understand possible reasons for subcritical transition, one must appeal to the nonlinear theory (not done here) and consider the effects three-dimensional perturbations as was done by Orszag and Patera (1983).

The pair of eigenvalues discussed in the plots in figures 15 and 16 correspond to $c = 0.96463092 - 0.03516728i$ and $c = 0.96464251 - 0.03518658i$ respectively. This nearly

degenerate pair of modes are not exactly degenerate as the values do not change when the order of truncation of the Chebyshev expansion is varied. This was the same conclusion arrived at by Orszag (1971) in the analysis of the 32 least stable eigenvalues. Below shown in figures 17a-17b is an example of a highly oscillatory antisymmetric eigenfunction with the vector field demonstrating the boundary layers moving in opposite directions adjacent to each other. The highly oscillatory nature of the antisymmetric eigenfunction is clearly

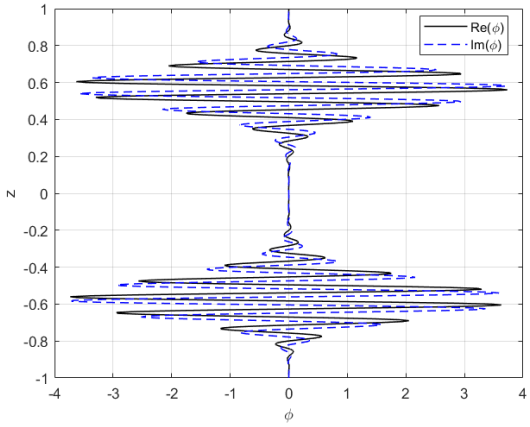


(a)

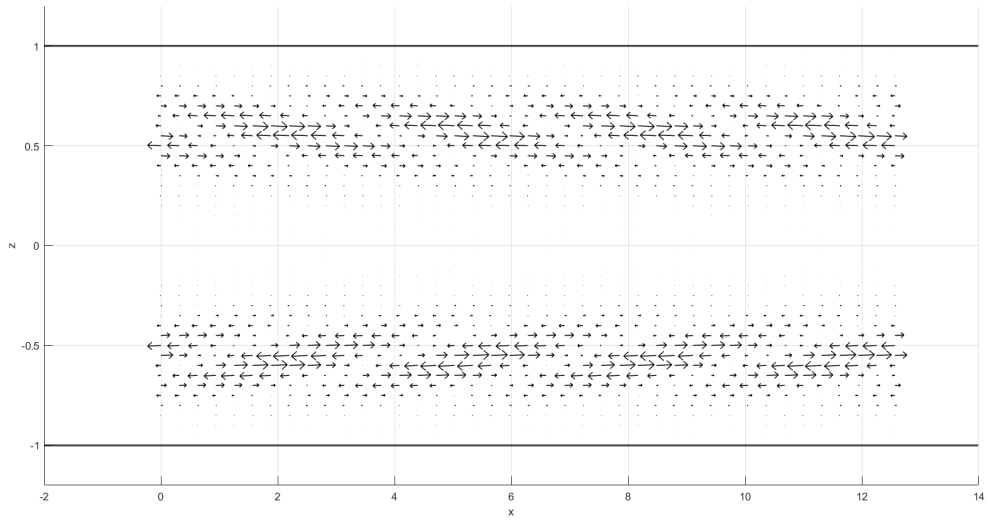


(b)

FIGURE. 17 (a) Eigenfunction; (b) Vector field, corresponding to the eigenvalue $c = 0.67133819 - 0.557665105i$ found with values $Re = 10,000$ and $\alpha = 1.0$.

visible in the plot of the vector field which is plotted over two cycles of the perturbation wave. As the gradient of the eigenfunction rapidly changes sign over the channel, the $x$-coordinate of the vector field $\hat{u}$ from equation (10.5) does as well. The phase speed of this mode given by $c_r = 0.67133819$ which is close to the average velocity in the channel $\mathrm{Re}(c) = \frac{2}{3}$ Orszag (1971). If we simply look to the eigenvalue spectrum again we observe that there are many eigenvalues with $\mathrm{Re}(c) \approx \frac{2}{3}$ located very close to each other in the lower branch of the spectrum, hence it appears that the majority of modes have a phase

speed of $\mathrm{Re}(c) \approx \frac{2}{3}$.

From figure 17b we once again observe the vector field with a corresponding highly oscillatory eigenfunction has many layers adjacent to each other travelling in opposite directions. If the no-slip condition is enforced then the velocity must decrease to zero as one approaches the boundary, the inertial forces outside the boundary layer must balance with the viscous forces which dominate outside the boundary layer. The boundary layers can be analysed by deriving the boundary layer equations from the two-dimensional, incompressible Navier-Stokes equations. This results in a parabolic system of partial differential equations, where scaling arguments must be used as the boundary layer is assumed to be very thin. Hence by introducing different scales for the $x$ and $z$ directions we can obtain the governing equations for boundary layers. The boundary conditions are derived by matching the flow inside the boundary layer to the flow outside the boundary layer. The characterisation and understanding of boundary layers is not only important in parallel flows but it is applicable to real situations particularly in aerodynamics and lubrication.

## 10.3 Curves of neutral stability

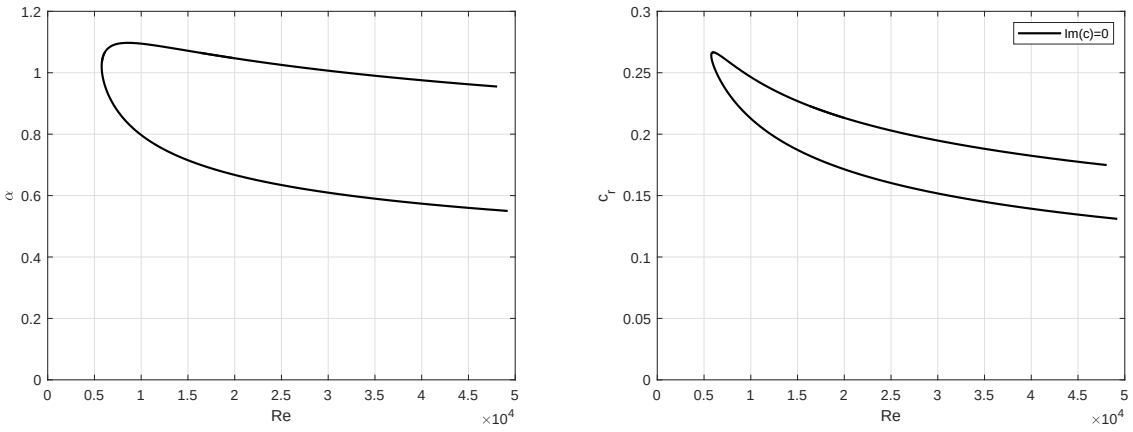


(a) (b)

FIGURE. 18 Neutral stability curves in the (a) $(Re, \alpha)$- (b) $(Re, c_r)$-planes.

The famous Newton-Raphson root-finding method was implemented numerically to obtain the neutral curves. A function was created that takes a Reynolds number, wavenumber and $N$ representing the number of Chebyshev polynomials used to solve the generalized eigenvalue problem as input. This function then returns the approximation to the least stable eigenvalue. The wavenumber $\alpha$ is fixed and the Reynolds number is varied up to $50,000$ to find at which Reynolds numbers the imaginary part of the least stable eigenvalue changes sign. Then, the root-finding method is used with guesses found from this process. It is known from table 7 that it is possible to solve the generalized eigenvalue problem approximately 40 times a second ($\frac{1}{0.023} \approx 43.5$). This coupled with the second-order convergence of the Newton-Raphson method allow for the computation of points on the neutral curves at relatively low cost.

For example, if we fix the wavenumber $\alpha = 1.02056$, we should expect the first Reynolds number that lies on this curve to be approximately $Re_{crit} = 5772.22$. A first-order central-difference scheme was used to approximate the derivative of the numerical function created. Although this would appear to be a limitation in converging to the root, the number of iterations taken to converge is still $\mathcal{O}(1)$. The accuracy of this approximation depends, not only on the number of Chebyshev polynomials used, but also on the threshold at which the Newton-Raphson method considers a value to have converged. In computing the neutral curve, the threshold of the magnitude of the correction to the guess of the Reynolds number was 1. Using this value as the threshold and with fixed wavenumber $\alpha = 1.02056$ yields approximations of 5772.22 and $26,254.29$ as the first and second time respectively the line $\alpha = 1.02056$ passes through the neutral stability curve.

One of the critical limitations of the Newton-Raphson method is that the method will fail to work if the derivative vanishes to zero. Therefore from the formulation discussed above, the Newton-Raphson method will fail to find the Reynolds number corresponding to the top of the neutral curve. In order to overcome this problem, the same root finding method was implemented where instead of fixing the wavenumber $\alpha$ the Reynolds number is fixed. The root-finding method then converges to a wavenumber that corresponds to a $(Re, \alpha)$ combination that lies on the neutral curve. The data obtained from using the root-finding algorithm is then also used to produce a curve of the phase speed, shown in figure 18b.

# 11 Comparison with finite-difference methods

In comparison to finite-difference approximations the exponential behaviour exhibited by the errors of spectral methods are far superior not only to the second-order finite-difference scheme employed here but to finite-difference schemes of higher orders. The implementation of the spectral method, usually achieved by collocation, Galerkin or tau techniques, has been extensively applied to many problems in fluid mechanics due to the excellent error properties. The solution to the Orr-Sommerfeld eigenvalue problem has been found using both finite-difference methods and the spectral-tau approach, and in this section the various properties of these methods will be compared by analysing the numerical results obtained. If we wish to obtain a reasonably accurate solution to the Orr-Sommerfeld problem, then the time taken to solve the generalized eigenvalue problem outlined in the finite-difference approach is known to be very high. For this reason we can compare the spectral method with the local iterative method employed to obtain an approximation of higher accuracy to the least stable eigenvalue.

## 11.1 Comparison of the local iterative method and the spectral-tau method

In order to compare the local iterative method with the spectral-tau method we can analyse the accuracy achieved by both methods and the associated run times in seconds to achieve a particular degree of accuracy. The corresponding run time for both methods is used a means of quantifying the computational expense to achieve comparatively accurate results. In table 10 and table 11 approximations to the least stable eigenvalue are shown. These approximations to the least stable eigenvalue correspond to the onset of instability in plane Poiseuille flow, that is the following critical values for the parameters are used $(Re, \alpha) = (5772.22, 1.02056)$ in the numerical methods employed here. The main difference in these methods is that the local iterative method only provides an approximation to the least stable eigenvalue and the corresponding eigenfunction, whereas the spectral-tau method solves the full Orr-Sommerfeld eigenvalue problem.

The computational expense of converging to an approximation to the least stable eigenvalue to an accuracy of five decimal places is significantly greater if the local iterative method is used in comparison to the spectral-tau method. From table 10 and table 11 we observe that the spectral-tau approach requires approximately 40 Chebyshev polynomials in order to provide an accuracy of five decimal places, whereas the local iterative method requires $N = 8192$ grid points over the channel to achieve the same accuracy. The corresponding eigenvalue problem from the spectral-tau approach is relatively small and the associated run time is therefore very small, taking only 0.000954 seconds to solve the generalized eigenvalue problem.

On the other hand the local iterative method takes approximately 1058.745 seconds to be accurate to five decimal places $0.26400257 - 0.00000132i$, this significantly larger run time is due to the fact that $N = 8192$ grid points are required. Furthermore there are two unknowns at each nodal grid point as the local iterative method is derived from the second-order finite-difference method employed prior, therefore at each iteration of the method a matrix with dimensions $16384 \times 16384$ must be inverted. Clearly this is extremely computationally expensive and is the primary reason for the large run time. Moreover, although the method generally converges to a given threshold in three or four iterations, the method is only second-order in comparison to the infinite-order convergence

| $N+1$ | $c$ | Factor of decrement of $\mathbb{I}m(c)$ | Run time |
|---|---|---|---|
| 25 | $0.2639901360 + 0.0016436578i$ | 0.538 | 0.000427 |
| 30 | $0.2640724022 + 0.0000562976i$ | 29.196 | 0.000637 |
| 35 | $0.2639943854 + 0.0000023313i$ | 24.148 | 0.000810 |
| 40 | $0.2640009500 + 0.0000004329i$ | 5.386 | 0.000954 |
| 45 | $0.2640017561 - 0.0000000096i$ | 45.146 | 0.001384 |
| 50 | $0.2640017405 - 0.0000000031i$ | 3.080 | 0.001753 |
| 55 | $0.2640017394 - 0.0000000031i$ | 1.017 | 0.001894 |
| 60 | $0.2640017396 - 0.0000000030i$ | 1.016 | 0.002482 |
| 65 | $0.2640017396 - 0.0000000030i$ | 0.996 | 0.003286 |
| 70 | $0.2640017397 - 0.0000000031i$ | 0.986 | 0.003350 |

TABLE. 10 Approximation to the least stable eigenvalue for critical values $(Re, \alpha) = (5772.22, 1.02056)$ obtained using the spectral-tau method (to 10 d.p). Also tabulated is the increasing number of Chebyshev polynomials $N+1$ retained in the truncation, factor of decrement of $\mathbb{I}m(c)$ and the associated run time in seconds to obtain the approximation.

| Grid points | $c$ | Factor of decrement of $\mathbb{I}m(c)$ | Run time |
|---|---|---|---|
| 1024 | $0.26405519 - 0.00008075i$ | 3.8169 | 1.371 |
| 2048 | $0.26401511 - 0.00002068i$ | 3.9048 | 8.030 |
| 4096 | $0.26400508 - 0.00000524i$ | 3.9501 | 70.797 |
| 8192 | $0.26400257 - 0.00000132i$ | 3.9697 | 1058.745 |

TABLE. 11 Approximation to the least stable eigenvalue for critical values $(Re, \alpha) = (5772.22, 1.02056)$ obtained using the second-order finite-difference method outlined previously. The factor of decrement of $\mathbb{I}m(c)$ is also tabulated along with the run time in seconds. The values in this table were obtained using an initial guess obtained from solving the generalized eigenvalue problem on $N = 256$ grid points.

exhibited by the spectral-tau method. If the number of grid points are doubled, the imaginary part of the least stable eigenvalue decreases by approximately a factor of four (see 3rd column in table 11). In order to invert an $N \times N$ matrix the number of operations is generally $\mathcal{O}(N^3)$, hence increasing the number of grid points by a factor of two increases the number of operations by a factor of eight. We note that to invert a matrix with dimensions $16384 \times 16384$ the number of operations is $\mathcal{O}(10^{12})$. Although the sparsity of the matrix is high, the run time of the local iterative algorithm is still high for $N = 8192$ grid points as $\mathcal{O}(10^{12})$ operations need to be performed at each iteration.

The numerical results shown in table 10 demonstrate the rapid convergence of the spectral method. We note that the real part of the least stable eigenvalue does not appear to improve with accuracy in the first three approximations. For example, if 25 Chebyshev polynomials are retained then the approximation to the real part $\mathbb{R}e(c) = 0.2640$ is accurate to four decimal places, when we compare it the value of the real part if 70 Chebyshev polynomials are retained $\mathbb{R}e(c) = 0.2640017397$. However, if the number of Chebyshev polynomials retained is increased to 35 the approximation to the real part of $c$ remains only correct to four decimal places, while the approximation to the imaginary

part of $c$ improves significantly. In the subsequent approximations to $c$ where the number of Chebyshev polynomials is increased beyond 45, we have rapid convergence to a value of $0.2640017397 - 0.0000000031i$ (obtained with 70 Chebyshev polynomials). Although the spectral-tau method exhibits the expected infinite-order convergence here as described by Orszag (1971), the number of Chebyshev polynomials must be increased in order to confirm convergence to the solution. If more Chebyshev polynomials are retained then the matrices in the generalized eigenvalue problem will increase in size, however this results in an eigenvalue problem that is only marginally more computationally expensive as one can see that the run time remains small.

The rapid convergence to an accurate solution of the Orr-Sommerfeld eigenvalue problem demonstrated by the spectral-tau method confirms the conclusions that were made by Orszag (1971), when spectral methods were first applied to study the linear stability of plane Poiseuille flow. The results shown here demonstrate not only the high accuracy of the solution but also that this accuracy is obtained very economically. These properties of spectral methods make them far superior to finite-difference methods and the local iterative method employed here. The second-order convergence of the local iterative method means that great computational expense is required to improve the accuracy of the solution. In the finite-difference implementation the method is known to exhibit second-order convergence, where doubling the number of grid points reduces $\mathbb{I}m(c)$ by a factor of four (for $(Re, \alpha) = (5772.22, 1.02056)$ as the parameter values). Therefore in order to reduce $\mathbb{I}m(c)$ by a factor of 64 we are required to increase the number of grid points by a factor of eight significantly increasing the computational expense required to converge to a solution for the local iterative method. In contrast, by retaining ten more Chebyshev polynomials in the truncation from 40 to 50 polynomials $\mathbb{I}m(c)$ is reduced by more than double this factor with a very marginal increase in computational expense. This clearly illustrates the limitation of a second-order method in comparison to the exponential convergence possessed by spectral methods.

Prior to the development and application of spectral methods to problems in fluid dynamics, finite-difference techniques were one of the few ways to obtain numerical approximations to complex differential equations. The solution obtained by Thomas (1953) replaced the fourth-order Orr-Sommerfeld equation with a difference system of the same order, with truncation error that involved the eighth derivative. In the study conducted by Thomas (1953) central-differences were used to obtain an approximation of $Re = 5780$ for the critical Reynolds number, which interestingly was the first solution to the Orr-Sommerfeld equation obtained by an electronic computer. The value of the least stable eigenvalue obtained by Thomas (1953) for $(Re, \alpha) = (5780, 1.026)$ was found to be $0.26457279 - 0.00000058i$. Thus, by using these finite-difference techniques and an early computer, Thomas (1953) achieved a reasonable estimation for the theoretical critical parameter values corresponding to the onset of instability of plane Poiseuille flow. This was a significant improvement over the numerical and asymptotic techniques that were being used at the time.

## 11.2 Computation of the critical Reynolds number

An accurate approximation of the theoretical critical Reynolds number has been sought after ever since the instability of plane Poiseuille flow was discovered. The work by Orszag (1971) produced the first accurate approximation to the critical Reynolds number of $Re = 5772.22$ with the first unstable mode appearing for $\alpha = 1.02056 \pm 0.00001$. By using

the Newton-Raphson root-finding method for fixed disturbances $\alpha$ on an interval about the level of disturbance for which the first unstable mode appears, we arrive at the same conclusion. That is, the critical Reynolds number is obtained with $\alpha = 1.02056 \pm 0.00001$ and is approximately $Re = 5772.22$. In a similar fashion to the computation of the neutral curve, the root-finding method is set up numerically so that the algorithm converges to a Reynolds number with $\mathbb{I}m(c) = 0$ for the corresponding least stable eigenvalue.

| $N$ | $Re_{crit}$ |
|---|---|
| 30 | 5736.27 |
| 40 | 5770.82 |
| 45 | 5771.96 |
| 50 | 5772.23 |
| 55 | 5772.22 |
| 60 | 5772.22 |
| 65 | 5772.22 |

TABLE. 12 Approximations to the critical Reynolds number obtained using the Newton-Raphson root-finding method for the fixed level of disturbance $\alpha = 1.02056$, with varying number of Chebyshev polynomials $N$ retained in the truncation.

| Grid points | $Re_{crit}$ |
|---|---|
| 1024 | 5821.89 |
| 2048 | 5784.81 |
| 4096 | 5775.40 |
| 8192 | 5773.02 |
| $\infty$ | 5772.22 |

TABLE. 13 Approximations to the critical Reynolds number obtained using the Newton-Raphson root-finding method for the fixed level of disturbance $\alpha = 1.02056$, with varying number of grid points. The approximations to the least stable mode were made using the local iterative method derived from the second-order finite-difference scheme.

In table 12, the approximations to the critical Reynolds number obtained with $N$ Chebyshev polynomials are shown, where the spectral-tau method has been utilised to obtain approximations to the least stable eigenvalue. We observe that as the number of Chebyshev polynomials retained is increased the approximation does indeed converge a value of $Re = 5772.22$, which is in agreement with the widely accepted theoretical value for the critical Reynolds number. The behaviour observed here using the root-finding method can also been seen in table 10. The local iterative method derived from the finite-difference approach demonstrates clear second-order convergence by measuring the factor of the decrement in $\mathbb{I}m(c)$. Conversely for the spectral-tau method the factor of decrement of $\mathbb{I}m(c)$ does not clearly indicate the infinite-order of convergence in the same way the order of convergence is exhibited in the local iterative method. However the factor of decrement can still be analysed as we observe that the spectral method appears to have converged if 50 or more Chebyshev polynomials are retained in the truncation, as the factor of decrement of $\mathbb{I}m(c)$ is approximately 1. Now, in table 12, we observe that

the approximation has converged to a value of 5772.23 with $N = 50$ and $Re = 5772.22$ for $N \geq 55$. Therefore as we expected retaining $N > 50$ Chebyshev polynomials in the truncation the critical Reynolds number is approximately $Re_{crit} = 5772.22$.

Now, if the Newton-Raphson method is used in conjunction with the local iterative method to compute the critical Reynolds number, then the number of grid points used in the central-difference system dictate the accuracy instead of the number of Chebyshev polynomials retained. In table 13 the estimates of the critical Reynolds number are shown for a varying number of grid points used in the local iterative method. We observe that with $N = 1024$ grid points, the approximation for the critical Reynolds number is given by $Re = 5821.89$ which is a somewhat reasonable approximation for a second-order finite-difference scheme as the error is $\mathcal{O}(10)$. Moreover, we see that to achieve an approximation to the critical Reynolds number greater accuracy than Thomas, $N = 4096$ grid points are required by the local iterative method. The local iterative method is known to have second-order convergence, this is observed in the computation of the critical Reynolds number as the factor of decrement in the approximation is roughly a factor of four as the number of grid points are doubled. Therefore, if we extrapolate the number of grid points to $\infty$ we observe that the critical Reynolds number is indeed $Re = 5772.22$. In comparison to the utilisation of the spectral-tau method, an approximation of greater accuracy is more attainable and significantly less computationally expensive.

In summary the spectral-tau method is more accurate and less computationally expensive than the local iterative method employed. Although the iterative method derived from the finite-difference approach clearly has second-order convergence, this cannot compete with the infinite-order convergence demonstrated by the spectral-tau method. The finite order of accuracy exhibited by finite-difference approximations give errors that behave like a finite power of $1/N$ as $N \to \infty$, where $N$ is the number of grid points. In the case of second-order convergence the errors behave like $1/N^2$ as $N \to \infty$, whereas the Chebyshev polynomial approximations in the spectral-tau method give errors that decrease faster than any power of $1/N$ as $N \to \infty$ ($N$ is the number of Chebyshev polynomials retained in the truncation). Overall the local iterative method is an improvement, when compared to solving the generalized eigenvalue problem using finite-difference methods, as it reduces the computational expense to obtain features of the solution that we are truly concerned with.

# 12 Conclusions and discussion

The canonical problem in hydrodynamic stability theory of the critical flow speed at which laminar, plane Poiseuille flow becomes linearly unstable to travelling wave disturbances has been studied by the implementation of two numerical methods. In a similar fashion to the historic investigations and studies into the solution of the Orr-Sommerfeld eigenvalue problem, finite-difference methods were first applied here with the spectral approach utilised later. The numerical solution to the eigenvalue problem arising from the famous Orr-Sommerfeld equation was analysed in terms of the order of convergence, computational expense and accuracy achieved. As expected, the implementation of the spectral-tau method here has been shown to be far superior in computing an accurate solution to the Orr-Sommerfeld equation in comparison to that of a second-order finite-difference scheme. A local iterative method was also derived from the second-order central-difference system, which allowed for the computation of a more accurate approximation to the least stable mode at less computational expense than solving the whole eigenvalue problem. The spectral-tau approach, accomplished by expanding the solution to the eigenvalue problem in terms of Chebyshev polynomials, was also proven to be superior to the local iterative method employed. The primary reason for the superiority of the spectral-tau method over this approach using finite-difference methods is their infinite-order convergence, which allows for a very accurate solution to be obtained by means of significantly less memory intensive computation.

In the formulation of the spectral-tau method it is clear the spectral implementation is more complicated than the finite-difference approach carried out earlier in this report. The spectral-tau method, which is often much simpler to formulate when compared with collocation or Galerkin techniques, is very useful if a parameter is required to be changed frequently. This is particularly useful in analysing the stability of plane Posieuille flow, as the Reynolds number $Re$ and wavenumber $\alpha$ parameters are frequently varied. By using the Newton-Raphson root-finding algorithm the neutral stability curves in the $(Re, \alpha)$ and $(Re, c_r)$ planes were computed using the spectral-tau method to compute the solution for a given set of parameter values $(Re, \alpha)$. A naive parameter search in the $(Re, \alpha)$ plane was employed to compute the neutral curves using the local iterative method to obtain values on the curve (corresponding to $\mathbb{I}m(c) = 0$). Furthermore by fixing the level of disturbance at $\alpha = 1.02056$ the critical Reynolds number was confirmed to be $Re_{crit} = 5772.22$ where the Newton-Raphson method was employed. This result along with the approximation to the least stable eigenvalue $0.26400174 - 6.6i(-10)$ are in strong agreement with the work conducted by Orszag (1971), where an accurate solution to the Orr-Sommerfeld equation was first obtained. The critical Reynolds number obtained by using finite-difference methods was found to be $Re_{crit} = 5773.02$ on $N = 8192$ grid points over the channel. This value is a reasonable approximation to the well-known value $Re = 5772.22$, as the central-difference scheme and local iterative method only have second-order convergence. Although this critical value was obtained with reasonably high computational expense, if one considers other implementations of finite-difference methods to solve the Orr-Sommerfeld eigenvalue problem, the accuracy of the approximation to the critical Reynolds number achieved here is very reasonable. The neutral curve obtained in the linear stability analysis conducted illustrates the regions in the $(Re, \alpha)$ plane where the flow is stable and unstable to infinitesimal disturbances. Furthermore, a curve of the speed at which the perturbation wave propagates was produced.

## 12.1 Extension to Poiseuille-Couette flow

In this investigation the conditions under which plane Poiseuille flow becomes linearly unstable were studied. Now if the boundaries adjacent to the viscous fluid are not required to be fixed, plane Poiseuille flow may be extended to a hybrid flow in which the parallel boundaries are allowed to move tangentially relative to one another. In the absence of a pressure gradient parallel to the channel walls, the movement of the boundaries of the flow results in a shear stress on the fluid inducing a flow, this is known as Couette flow. The combination of Couette and Poiseuille flow corresponds to a flow in which both channel boundaries may move tangentially relative to one another and a constant pressure gradient also acts on the fluid. This hybrid flow is known as Poiseuille-Couette flow. A diagram of Poiseuille-Couette flow is shown in figure 19 where the lower boundary is fixed and the upper boundary is moving to the right with velocity $u_w$. We observe the parabolic profile of plane Poiseuille flow is no longer symmetric about the centreline of the channel as the motion of the upper boundary induces a shear on the viscous fluid.

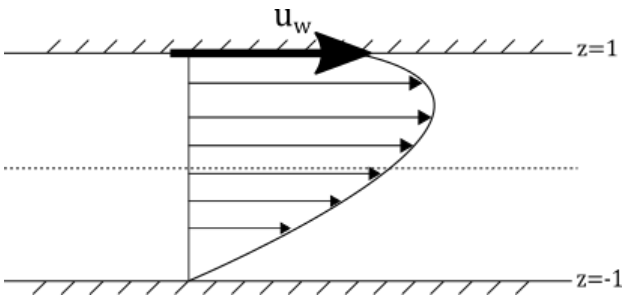


FIGURE. 19 Diagram of hybrid Poiseuille-Couette flow, where the upper boundary is moving to the right with velocity $u_w$ and the lower boundary is stationary.

The numerical solution to the linear stability problem concerning plane Poiseuille flow has been studied here with regard to two differing numerical schemes. From the numerical results of these methods, we have observed that plane Poiseuille flow is linearly unstable to two-dimensional infinitesimal disturbances with $Re > 5772.22$. If we once again consider the inviscid approximation then we arrive at the conclusion that plane Couette flow is inviscidly stable, by checking that the base flow $U(z) = z$ indeed has no inflection point (where the equations have been non-dimensionalised). Although the velocity profile of shear flow would seem simpler than that of plane Poiseuille flow, the determination of the stability of such a flow has proven more complex in comparison. Unlike plane Poiseuille flow it has been found that plane couette flow is linearly stable to infinitesimal disturbances, that is no unstable modes have been found to exist for all Reynolds numbers for waves of all lengths. This was demonstrated by Davey (1973) by use of asymptotic analysis and numerical computation of the least stable eigenvalue $c$ of the two dimensional Orr-Sommerfeld problem. Similar to plane Poiseuille flow, there are disagreements between the experimental results and the theoretical results. Experimentally it is known plane Couette flow is unstable for modest Reynolds numbers, thus it would seem the conclusions drawn from the linear stability analysis are in complete conflict with the physical evidence. By considering the combination of the two flows, the stability of the hybrid flow may be analysed.

The stability of plane Poiseuille flow is more easily understood as linear analysis yields a neutral curve (see figure 18a), whereas the stability of plane Couette flow is less understood as the linear stability analysis fails to predict a linear instability. As has

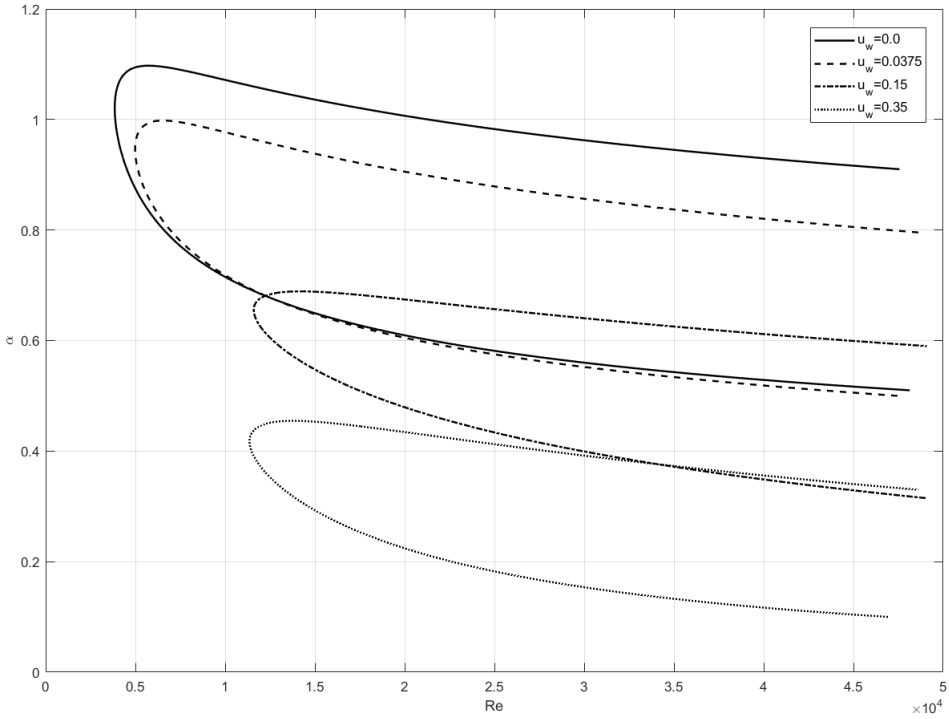


FIGURE. 20 Neutral stability curves (linear) of plane Poiseuille-Couette flow for boundary speeds, $u_w = 0$, $u_w = 0.0375$, $u_w = 0.15$ and $u_w = 0.35$, where the base velocity is given by $U(z) = \frac{3}{2}(1 - z^2) + u_w z$.

already been discussed the linear stability analysis of plane Poiseuille flow does not fully describe the transition to turbulence, as there are nonlinear effects that may contribute to subcritical transition under certain conditions. If the walls are kept stationary then we recover plane Poiseuille flow, hence by allowing the boundaries to move tangentially we introduce components of Couette flow, where the stability of the flow is then analysed. In figure 20 the effect of increasing the wall velocity on the stability of the flow to infinitesimal disturbances is illustrated, where the neutral curve is observed to move down the $Re$-$\alpha$ plane as the boundary speed increases.

The study carried out by Cowley and Smith (1985) analyses the hybrid Poiseuille-Couette flow in terms of both the linear and weakly nonlinear stability. The weakly nonlinear stability analysis, aims to describe the evolution of perturbations in the unstable regime, where the nonlinear terms previously neglected in the linear analysis become important. Instead of fixing one boundary and allowing one boundary to move tangentially, (without loss of generality) both boundaries move with the same speed $u_w$ but in opposite directions with an applied pressure gradient. By adding components of Couette flow to Poiseuille flow we may analyse the linear stability of the resultant flow by producing a linear neutral curve. As Couette flow is linearly stable it is natural to determine the speed of the boundary at which the contribution of Couette flow stabilizes the hybrid flow, that is the hybrid flow is stable to infinitesimal disturbances for wall speeds that exceed this speed and the neutral stability curve disappears. Cowley and Smith (1985) studied the stability of the hybrid flow for various values of the wall velocity $u_w$, so the 'cut off' velocity of $u_w^*$ at which each neutral curve disappears was determined. From

the analysis conducted two main neutral curves and one minor neutral curve were discovered, and Poiseuille-Couette flow was shown to be linearly stable above the cut-off value for the wall velocity $u_w^* = 0.5279$ (Cowley and Smith, 1985). That is above a wall velocity of approximately 53% of the mean velocity in the flow Poiseuille-Couette flow is stabilized and the neutral curves cease to exist. The branches of the main neutral curves are expected to coalesce when $u_w = u_w^*$. This appears to be in agreement with the behaviour of the neutral curves in figure 20 as $u_w$ is increased. The curves shown in figure 20 are not the complete picture as only one neutral curve is shown for varying wall speeds, whereas the stability analysis undertaken by Cowley and Smith (1985) discovered more. For increasing values of $u_w$ the critical wavenumber approaches zero and the Reynolds number approaches infinity, therefore the neutral curve ceases to exist and above the cut-off value ($u_w^* = 0.5279$) the hybrid flow is then stable to infinitesimal disturbances. It was concluded from the study by Cowley and Smith (1985) a number of linear neutral curves exist in Poiseuille-Couette flow, and further that the two main neutral curves disappear when $u_w$ is $\mathcal{O}(1)$. In contrast, the analysis for plane Poiseuille flow ($u_w = 0$) is less complex as there is only one linear neutral curve.

The weakly nonlinear stability analysis of Poiseuille-Couette flow conducted by Cowley and Smith (1985) demonstrated the existence of unstable finite-amplitude solutions, one of which bifurcates from just below $u_w^*$, the other bifurcates from infinity. As expected the nonlinear solutions which are closest to $u_w^*$ are most likely the more physically significant results in regard to experimental testing. It has been shown numerically that two-dimensional and three-dimensional finite-amplitude disturbances play a role in the transition at Reynolds numbers of order 1000 in both plane Poiseuille and Couette flow, with three-dimensional effects driving the transition in plane Couette flow (Orszag and Kells, 1980). As the two-dimensional linear stability analysis applied to plane Poiseuille and Couette flow yield critical Reynolds numbers that are often in conflict with experiment, the inclusion of the nonlinear theory in the prediction of transition in both flows has allowed for better agreement among the theoretical and experimental results.

## 12.2 Conclusions

The numerical results obtained here concerning the linear stability of plane Poiseuille flow are in strong agreement with the literature. The implementation of both numerical methods employed here have advantages and disadvantages. The superior error properties of spectral methods benefit from convergence of infinite-order whereas finite-difference methods, will only ever be of finite-order convergence (second-order in this case). The central-difference scheme employed, constructed with second-order convergence, clearly exhibits this order of convergence by the analysis of the solution to the Orr-Sommerfeld eigenvalue problem. Although finite-difference methods are more intuitively implemented when compared with the spectral approach, the finite-order of the convergence rate means that difference schemes of further complexity are often required to obtain a similar order of accuracy to that of spectral methods. We note that Gary and Helgason (1970) made use of a sixth-order finite-difference scheme, with a variable mesh being utilised while only seeking symmetric modes in order to obtain a solution of similar accuracy to spectral methods. In the finite-difference approach here a local iterative method was employed, which used an initial guess to obtain a more accurate approximation to the least stable eigenvalue at less computational expense when compared with solving the

complete generalized eigenvalue problem.

The development of spectral methods has allowed the solution to the linear stability problem of plane Poiseuille flow, characterised by numerically solving an eigenvalue problem, to be obtained with great accuracy more economically in comparison to finite-difference methods. This was clearly observed here in the analysis of the solution to the Orr-Sommerfeld eigenvalue problem from the implementation of the spectral-tau method. In the solution obtained by the spectral-tau method, features of the solution were found to be spurious. This is not out of line of similar results obtained in the literature. These non-physical features arising in the solution required more care numerically when compared with the solution obtained by finite-difference methods which did not exhibit such artifacts. Nonetheless the spurious eigenvalues may be eliminated from the solution by modifying the spectral-tau method. This was not done here, however the modification to the tau method by McFadden *et al.* (1990) was illustrated and the significant growth of the non-physical eigenvalues discussed.

The linear neutral stability curve along with approximations to the critical Reynolds number were computed using both numerical methods. The breakdown in laminar flow leading to the transition to turbulence is only partially described by the linear theory, as nonlinear effects as described by the weakly nonlinear theory may have a significant effect on the transition. The observation of subcritical transition in plane Poiseuille flow demonstrates that a flow which is stable to infinitesimal disturbances is perhaps unstable to finite disturbances. Although nonlinear effects may influence subcritical transition, we may recall the stability experiments conducted by Nishioka *et al.* (1975), that demonstrate encouraging agreement between the linear theory and experimental observations provided the background turbulence is carefully controlled. Therefore there is evidence that for small disturbances the linear theory is valid. On the other hand observations from the experiments found that a nonlinear subcritical instability occurs when the intensity of subcritical disturbances exceed a certain threshold value, which was found to be a function of Reynolds number and frequency of disturbance (Nishioka *et al.*, 1975). The subcritical instability termed the secondary instability was found to have a critical Reynolds number for plane Poiseuille flow of roughly $Re = 1000$, which is in agreement with transition observed in typical flows (Orszag and Patera, 1983). The secondary instability discussed by Orszag and Patera (1983), said to be the prototype of transitional instability in plane Poiseuille flow, is characterised by two-dimensional finite-amplitude waves that are unstable to three-dimensional infinitesimal disturbances. The two-dimensional instability of the linear theory with Squire's transformation contrasts with the observed transition which demonstrates the intrinsic three-dimensionality of turbulence.

In summary a linear stability analysis on plane Poiseuille flow has been conducted with the implementation of two numerical methods to solve the Orr-Sommerfeld eigenvalue problem in hydrodynamic stability theory. The results achieved here are in strong agreement with well-known results and concepts in the literature. A natural extension to the stability analysis of plane Poiseuille flow performed here would be to study the stability of other flows and jets such as plane Poiseuille-Couette flow, Plateau-Rayleigh instability (Capillary instability of a liquid jet), Kelvin-Helmholtz instability or instability of flow past an circular cylinder. Alternatively one could extend to the theoretical discussion on the transition to turbulence by conducting a weakly nonlinear stability analysis on plane Poiseuille flow, and further discuss the subcritical transition observed not only in plane Poiseuille flow but also in other parallel flows.

# Appendices

## A Spectral-tau method for Poiseuille-Couette flow

The linear stability analysis of the hybrid plane Poiseuille-Couette flow can be implemented by making use of the spectral-tau formulation already formalised previously. The process of non-dimensionalisation of the Navier-Stokes and continuity equations and obtaining an expression for the base flow is unchanged. The only difference in this case, is that since the boundaries are allowed to move tangentially relative to each other, the boundary conditions are no longer zero at the walls. The linear combination of plane Poiseuille and plane Couette flow examined here is produced by an applied pressure gradient on the fluid in the channel and (without loss of generality) allowing the walls to move with the same speed $u_w$ but in opposite directions.

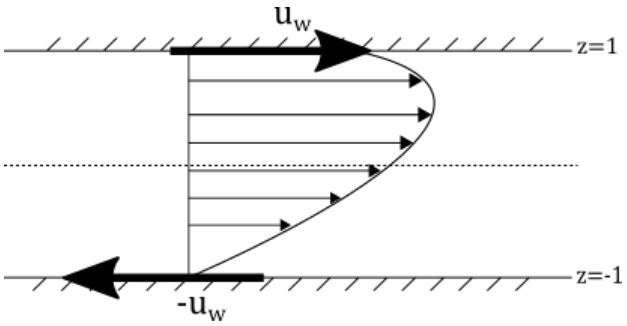


FIGURE. 21 Diagram of the hybrid flow where both walls move tangentially relative (in opposite directions) to each other with the same speed $u_w$ and a pressure gradient also acts on the fluid. The relative velocity of the walls is therefore $2u_w$.

By considering the non-dimensionalised Navier-Stokes and continuity equations that were established in the derivation of the Orr-Sommerfeld equation along with the altered boundary conditions we have,

$$\frac{\partial \mathbf{u}^*}{\partial t^*} + (\mathbf{u}^* \cdot \nabla^*)\,\mathbf{u}^* = -\nabla^* p^* + \frac{1}{Re}\nabla^{*2}\mathbf{u}^*, \tag{A-1}$$

$$\nabla \cdot \mathbf{u}^* = 0, \tag{A-2}$$

with boundary conditions,

$$u^* = u_w, \quad w^* = 0, \quad at \quad z = 1, \tag{A-3}$$

$$u^* = -u_w, \quad w^* = 0, \quad at \quad z = -1. \tag{A-4}$$

The base flow is then represented by the following linear combination of plane Poiseuille and Couette flow.

$$U(z) = \frac{3}{2}(1 - z^2) + u_w z. \tag{A-5}$$

In conducting a linear stability analysis on the hybrid Poiseuille-Couette flow, this base flow is perturbed to infinitesimal disturbances. The Orr-Somerfeld eigenvalue problem must therefore be solved again for this different base flow. The boundary conditions for the Orr-Sommerfeld problem remain the same and if we make use the spectral-tau formulation with Chebyshev polynomials, the only terms in the equations that need be

altered are those involving the base flow $U(z)$. In order to incorporate the extra term $u_w z$ into the spectral formulation, we begin by rewriting the base flow in terms of Chebyshev polynomials.

$$U\phi = \frac{3}{4}(T_0 - T_2)\sum_{n=0}^{\infty}\phi_n T_n + u_w T_1 \sum_{n=0}^{\infty}\phi_n T_n. \tag{A-6}$$

Recalling the recurrence relation for the product of Chebyshev polynomials, for integers $n$ and $m$,

$$2T_n(z)T_m(z) = T_{n+m}(z) + T_{|n-m|}(z), \tag{A-7}$$

After utilising the recurrence relation we obtain,

$$U\phi = \frac{3}{4}\sum_{n=0}^{\infty}\phi_n T_n - \frac{3}{4}\sum_{n=0}^{\infty}\phi_n\left(T_{n+2} + T_{|n-2|}\right) + \frac{u_w}{2}\sum_{n=0}^{\infty}\phi_n(T_{n+1} + T_{|n-1|}), \tag{A-8}$$

$$= \frac{3}{4}\sum_{n=0}^{\infty}\phi_n T_n - \frac{3}{8}\sum_{n=0}^{\infty}\phi_n\left(T_{n+2} + T_{|n-2|}\right) + \frac{u_w}{2}\left(\sum_{n=0}^{\infty}\phi_n T_{n+1} + \sum_{n=0}^{\infty}\phi_n T_{|n-1|}\right), \tag{A-9}$$

Collecting the coefficients of each Chebyshev polynomial we have,

$$\begin{aligned} U\phi = &\left(\frac{3}{4}\phi_0 - \frac{3}{8}\phi_2 + \frac{u_w}{2}\phi_1\right)T_0 + \left(\frac{3}{8}\phi_1 - \frac{3}{8}\phi_3 + u_w\phi_0 + \frac{u_w}{2}\phi_2\right)T_1 \\ &+ \left(\frac{3}{4}\phi_2 - \frac{3}{4}\phi_0 - \frac{3}{8}\phi_4 + \frac{u_w}{2}\phi_1 + \frac{u_w}{2}\phi_3\right)T_2 \\ &+ \left(\frac{3}{4}\phi_3 - \frac{3}{8}\phi_1 - \frac{3}{8}\phi_5 + \frac{u_w}{2}\phi_1 + \frac{u_w}{2}\phi_3\right)T_3 + \ldots. \end{aligned} \tag{A-10}$$

Recalling the coefficient $c_n$, where $c_0 = 2$ and $c_n = 1$ for $n > 0$, then the coefficient of the $n$-th Chebyshev polynomial can be written as,

$$U\phi = \sum_{n=0}^{\infty}\left[\phi_n - \frac{1}{4}\left(c_{n-2}\phi_{n-2} + \phi_n\left(c_n + c_{n-1}\right) + \phi_{n+2}\right) + \frac{u_w}{2}\left(c_{n-1}\phi_{n-1} + \phi_{n+1}\right)\right]T_n,$$

where $c_n = 0$ for $n < 0$. Similarly,

$$U\phi'' = \sum_{n=0}^{\infty}\left[\phi_n^{(2)} - \frac{1}{4}\left(c_{n-2}\phi_{n-2}^{(2)} + \phi_n^{(2)}\left(c_n + c_{n-1}\right) + \phi_{n+2}^{(2)}\right) + \frac{u_w}{2}\left(c_{n-1}\phi_{n-1}^{(2)} + \phi_{n+1}^{(2)}\right)\right]T_n.$$

The formulation of the cross terms $U\phi$ and $U\phi''$ in terms of Chebyshev polynomials can then used in the spectral-tau method analogously with the formulation for plane Poiseuille flow. Note that if the wall velocity is set to zero, $u_w = 0$, we recover plane Poiseuille flow. However the value for the critical Reynolds number for plane Poiseuille flow is no longer $Re = 5772.22$, the value is in fact $Re = 3848.08$. The analysis performed on plane Poiseuille flow can be applied to the hybrid flow for various values of the wall velocity. Such analysis is not performed here, however the spectral-tau formulation developed is able to produce results that are in strong agreement with the literature Potter (1966), Reynolds and Potter (1967). Plots of the linear neutral curves are displayed in the conclusions and discussion.

# B Examples of MATLAB code used

Displayed below are the implementations of both methods.

## B.1 Finite-difference implementation

```
% ========================================================================
% ------ Finite-difference implementation - Orr-Sommerfeld equation -------
% ========================================================================
Re = 5772.22; % Reynolds number
alpha = 1.02056; % wavenumber
m=12;
N = 2^m;
gridpts = 2^(m-1); % # grid points
h = 2/(gridpts-1);
U = zeros([gridpts 1]);
for i = 1:gridpts-1
    U(i)= 1-(-1 + h*(i-1))^2;
end
A = zeros(N);
B = zeros(N);
b = (-1)^0.5 / (alpha*Re);
% phi' = 0 BC
A(1,2) = -3;
A(1,4) = 4;
A(1,6) = -1;
% phi' = 0 BC
A(2,2) = 1;
for j = 2:N/2 - 1
    k = 2*j-1;
    B(k,k) = 1;
    A(k,k-2) = b/h^2 ; %psi_j-1
    A(k,k) = U(j) - (2/h^2 + alpha^2)*b ; %psi_j
    A(k,k+1) = 2 ; %phi_j
    A(k,k+2) = b/h^2; %psi_j+1
    k = k+1;
    A(k,k-2) = -1/h^2;
    A(k,k-1) = 1;
    A(k,k) = 2/h^2 + alpha^2;
    A(k,k+2) = -1/h^2;
end
% phi' = 0 BC
A(N-1,N-4) = 1;
A(N-1,N-2) = -4;
A(N-1,N) = 3;
% phi = 0 BC
A(N,N) = 1;
```

```
[eigvec,v] = eig(A,B);
% v generalized eigenvalues as entries on a diagonal matrix, eigvec matrix
of eigenvectors
vsorted = sort(diag(v));
vsorted(1) % least stable eigenvalue
```

---

### B.2 Spectral-tau method implementation

---

```
% ======================================================================
% ----- Spectral method implementation - Orr-Sommerfeld equation ------
% ======================================================================
%% Formulate the generalized eigenvalue problem
Re = 5772.22; % Reynolds number
alpha = 1.02056; % Wavenumber
N=54; % N+1 Chebyshev polynomials
% Working out E matrix
A = zeros(N);
B = zeros(N);
C = zeros(N);
for i=1:N
    if i==1
        C(i,i)=2;
    else
        C(i,i)=1;
    end
    if i<=N-2
        C(i,i+2)=-1;
    end
    A(i,i+1)=2*i;
end
E = C\A;
E(N+1,N)=0; % Add another row to make the matrix square

% Constructing the matrix which is used to determine the matrix formulation
% of the cross terms in the Orr-Sommerfeld equation U*phi, U*phi"
Q = zeros(N+1); % has same dimensions as E
for j=1:N-3
    if j<N
        Q(j,j+2) = -0.25;
    end
    % Diagonal entries
    if j-1 == 1
        Q(j,j)=0.25;
    else
        Q(j,j)=0.5;
```

```
    end
    % Other off-diagonal entries
    if j>2
        if j==3
            Q(j,j-2) = -0.5;
        else
            Q(j,j-2)=-0.25;
        end
    end
end
% Constructing generalized eigenvalue problem in the form Dx=cFx
% Identity matrix
I = zeros(N+1);
for j=1:length(E)-4
   I(j,j) = 1;
end
% Solving the generalized eigenvalue problem
D = (sqrt(-1)/(alpha*Re))*( E^4-2*(alpha^2)*I*(E^2)+(alpha^4)*I )+ 2*I -
(alpha^2)*Q + Q*(E^2); % LHS
F = I*E^2 - (alpha^2)*I; % RHS
%Boundary conditions
for k = 1:length(D)
   D(N-2,k) = 1; % phi(1)=1
   D(N,k) = (k-1)^2; % phi'(1)=n^2
   D(N-1,k) = (-1)^(k-1); % phi(-1)=(-1)^(n-1)
   D(N+1,k) = ((-1)^(k-1))*(k-1)^2; % phi'(-1)= n^2 (-1)^(n-1)
end
% Solving for the eigenvalues and eigenvectors
% Columns of V are the eigenvectors, with W a diagonal matrix with
% eigenvalues as the entries
format long
[V,W] = eig(D,F); %
eigvals = diag(W);
eigvals = sort(eigvals) % Display eigenvalues

% Sanity check
eig_crit = min(eigvals);
for k=1:length(eigvals)-6 %-6 as we need to remove the spurious eigenvalues
    if imag(eigvals(k)) > imag(eig_crit)
        eig_crit = eigvals(k);
    end
end
eig_crit % display least stable eigenvalue
```

---

# References


Alavyoon, F., Henningson D. S. and Alfredsson, P. H.(1986) 'Turbulent spots in plane Poiseuille flow – flow visualization', *The Physics of Fluids* **29**, pp. 1328-1331.

Cowley, S. J. and Smith, F. T.(1985) 'On the stability of Poiseuille-Couette flow: a bifurcation from infinity', *Journal of Fluid Mechanics*, **156**, pp. 83-100.

Davey, A.(1973) 'On the stability of plane Couette flow to infinitesimal disturbances', *Journal of Fluid Mechanics* **57**(2), pp. 369-380.

Davey, A. and Drazin, P. G.(1969) 'The stability of Poiseuille flow in a pipe', *Journal of Fluid Mechanics* **36**(2), pp. 209-218.

Drazin, P. G. and Howard, L. N.(1966) 'Hydrodynamic Stability of Parallel Flow of Inviscid Fluid', *Advances in Applied Mechanics* **9**, pp. 1-89.

Gary, J. and Helgason, R.(1970) 'A matrix method for ordinary differential eigenvalue problems' , *Journal of Computational Physics* **5**(2), pp. 169-187.

Grosch, C. E. and Salwen, H.(1968) 'The stability of steady and time-dependent plane Poiseuille flow' , *Journal of Fluid Mechanics* **34**(1), pp. 177-205.

Gustavsson, L. H.(1981) 'Resonant growth of three-dimensional disturbances in plane Poiseuille flow', *Journal of Fluid Mechanics* **112**, pp. 253-264.

Helmholtz, H.(1868) 'XLIII. On discontinuous movements of fluids' , *The London, Edinburgh, and Dublin Philosophical Magazine and Journal of Science* **36**(244), pp. 337-346

Howard, L. N.(1961) 'Note on a paper of John W. Miles' , *Journal of Fluid Mechanics* **10**(4), pp. 509-512.

Kelvin, Lord(1871) 'XLVI. Hydrokinetic solutions and observations', *The London, Edinburgh, and Dublin Philosophical Magazine and Journal of Science* **42** 281, pp. 362-377.

Koch, W.(1986) 'Direct resonances in Orr-Sommerfeld problems.', *Acta Mechanica* **59**, pp. 11-29.

McFadden, G.B. and Murray, B.T. and Boisvert, R.F.(1990) 'Elimination of spurious eigenvalues in the Chebyshev tau spectral method', *Journal of Computational Physics* **91**(1),pp. 228-239.

Nishioka, M and Asai, M.(1985) 'Some observations of the subcritical transition in plane Poiseuille flow', *Journal of Fluid Mechanics* **150**, pp. 441-450.

Nishioka, M., A, S. I. and Ichikawa, Y.(1975) 'An experimental investigation of the stability of plane Poiseuille flow', *Journal of Fluid Mechanics* **72**(4), pp. 731-751.

Orr, W. McF.(1907a) 'The stability or instability of the steady motions of a liquid. Part I' , *Proceedings of the Royal Irish Academy* , A **27**, pp. 9-68.

Orr, W. McF.(1907b) 'The stability or instability of the steady motions of a liquid. Part II' , *Proceedings of the Royal Irish Academy* , A **27**, pp. 69-138.

Orszag, S. A.(1971) 'Accurate solution of the Orr-Sommerfeld stability equation', *Journal of Fluid Mechanics* **50**(4), pp. 689-703.

Orszag, S. A. and Kells, L. C.(1980) 'Transition to turbulence in plane Poiseuille and plane Couette flow' **96**(1), pp. 159-205.

Orszag, S. A. and Patera, A. T.(1983) 'Secondary instability of wall-bounded shear flows', *Journal of Fluid Mechanics* **128**, pp. 347-385.

Potter, M. C.(1966) 'Stability of plane Couette-Poiseuille flow', *Journal of Fluid Mechanics* **24**(3), pp. 609-619.

Rayleigh, Lord.(1880) 'On the Stability, or Instability, of certain Fluid Motions', *Proceedings of the London Mathematical Society* **s1-11**(1), pp. 57-70.

Reynolds, O.(1883) 'XXIX. An experimental investigation of the circumstances which determine whether the motion of water shall be direct or sinuous, and the law of resistance in parallel channels.', *Philosophical Transactions of the Royal Society of London* **174**, pp. 935-982.

Reynolds, W. C. and Potter, M. C.(1967) 'Finite-amplitude instability of parallel shear flows' **27**(3), pp.465-492.

Shanthini, R.(1989) 'Degeneracies of the temporal Orr-Sommerfeld eigenmodes in plane Poiseuille flow', *Journal of Fluid Mechanics* **201**, pp. 13-34.

Sommerfeld, A.(1908) 'Ein Beitrag zur hydrodynamische Erklärung der turbulenten Flüssigkeitsbewegungen', *Proceedings of the 4th International Congress of Mathematicians*, **III**, Rome, pp. 116–124.

Squire, H. B.(1933) 'On the stability of three-dimensional disturbances of viscous flow between parallel walls', *Proceedings of the Royal Society A*, **142**, pp. 621-628.

Taylor, G. I.(1915) 'I. Eddy motion in the atmosphere', *Philosophical Transactions of the Royal Society of London* **215**, pp. 1-26.

Thomas, L. H.(1953) 'The Stability of Plane Poiseuille Flow', *Physical Review* **91**(4), pp. 780-783.